INVESTIGATIONS ON NANOMATERIALS FOR POTENTIAL BIOMEDICAL APPLICATIONS

TAPAS RANJAN NAYAK

NATIONAL UNIVERSITY OF SINGAPORE

2010

INVESTIGATIONS ON NANOMATERIALS FOR POTENTIAL BIOMEDICAL APPLICATIONS

TAPAS RANJAN NAYAK

A THESIS SUBMITTED

FOR THE DEGREE OF DOCTOR OF PHILOSOPHY

DEPARTMENT OF PHARMACY

NATIONAL UNIVERSITY OF SINGAPORE

2010

ACKNOWLEDGEMENTS

I take this as an opportunity to express my deep sense of regards and gratitude to my supervisor, **Dr Giorgia Pastorin**, Assistant Professor, Department of Pharmacy, National University of Singapore, for her valuable suggestions, encouragement, inspiring guidance, constructive criticism and kind cooperation during the period of my PhD.

I would also like to thank Prof Hans Junginger, Faculty of Pharmaceutical Sciences, Naresuan University, Phitsanulok, Thailand, for volunteering to become a subject for TEWL and Tape stripping experiments and Dr S Ramaprabhu, Indian Institute of Technology, Madras, India, for providing me ultrapure MWCNTs for my research.

I sincerely thank Dr Gigi Chiu, thesis committee member for her valuable advice on my project; Dr Paul Ho, for taking time to be my PhD qualifying examination examiner: Dr EE Pui Lai, Rachel, Dr Ho Han Kiat for providing access to their lab facility for carrying out important experiments.

My special thanks and appreciation to Dr Clement Khaw and SBIC Nikon Imaging Centre for providing me access to fluorescence and confocal microscopy facilities, Dr Jan Fric and Dr Florent Ginhoux (Singapore Immunology Network) for helping me in *in vivo* immunization study.

I would like to thank the Department of Pharmacy, National University of Singapore for granting me the scholarship that enabled me to pursue this study, and for providing the premises and equipment for me to conduct the experiment. I would also like to thank Dr Chan Sui Yung, Head of the Department and all other faculty members of Department for their cooperation whenever I needed.

My deep gratitude and regards are due for my friends and lab mates, specifically Mr Henrik Anderson, Mr Zheng Minrui, Miss Siew Lee and Mr Li Jian for extending their help whenever I needed during the course of my PhD study.

I am deeply indebted to my family. I thank my parents and brother for their love and encouragement when I faced difficulties. Special appreciation is due to my wife, Purnatoya Nayak. She has been a great source of support, providing a happy family life for me during my PhD study, and for standing with me during my difficult periods.

Content

Summary

Recent advances in creating nanomaterials have led to several opportunities in biomedical research and clinical applications. Some of these opportunities are becoming realities (liposomes as first generation of nano delivery systems), while others are generating promise in their early phases of development and are expected to experience vigorous growth in the foreseeable future. The current and most promising applications of these nanomaterials include, but are not limited to, drug delivery, *in vitro* diagnostics, *in vivo* imaging, therapy techniques, biomaterials, and tissue engineering. A variety of organic/inorganic nanomaterials and devices are currently being investigated world over for these purposes. We, as part of that, have considered and studied suitably functionalized carbon nanotubes (CNTs) as scaffold for bone tissue engineering and Zinc oxide nanorods for transdermal delivery of vaccine. While Zinc oxide nanoparticles are already approved by USFDA as a safe product for their application in several skin care products, carbon nanotubes (CNTs) are still being elucidated for their solubility, cytotoxicity and biocompatibility. Therefore we also studied covalent functionalization of carbon nanotubes as part of the enhancement of their solubility and simultaneous characterization of several parameters owing to improvement of their biocompatibility.

The objectives of our first study were 1) to modify carbon nanotubes' (CNTs) surface with appropriate functional groups to improve their water solubility and decrease their tendency to aggregate, and 2) to characterize their biocompatibility and cytotoxicity in terms of several parameters such as sidewall functionalization, concentration, degree of dispersibility, length and purity. Pristine CNTs were not only insoluble in water but also insoluble in most of organic solvents (ethyl acetate, DMF, ethanol etc). In contrast covalent functionalization of CNTs to form *f*-CNTs increased their dispersibility, which

was directly correlated to the polarity of the functional groups covalently bond to CNTs. In particular functionalization of CNTs with longer chains such as poly(ethylene glycol) resulted in dramatic improvement of aqueous dispersibility of CNTs by a factor of 5 in case of SWCNTs and a factor of 25 in case of MWCNTs. As part of the evaluation of parameters with respect to biocompatibility of CNTs we found the cell viability of MCF7 cells in direct correlation with water dispersibility and hence functionalization. PEG-CNTs, being the most hydrophilic, displayed higher cell viability compared to Pristine CNTs, which had the worst toxicological profile. Similarly, evaluation of cell viability in terms of length of CNTs resulted in higher cell viability for shorter tube length. Cell viability of MCF-7 and HL-60 cells showed an an inverse correlation with concentrations: the higher the dose of CNTs, the lower the cell viability. Among all these parameters, purity was found to be the most crucial in terms of biocompatibility of CNTs as one of our samples (the so called ultrapure MWCNTs with a purity of around 98%) showed no sign of toxicity in case of both tumoral cell line (MCF-7) and normal cell line (hMSCs) till a concentration of 150 μg /ml compared to SWCNTs (90% purity) and MWCNTs (95% purity), which showed sign of toxicity even in in the range of 10μg/ml. The above result found via MTT cell viability assay was also confirmed by CyQUANT cell viability assay.

The objective of our second study was to prepare compact and uniform thin film of PEG functionalized carbon nanotubes as a biocompatible scaffold to provide suitable microenvironment for growth, proliferation and specific differentiation of human mesenchymal stem cells (hMSCs) into osteogenic lineages, without the need of any additional biochemical inducer in osteogenic medium. As part of the purpose, PEGylated ultrapure multiwalled carbon nanotubes (MWCNT-PEG) graft copolymers were synthesized following an earlier published procedure. These samples were coated on to

normal 12 mm cover slips in form of a uniform thin film using an air brush. Subsequently hMSCs were cultured and the cell viability was determined by calcein AM cell viability assay and MTT assay. hMSCs were able to maintain their growth and morphology on these coated cover slips preserving a morphology comparable to plain uncoated cover slips used as control. Furthermore, hMSCs growing on these cover slips were osteoinduced for osteogenesis for two weeks by using an osteogenic medium with or without the addition of BMP-2 (biochemical inducer). Alizarin red quantification was done to quantify calcium deposits as part of bone mineralization. In a remarkable result, hMSCs growing on MWCNT-PEG coated cover slips showed calcium deposition comparable ($p>0.05$) to BMP-2 treated substrates even without osteoinduction with BMP-2. In a simultaneous experiment of immunofluorescence performed after using two common protein markers, *CD44* for hMSCs and osteocalcin (*OCN*) for osteoblasts, it was found that hMSCs growing on MWCNT-PEG thin films did not show expression of *CD44*, but displayed a high fluorescence with respect *OCN* immunostaining. This result was in clear contrast to hMSCs growing on plain uncoated cover slips, which confirmed the successful differentiation of hMSCs in to osteoblasts even in absence of BMP-2. The above result was further confirmed by qPCR analysis of transcriptional upregulation of osteopontin (*OPN*), an early biomarker for osteogenesis. hMSCs, growing on MWCNT-PEG thin films demonstrated an elevated *OPN* transcript level that was comparable ($p>0.05$) to the hMSCs undergoing BMP-2 stimulation on plain uncoated cover slips. Altogether, MWCNT-PEG successfully transformed hMSC into bone-like cells even in the absence of any additional osteogenic inducer, as evidenced by multiple independent criteria at the transcript (e.g. osteopontin), protein (e.g. osteocalcin) and functional (e.g. calcium deposition) levels.

The objective of our third study was to carry out a preliminary study of transdermal delivery of a vaccine prototype using aligned ZnO nanorods grown successfully on silicon chip as part of a future platform for transdermal delivery of therapeutics including pertussis, tetanus and influenza vaccines. As part of that study, we functionalized the nanorod chips with albumin-FITC and *in vitro* skin permeation study was conducted to investigate the degree of penetration of these nanorods through human skin samples using Franz diffusion cells. SEM image of these chips done before and after skin penetration study showed that there was no reduction in density and nanorods preserved certain degree of alignment except for the tips, which were slightly affected. The fluorescence microscopy of the chips before the skin penetration study showed uniform distribution of vaccine prototype, but after skin penetration study, there were blank patches owing to detachment of albumin-FITC. The detached albumin-FITC was confirmed to be adsorbed in to the skin in the form of fluorescent tunnels during the process from the confocal microscopy of the skin. This was further confirmed by *in vivo* skin penetration studies, where the average length of the fluorescent tunnels was found to be 11.19 μm, which is greater than the normal thickness of the stratum corneum of the human skin. Bradford analysis for the quantification of the vaccine solution (collected every three hours during Franz diffusion cell experiment), showed maximum peak of albumin diffusion during the first 4 hours. In an another experiment, transepidermal water loss carried out on the forearms of a 64-year old volunteer demonstrated the increase in permeability through enhancement of water loss; this in turn confirmed the efficacy of these nanorods in penetrating the skin without any pain. Similarly tape stripping experiment done on the same volunteer confirmed the effective penetration of the nanorods through the skin as seen in form of fluorescent layers through the whole18 skin samples analyzed under confocal microscope. In subsequent steps, *in vivo* immune response was determined by

ELISA of the serum collected from the mice subjected to chips with different OVA formulations. Overall the antibody titer found in case of serum of test mice was at a serum dilution of 1:160 compared to serum of mice applied with PBS adsorbed chips (negative control). However immune response obtained in case of OVA applied to stripped ear (1:640) did not show any significant difference ($P>0.05$) compared to OVA with alum as adjuvant. Anyhow, it showed better antibody titer compared to mice applied with chips adsorbed with only OVA (1:160). This proves the role of alum as an adjuvant, which led to better immune response even at a lower dose of the prototype vaccine. Finally significant increase in antibody titer as part of the immune response against our prototype vaccine confirms the efficacy of this novel nano device. In summary these results pave the way for a further development of the project for transdermal delivery of vaccines using this nanometric platform.

List of Tables

List of Figures

List of Abbreviations

AFM	Atomic force microscopy
APC	Antigen presenting cells
ASC	Antibody secreting cells
AuNP	Gold nanoparticle
BMP-2	Bone morphogenic protein
BOC	Di-tert-butyl dicarbonate
BSA	Bovine serum albumin
CNT	Carbon nanotube
CTL	Cytotoxic lymphocyte
CVD	Chemical vapor deposition
DAPI	4',6-diamidino-2-phenylinoindole
DC	Dendritic cell
DIPEA	N,N-di-isopropyl ethylamine
DMEM	Dulbecco’s modified eagle's media
DMF	Dimethyl formamide
DMSO	Dimethyl sujphoxide
DOX	Doxorubicin
EDC	1-ethyl-3-(3-dimethylaminopropyl) carbodiimide
EDS	Energy dispersive X-ray spectroscopy
ELISA	Enzyme-Linked Immunosorbent Assay
FBS	Fetal bovine serum
FITC	Fluorescein isothiocyanate
FMOC	Fluorenylmethyloxycarbonyl
GFP	Green fluorescent protein
GO	Graphene oxide
GPC	Gel permeation chromatography
hMSC	Human mesenchymal stem cell
HRP	Horse radish peroxidase
IgG	Immunoglobulin G
INM	Inorganic nanomaterial

KCN	Potassium cyanide
LC	Langerhans cell
MES	2-(N-Morpholino)ethane-sulphonic acid
MRI	Magnetic resonance imaging
MSC	Mesenchymal stem cells
MTT	(3-(4,5-Dimethylthiazol-2-yl)-2,5-diphenyltetrazolium bromide
MWCNT	Multiwall carbon nanotube
MWNT	Multiwall nanotube
ND	Nanodiamond
NEAA	Non-essential amino acid
NGO	Nanographene oxide
NGS	Nanographene sheet
NHS	N-hydroxysuccinimide
NIR	Near infra-red
NP	Nanoparticle
OCN	Osteocalcin
OPN	Osteopontin
PBS	Phosphate buffered saline
PDT	Photodynamic therapy
PEB	Paclitaxel embedded buckysomes
PEG	Polyethylene glycol
PTFE	Polytetrafluoroethylene
QD	Quantum dot
qPCR	Quantitative Polymerase chain reaction
RDX	Research Department Explosive
RMS	Root mean square
ROS	Reactive oxygen species
RPMI	Rosswell park memorial institute
SC	Stratum corneum
SDBS	Sodiumdodecyl benzene sulphonate
SDS	Sodium dodecyl sulphate
SEM	Scanning electron microscope

SWCNT	Single wall carbon nanotube
SWNT	Single wall nanotube
TEG	Triethylene glycol
TEM	Transmission electron microscopy
TEWL	Transepidermal water loss
TGA	Thermogravimetric analysis
TGF	Transforming growth factor
THF	Tetrahydrofuran
TMB	3.3',5,5'-tetramethylbenzidine
TNT	Trinitrotoluene
TVD	Transdermal vaccine delivery
UDD	Ultradispersed diamond
UNCD	Ultracrystalline diamond
ZnO	Zinc oxide

List of publications and conference Presentations

Publications:

1. Ren, Y., Paira, P., **Nayak, T.R**., Ang, W.H and Pastorin, G. (2011). Encapsulation of Pristine Fullerene in Gold Nanoshells, ***Chem Comm*** (Accepted, in press).

2. **Nayak, T.R**., Andersen, H., Makam, V.S., Khaw, C., Bae, S., Xu, X., Ee, P.L., Ahn, J.H., Hong, B.H., Pastorin, G., and Ozyilmaz, B. (2011). Graphene for Controlled and Accelerated Osteogenic Differentiation of Human Mesenchymal Stem Cells, ***ACS Nano*** (DOI: 10.1021/nn200500h).

3. **Nayak, T.R**., Jian, L., Phua, L.C., Ho, H.K., Ren, Y., and Pastorin, G. (2010). Thin films of functionalized multiwalled carbon nanotubes as suitable scaffold materials for stem cells proliferation and bone formation, ***ACS Nano***, Vol. 4, No. 12, pp. 7717-7725(9).

4. **Nayak, T.R**., Leow, P.C., Ee, P.R., Arockiadoss, T., Ramaprabhu, S. and Pastorin, G. (2010). Crucial Parameters responsible for Carbon Nanotubes toxicity, ***Curr Nano Sci***, Vol. 6, No. 2, pp. 141-154(14).

5. Pastorin, G., **Nayak, T.R**. and Ren, Y. (2010). Achievements and challenges in the delivery of bioactive molecules by nano-carbon-based systems, ***Int. J. Biomedical Nanoscience and Nanotechnology***, Vol. 1, Nos. 2/3/4, pp.267-289.

6. **Nayak, T.R**. and Pastorin, G. (2010). Toxicity of Carbon nanotubes, *Carbon Nanotubes: from bench Chemistry to promising Biomedical Applications*, Pan Stanford Publishing, Singapore, Chapter 8, pp-223.

Oral and Poster Presentations:

1. Nayak, T.R., Zheng, M., Pastorin, G., Fric, J. and Ginhoux, F. (2010). *Nanoneedles Devices for Transdermal Vaccine Delivery: in Vitro and in Vivo Evaluation*, Poster presented at the Singapore Symposium on Drug Delivery Systems, Jan (20-22).

2. Nayak, T.R. and Pastorin, G. (2009). *Functionalization and Characterization of Carbon Nanotubes for enhancing their Biocompatibility in terms of Drug Delivery*, Poster presented at the AAPS Annual Meeting, Los Angeles, Nov (8-12).

3. Ren, Y., Tiang, H.Y., Nayak, T.R., Li, J. and Pastorin, G. (2009). *Nano-bottles for incorporation, storage and drug release from carbon nanotubes*, Poster presented at the IEEE-NANOMED conference, Taiwan, Oct (18-21).

4. Nayak, T.R. and Pastorin, G. (2008). *Functionalization and Characterization of Carbon Nanotubes for Biomedical Applications*, Oral presentation at the Asian Conference on Nanoscience and Nanotechnology, Singapore, Nov (3-7).

5. Nayak, T.R. and Pastorin, G. (2008). *Functionalization and Characterization of Carbon Nanotubes for Biomedical Applications*, Poster presented at the Singapore Nanomedicine Workshop, Oct (22-25).

6. Nayak, T.R., Zheng, M., Junginger, H. and Pastorin, G. (2008). *Functionalization and Characterization of Aligned Nanodevices as potential Vaccine Delivery Systems*, Poster presented at the 35th Annual Meeting & Exposition of the Controlled Release Society, New York, July (12-16).

7. Ren, Y., Nayak, T.R., Dumortier, H., Wu, W., Bianco, A. and Pastorin, G. (2007). *Characterization of Functionalized SWNT and A Preliminary study on their impact on Immune cells*, Poster presented at PharmSci@Asia Symposium, Fudan University, Shanghai, China, June (28-29).

Chapter 1

Introduction

1.1 Nanotechnology & nanomaterials

Every so often, a new term comes along that represents an emerging scientific trend. Biotechnology, genetic engineering, tissue engineering, gene therapy, combinatorial chemistry, high throughput screening, and stem cells are some examples of past terms. Recently, nanotechnology has become a popular term representing the main efforts of the current science and technology.

Nanotechnology, which is still not a mature technology and thus, more appropriately called nanoscience, can be defined as a combination of techniques aimed to conceive, characterize, produce and utilize materials of at least one dimension ranging within 100 nm, down to the atomic level (approximately 0.2 nm) (Lanone and Boczkowski 2006). When only one dimension is nanometric, these materials can be referred to be a layer (such as with graphene), when they have bidimentional nanometric structure, they can be referred to nanotubes or nanofibers (with the ratio between the longest diameter and the shortest perpendicular greater than 3:1) and finally when all three dimensions are at the nanometric scale, they are referred to be nanoparticles.

These nanomaterials possess unique optical, magnetic, electronic, mechanical and chemical properties and therefore can serve as model systems for providing fundamental understanding of structure-property correlation at the nanoscale level and guide the creation of new structures, systems, devices with novel properties (Wang, Liu et al. 2009) and core frameworks for their area of applications (Gonsalves, Halberstadt et al. 2007).

1.2 Nanobiotechnology

Nanotechnology is unique in that it is not just limited to one specific area, but it includes a vast variety of disciplines ranging from basic material science to personal care

applications (Park 2007). One of the important areas of nanotechnology is "Nanomedicine," or "Nanobiotechnology," which refers to highly specific medical intervention at the molecular and biological scale for diagnosis, prevention and treatment of diseases.

In other words the development of nanotechnology is penetrating biology and medicine at a remarkable speed (Roco 2003). Nanobiotechnology is poised to provide new tools to measure and understand Biosystems (Ishijima and Yanagida 2001; Dubertret, Skourides et al. 2002), bring insights to challenges in biotechnology and biomedicine (Curtis and Wilkinson 2001; Bogunia-Kubik and Sugisaka 2002), and offer fundamental components for advanced biomaterials (Seeman and Belcher 2002; Whitesides and Boncheva 2002). Therefore the use of nanomaterials for biomedical and biotechnological applications is an area of research that holds great promise and intense interest (Martin and Kohli 2003).

1.3 Types of nanomaterials

Depending upon their source, nano materials can be classified into three main types:

- Natural Nanomaterials: Materials with a structure between approximately 1 nm and 100 nm produced as a result of natural processes. Particles arising from volcanic emissions, sea spray, and atmospheric gas-to-particle conversion would be considered natural nanomaterials.

- Incidental Nanomaterials: Materials with a structure between approximately 1 nm and 100 nm that are produced as a by-product of a process. For instance, welding fume and diesel emission particulates would be considered incidental nanomaterials.

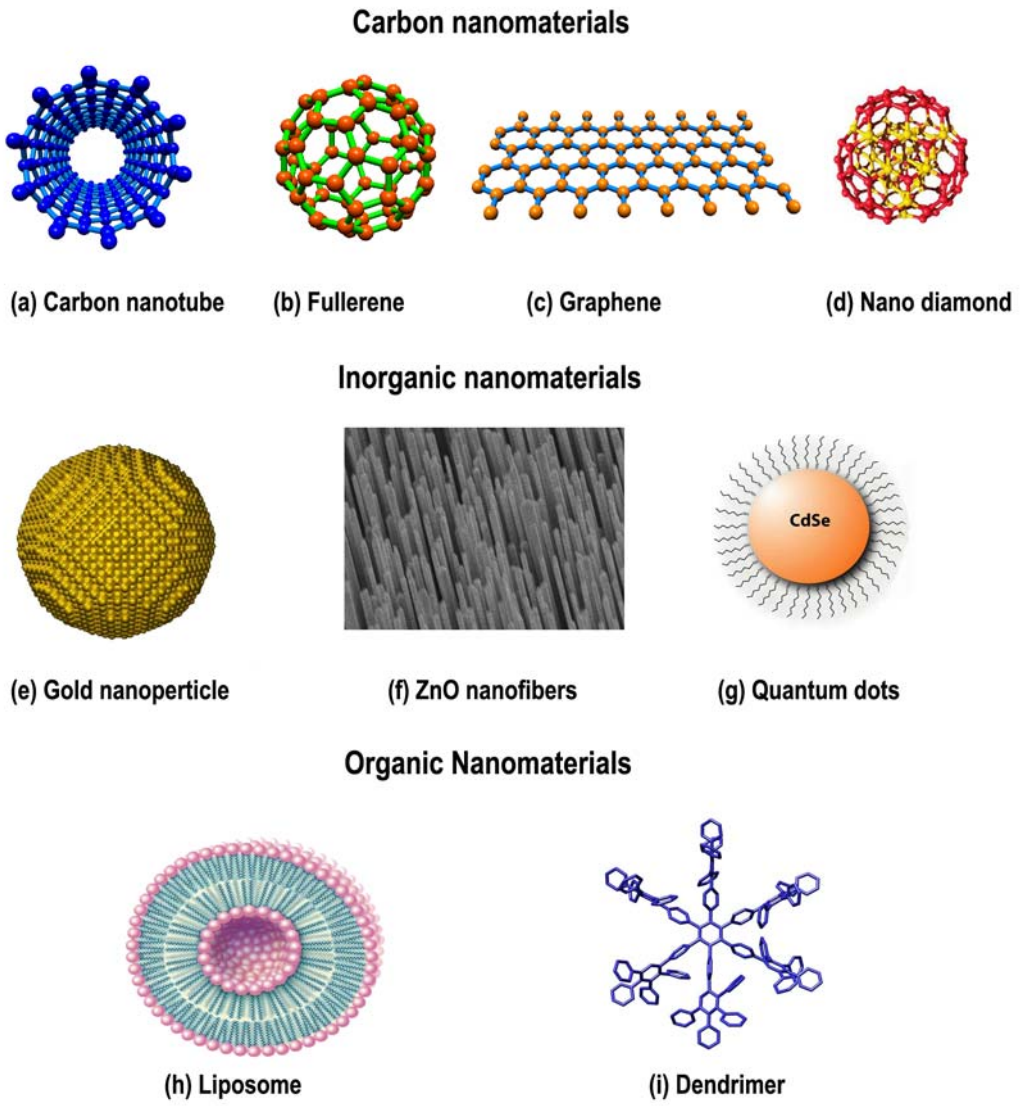

Figure 1.1: Types of engineered nanomaterial. Images of Carbon nanotube, Fullerene and Graphene are made in Nanotube modeller. Nanodiamond (http://abba.com.tw/html/Eng/index.html), Gold nanoparticle (http://www.nd.edu/~gezelter/Research/MetallicNanoparticles.html), Liposome and Dendrimer (Wikipedia), Quantum dot (http://www.phys.uu.nl/~koole/).

- Engineered Nanomaterials: Materials intentionally manufactured as engineered structure between approximately 1 nm and 100 nm. There are many types of intentionally produced nanomaterials, and a variety of others are expected to appear in the future. However currently available engineered nanomaterials can be organized into three types: 1) **Carbon based nanomaterials**, 2) **Inorganic nanomaterials**, 3) **Organic nanomaterials**. These engineered nanomaterials have

pervaded every sphere of human society with their interminable scope for wide area of applications. It is difficult to comprehend all these applications of engineered nanomaterials, as it is beyond the scope of this chapter of the thesis except their special mention with regard to biomedical applications in general, and drug delivery in more detail.

1.4 Carbon nanomaterials

Nanostructured carbons or carbon nanomaterials are mostly composed of carbon in the form of carbon nanotubes, spherical or ellipsoidal fullerenes, graphene/graphite polyhedral crystals and nano-diamonds. Recently they have also been obtained in form of cones, fibers, scrolls and whiskers.

1.4.1 Carbon Nanotubes

Carbon nanotubes (CNTs; also known as Bucky tubes), not to be confused with Carbon Fibers, are allotropes of carbon with a cylindrical nanostructure (**Figure 1.1 a**). Although discovered in as early as 1952, the first reported observation of carbon nanotubes was by Iijima in 1991 for multi-wall nanotubes. It took, however, less than two years before single wall carbon nanotubes were discovered experimentally by Iijima at the NEC Research Laboratory in Japan and by Bethune at the IBM Almaden Laboratory in California. These experimental discoveries and the theoretical work, which predicted many remarkable properties for carbon nanotubes, launched this field and propelled it forward.

Carbon nanotubes exhibit many unique intrinsic physical and chemical properties (discussed in detail in **Chapter 3**) and therefore they have been intensively explored for biological and biomedical applications in the past few years. The recent expansion and

availability of chemical modification and bio-functionalization methods have made it possible to generate a new class of bioactive carbon nanotubes which can be conjugated with proteins, carbohydrates, or nucleic acids. The modification of carbon nanotubes (CNTs) on a molecular level using biological molecules is essentially an example of the 'bottom-up' fabrication principle of bionanotechnology (Yang, Thordarson et al. 2007). The availability of these modified CNTs constructs opens up an entire new and exciting research direction in the field of chemical biology, finally aiming to target and to alter the cell's behavior at the subcellular or molecular level.

Within the realm of biotechnology, CNTs have been utilized as platforms for ultrasensitive recognition of antibodies (Chen, Bangsaruntip et al. 2003), as nucleic acids sequencers (Wang, Liu et al. 2003), as bioseperators, biocatalysts (Mitchell, Lee et al. 2002), and ion channel blockers (Park, Chhowalla et al. 2003) for facilitating biochemical reactions and biological processes. As an emerging trend of utilizing nanomaterials for novel and alternative diagnostics and therapeutics in nanomedicine, CNTs have been utilized as scaffolds for neuronal and ligamentous tissue growth for regenerative interventions of the central nervous system and orthopedic sites (Hu, Ni et al. 2004), substrates for detecting antibodies associated with human autoimmune diseases with high specificity (Wang, Liu et al. 2004), and carriers of contrast agent aquated Gd^{3+}-ion clusters for enhanced magnetic resonance imaging (Sitharaman, Kissell et al. 2005).

In addition to the above mentioned biomedical applications, CNTs have shown intriguing properties as drug delivery systems. More precisely, the advantage of incorporating multiple functional groups and chains at their surface (which is critical to their behaviour in biological systems (Liu, Tabakman et al. 2009) which improves their water solubility (Hudson, Casavant et al. 2004)) has stimulated further investigation in

this regard. It has been reported that properly functionalized CNTs are able to enter cells without toxicity, shuttling various bio-molecular cargoes into cells (Bianco, Kostarelos et al. 2005; Kam and Dai 2005; Singh, Pantarotto et al. 2005). Another advantage of CNTs with regard to drug delivery aspect is that they have unique 1D structure (sometime also mentioned as pseudo one dimensional structure) with tunable length and thereby provide an ideal platform to investigate size and shape effects *in vivo*. Additionally, unlike conventional organic drug carriers, the intrinsic physical properties of SWNTs, including resonance Raman scattering, photoluminescence, and strong NIR optical absorption can provide valuable means of tracking, detecting and imaging. Lastly they are composed purely of carbon, while many inorganic nanomaterials (e.g. quantum dots) are composed of relatively more hazardous elements, such as heavy metals. Taken all these properties together, CNTs may serve as a unique platform for potential multimodality cancer therapy and imaging.

Further biomedical applications and biocompatibility of CNTs have been discussed in **Chapter 3** and **Chapter 4**.

1.4.2 Fullerenes

Fullerenes (of which the most common form is called Buckminsterfullerene or C_{60}) are truncated icosahedrons (**Figure 1.1b**) containing 60 carbon atoms with C_5-C_5 single bonds forming pentagons and C_5-C_6 double bonds forming hexagons (Kroto, Heath et al. 1985). Their diameter is extremely small (about 0.7 nm) and these nanoscale dimensions facilitate passive targeting and enhance their accumulation at tumor sites by entering through leaky vasculature present in endothelial cells of the affected areas. However their lack of water solubility and quick tendency to aggregate in aqueous media confer them with unfavorable characteristics for biological applications (Ruoff, Tse et al. 1993).

Fortunately, such boundary has been defeated through their chemical functionalization leading to excellent solubility in polar solvents (Da Ros and Prato 1999), thereby opening the doors to several biomedical applications including drug-delivery, reactive oxygen species (ROS) quenching, and magnetic resonance imaging (MRI) resolution.

Broad use of fullerenes and their analogues in biomedical fields have been documented over the last few decades (Murakami and Tsuchida 2008). Fullerenes have been employed as contrast agents for MRI (Okumura, Mikawa et al. 2002; Bolskar, Benedetto et al. 2003; Toth, Bolskar et al. 2005), sensitizers for photodynamic therapy (Tabata, Murakami et al. 1997; Rancan, Helmreich et al. 2005), and also for their intrinsic activity as bioactive systems, to be applied as anti-human immunodeficiency virus agents (Bosi, Da Ros et al. 2003; Marchesan, Da Ros et al. 2005; Mashino, Shimotohno et al. 2005), antioxidants (Gharbi, Pressac et al. 2005; Wang, Chen et al. 2006), anti-bacterial agents (Mashino, Nishikawa et al. 2003), and bone-disorder molecules (Gonzalez, Wilson et al. 2002).

Water soluble functionalized fullerenes have been demonstrated to be effective at reducing intracellular reactive oxygen species (ROS) production, with a potency inversely correlated with the size of the nanoparticles (Yin, Lao et al. 2009). More precisely, larger nanoparticles provided less reactive sites for the ROS, thereby decreasing the efficiency of scavenging reactive species and influencing the distribution of nanoparticles in cells and tissues. In another study fullerenes chemically functionalized with paclitaxel by a cleavable ester bond have been shown to deliver paclitaxel for its anticancer activity over a period of 4 hour by cleavage of the ester linkages (Zakharian, Seryshev et al. 2005). Moreover, with the purpose of a better targeting of the drug towards the lung, the C_{60}-

paclitaxel conjugates were further embedded in liposomes through the use of the hydrophobic portion of C_{60}, while maintaining their anticancer activities.

Similarly, paclitaxel-embedded buckysomes (PEBs), i.e. spherical nanostructures of about 100-200 nm, consisting of an amphiphilic fullerene embedding the anti-cancer drug paclitaxel inside its hydrophobic pockets (Partha, Mitchell et al. 2008), has been demonstrated to uptake and subsequently deliver paclitaxel to a higher extent than Abraxane®, which is a FDA-approved drug for treating diseases including metastatic breast cancer. In addition, the incorporation of the drug does not require non-aqueous solvents, which are often responsible for patient discomfort and unwanted side effects (Nakamura and Isobe 2003) and it helps in reduction of infusion times, increase in tumor uptake, and therefore greater anti-cancer efficacy.

1.4.3 Graphite and its derivatives

Graphite is the most stable form of carbon having a layered and planar structure. In each layer, the carbon atoms are arranged in a hexagonal lattice with separation of 1.4 angstroms, and the distance between planes is about 3.4 angstroms. All the atoms that lie in a plane are strongly connected with the surrounding carbons, but they are only weakly linked to the graphite sheets above and below; such week interaction is also responsible for the high softness and the lubricant properties of this mineral. Yet when these sheets are rolled up into tubular structures (such as in carbon nanotubes), the strength of the bonds becomes apparent. In the same way to carbon nanoparticles, and differently from diamond, graphite is an electrical conductor, and thus it can be used, for instance, in the production of advanced electronics, membranes, and composites.

Although graphene (**Figure 1.1 c**) (a novel one-atom-thick two-dimensional graphitic carbon system) has been extensively studied with regard to its application for

nanoelectronics (Geim and Novoselov 2007; Li, Muller et al. 2008; Li, Wang et al. 2008), sensors and nanocomposites (Stankovich, Dikin et al. 2006; Dikin, Stankovich et al. 2007; Watcharotone, Dikin et al. 2007), the biological use of graphene and graphene oxide (GO) represents a subject still poorly explored. This is mainly due to previous surface modifications, required in order to render this material suitable for biomedical applications: in fact GO and its derivatives usually form stable suspensions in water, but they generally aggregate in salt or other biological solutions (Li, Muller et al. 2008). In addition, it is necessary to achieve proper size control or size separation on various length scales to select uniform batches of graphene sheets. So far, very little is known about the physicochemical properties of graphite and derivatives when they reach nanometric dimensions.

Recently graphite in form of nanographene sheets (NGS) has been investigated for potential biomedical applications. One such study involving ultra-small nanographene oxide (NGO) showed increased water dispersion when covalently grafted with polyethylene glycol (PEG) chains (Sun, Liu et al. 2008). Interestingly, the NGO sheets displayed photoluminescence from visible to the near-infrared (NIR) range providing knowledge for its possible application in cellular imaging. Similarly the aromatic anticancer drug doxorubicin (DOX) was loaded to NGO conjugated with specific antibody, via simple physical adsorption. The obtained complex was subsequently targeted into cancer cells. Compared to other carbon-based materials (e.g. carbon nanotubes) used for drug adsorption through π-stacking (Liu, Sun et al. 2007), NGO demonstrated to be advantageous both in terms of costs and ready scalability. Drug release from NGO-PEG sheets was achieved under a more acidic environment (attributable to an increased hydrophilicity and solubility of DOX at this pH), thus mimicking both the extracellular tissues of tumors and the intracellular micro-

environment of lysosomes and endosomes. More precisely, this study demonstrated the potential of selective killing of cancer cells using NGO-PEG-antibody/drug conjugates *in vitro*. In a similar experiment PEGylated NGS was applied for *in vivo* photothermal therapy achieving ultraefficient tumor ablation after its intravenous administration and low power NIR laser irradiation on the tumor (Yang, Zhang et al. 2010), suggesting promising applications of graphene materials in biological and medical areas.

1.4.4 Nanodiamonds

Diamond nanoparticles or nano diamonds (**Figure 1.1d**) originate from detonation of explosive mixture of TNT/RDX. These diamond nanoparticles of 5 nm size are often also called as detonation diamond or ultradispersed diamond (UDD). They have attracted attention of many scientists in terms of their potential biomedical applications, due to several interesting properties like 1) an almost spherical aspect ratio an easily functionalizable carbon surface area (Kruger 2006; Kruger, Liang et al. 2006; Yeap, Tan et al. 2008), 2) an intrinsic good biocompatibility (Bąkowicz and Mitura 2002; Schrand, Huang et al. 2007) and 3) a well-defined particle distribution (Ozawa, Inaguma et al. 2007). Recently Nanodiamonds (ND) were coated with doxorubicin hydrochloride through simple physical adsorption (Huang, Pierstorff et al. 2007), in a similar way to that already reported with other carbon based nanomaterials. These drug-coated NDs were further embedded in polymer microfilms, where they demonstrated a constant moderate rate of drug elution over a period of months (Lam, Chen et al. 2008). Although preliminary, these results envisage that NDs are virtually able to carry any biologically relevant agent through an extremely controlled release and stimulate further research in this field. Similarly there have been several other reports on the non-covalent grafting of bioactive molecules onto the surface of nanodiamond particles. These include the

attachment of cytochrome *c*, apoobelin and protein lysozyme (Bondar', Pozdnyakova et al. 2004; Huang and Chang 2004; Yu, Kang et al. 2005; Chung, Perevedentseva et al. 2006; Nguyen, Chang et al. 2007). All the above biomedical applications involve physical adsorption on the surface of nanodiamond, however very little is known about the covalent attachment of biological moieties on diamond particles. There are two methods for surface functionalization of nano diamond particles. One involves oxidation of diamond particles with concentrated mineral acids at elevated temperatures leading to partially carboxylated particles (Liu, Cheng et al. 2007). These have been further coupled to thymidine and later modified with short DNA strain (Ushizawa, Sato et al. 2002). Another method for the surface functionalization involves reduction of surface carbonyl groups on detonation nanodiamonds with borane under mild conditions (Kruger, Liang et al. 2006). The resulting hydroxyl groups could be further modified for example using (3-aminopropyl) trialkoxysilane. This procedure could be applied for the immobilization of bioactive structures including biotin and streptavidin (Krueger, Stegk et al. 2008).

These covalent functionalization procedures, besides providing an increased stability, have also opened several opportunities for biological and medical applications. One of them is diamond molecule conjugates, to be employed as biocompatible fluorescent labels (due to their inherent fluorescence) as well as for drug delivery. Another interesting aspect is the preparation of ultracrystalline diamond (UNCD) based complexes, through the UNCD deposition on silicon surfaces (Huang, Chen et al. 2009), which let the incorporation of both therapeutically active collagen networks and the anti-inflammatory agent dexamethasone (DEX). In this way, it was demonstrated that a suitable interface between soft and hard materials is possible, by adopting a novel hybrid technology based on nanodiamond film bio-functionalization toward advanced translational applications. In fact, the incorporation of DEX at the interface between

artificial and biological materials could avoid potentially damaging effects on an implanted device, as it is known that inflammatory cells tend to surround foreign material, forming a fibrous capsule that dissociates the device with the body, a phenomenon known as biofouling (Gifford et al., 2005). On the contrary, this study confirmed the relevance of the UNCD-collagen hybrid as an active substrate for the regulation of cellular activity toward promising applications in nanomedicine.

1.5 Inorganic nanomaterials

Inorganic nanomaterials (INMs) and nanoparticles (NPs) are important in our lives because of their biomedical application in form of drugs, imaging agents, and antiseptics. Among the most promising INMs being developed are metal NPs or silica NPs. The Metal NPs can be further classified in to 1) pure metal NPs like gold and silver NPs, 2) metal oxides like Zinc oxide and iron oxide and 3) mixed metal NPs like quantum dots. INMs are basically obtained in the form of nanocrystalls, nanowires, nanospheres, nanoribbons, nanorods or nanofibers.

Gold nanoparticles (**Figure 1.1e**) or AuNPs are being studied recently for conjugation with biological and biocompatible ligands, plasmon-based labelling and imaging, optical and electrochemical sensing, diagnostics, therapy (drug vectorization, and DNA and gene delivery) for various diseases, in particular cancer therapy (Bawarski, Chidlowsky et al. 2008; Liong, Lu et al. 2008). Scientists distinguished between cancer and noncancer cells from the strong scattering images of the AuNPs conjugated to antibodies that bind only to the cancer cells (Louit, Asahi et al. 2009). AuNPs-enhanced optical coherence tomography showed the potential for molecular imaging and improved detection of diseases (Krumov, Perner-Nochta et al. 2009). Metallic nanoparticles like silver NPs have been shown to exhibit increased chemical activity due to their large

surface to volume ratios and crystallographic surface structure. In the size range of 1–100 nm they seem to have high bactericidal activity against Gram-negative bacteria. But they lose this property in their aggregated form (Morones, Elechiguerra et al. 2005).

Similarly Silicon dioxide NPs combined with zinc or silver have also shown antibacterial properties (Jia, Hou et al. 2008). Super paramagnetic iron oxide NPs are currently being studied for their application as MRI contrast agents and also for hyperthermic treatment of tumors (Di Marco, Sadun et al. 2007). Recently American elements (a leading manufacturer of rare earth and advanced material products) launched Z-MITE powders constituting inorganic zinc oxide nano particles (**Figure 1.1f**) with antibacterial, antifungal, anti-corrosion, catalytic and UV filtering properties. The bacteriostatic and fungistatic behaviour of zinc oxide is very well studied and additionally they are non-toxic and are highly compatible with skin, therefore have been approved by FDA along with Titanium dioxide nano particles for use in skin care products such as sunscreens. With regards to this last aspect, zinc oxide nanomaterial seems particularly indicated for the treatment of and/or delivery through the skin. Therefore, transdermal delivery of vaccine from solid-supported zinc oxide nanorods has been explored in **Chapter 5.**

Quantum dot (QD) (**Figure 1.1g**) nanocrystals are one of the very important members belonging to INMs family currently getting a lot of attention with regard to their biomedical applications. QDs are inorganic semiconductor nanocrystals having typical diameters between 2 and 8 nm. They are generally composed of atoms from groups II and VI elements (e.g., CdSe and CdTe) or groups III and V elements [e.g., indium phosphide (InP) and indium arsenide (InAs)] of the periodic table. In general, QDs consist of a semiconductor core, overcoated by a shell to improve optical properties, and a cap

allowing improved solubility in aqueous buffers. They have emerged as a new class of fluorescent labels with better brightness, resistance against photobleaching, and multicolour fluorescence emission. Therefore they are recently being systematically tried in virtually all fluorescence-based assays and in vivo imaging procedures (Smith, Gao et al. 2004; Medintz, Uyeda et al. 2005). QDs, in addition to being excellent fluorescent probes, can also be used as photoacoustic and photothermal contrast agents and sensitizers, thereby providing an opportunity for multimodal high-resolution (300 nm) photoacoustic photothermal fluorescent imaging as well as photothermal therapy (Shashkov, Everts et al. 2008).

Inorganic nanomaterials hold great promise in diagnostics, drug and gene delivery, sensing and biosensing, and in vivo imaging under the present scenario. Smartly engineered inorganic NPs can boost drug efficacy and can improve drug targeting to specific areas within the body, therefore making treatment less toxic and invasive (Sekhon and Kamboj 2010; Sekhon and Kamboj 2010).

1.6 Organic nanomaterials

These types of nanomaterials have organic materials such as polymers and lipids as their majority constituents. The two most important members of this nanomaterial family which are very well known in the field of biomedicine and biotechnology are **liposomes** and **dendrimers**.

Liposomes (**Figure 1.1h**) are vesicles made up of a lipid bilayer, resembling tiny cells with a cell membrane but nothing in the core. Although they do not constitute novel nanotechnology, and their sizes ranging from 90 to 150 nm, are slightly bigger than what would qualify as nanotechnology according to conventional definition (i.e., having a dimension of ≤100 nm), however liposome research constitute a significant portion of

what is considered as nanotechnology research in biomedicine today (Kim 2007). Liposomes because of their hollow core can be filled with drugs, and used to deliver certain drugs for cancer and other diseases. Liposomes of certain sizes, typically less than 200 nm, can rapidly enter tumors sites from the blood, but are kept in the bloodstream by the endothelial wall in healthy tissue vasculature. Anti-cancer drugs such as doxorubicin (Doxil), camptothecin and daunorubicin (Daunoxome) are currently being marketed in liposome delivery system. Further advances with liposome in form of stealth liposomes and polymerosome are being investigated to widen their biomedical applications.

Dendrimers (**Figure 1.1i**) are globular nanostructures of 5 nm in diameter with polymer branches that provide vast amount of surface area to which therapeutic agents and targeting molecule could be attached. They can also be specifically engineered to carry molecules encapsulated in their interior void spaces. Size, shape and reactivity of the dendrimers shells are determined by chemical composition of core, interior branching and surface functionalities. These parameters makes them as one of the customizable nanotechnologies commercially available materials (Byrne, Williams et al. 2007). They have been synthesized and characterized as multifunctional dendrimers conjugated with fluorescein isothiocyanate (for imaging), folic acid (for targeting cancer cells overexpressing folate receptors), and paclitaxel (chemotherapeutic drug). AuNPs stabilized inorganic-organic hybrid dendrimers have also been formed to provide new platforms for further modification with various biological ligands for the application of biosensing and targeted cancer therapeutics (Bentzen, House et al. 2005; Lin, Xie et al. 2007). Researchers also have synthesized water-soluble, biocompatible, fluorescent, and stable silver and gold host-guest nanocomposites that exhibited potential to be used as quantifiable cell biomarkers (Chang, Dai et al. 2009).

1.7 Conclusion

All the above nanomaterials are result of explosive growth of nanotechnology over past 30 years. Owing to their size-dependent effects, they exhibit new physical and chemical properties compared to conventional bulky and molecular materials (Bawendi, Steigerwald et al. 1990). Today these nanomaterials can be assembled on, encapsulated within, or integrated both inside and on the surface using different chemistries and techniques to create novel nanosystems or nanodevices. The new opportunities stemming from these novel nanodevices can in fact provide synergistic advantages leading to progress in their biomedical applications.

Chapter 2

Hypothesis and Objectives

2.1 Thesis rationale and hypothesis

Advances in engineering nanomaterials with exquisite size and shape control, elucidation of their unique properties, and demonstration of their broad applications including biomedical applications have made nanotechnology an exciting research area.

1) Carbon nanotubes are at the forefront of these nanomaterials currently being investigated for several applications such as probes for ultrasensitive molecular sensing and diagnostic imaging, agents for photodynamic therapy (PDT) and actuators for drug delivery, triggers for photothermal treatment, and precursors for building solar cells, electronics and light emitting diodes and scaffold for bone and cartilage tissue engineering. Several concerns and ambiguity have emerged regarding the toxicity of these carbon nanotubes from their previous reports related to nanotoxicity. Therefore it is quite imperative to evaluate certain physicochemical and biological parameters to determine their biocompatibility and eventual applicability in relation to specific biomedical applications.

With optimum purity, aspect ratio and functionalization, carbon nanotubes will show improved biocompatibility and solubility and thus can be used for various biomedical and therapeutic applications including tissue engineering and drug delivery.

2) Human mesenchymal stem cells (hMSCs) are critical for numerous ground breaking therapies in the field of regenerative medicine including bone tissue engineering. A myriad of environmental factors including their interaction with soluble growth factors, extracellular matrices (scaffold) and neighbouring cells are crucial for their survival, proliferation and differentiation into specific lineages. One of the main goals of tissue engineering is to control these factors by creating physical and chemical microenvironments designed to guide the ultimate fate of stem cells. A number of

materials with different elasticity, rigidity and texture have been fabricated to mimic the intrinsic characteristics of natural substrates such as muscles, bones and cartilages and recently they have been extensively investigated for this purpose.

Carbon nanotubes are viewed as a class of material with tremendous strength (strongest material on this earth), flexibility and elasticity, ultralight weight and high stability. The density of CNTs is similar to that of graphite, which in turn is much lower than other metal bone replacement materials, including steel and titanium. More importantly they can be modified at their surface with appropriate functional groups to enhance their biocompatibility. Therefore CNTs can be used as a suitable scaffold not only for growth and proliferation of osteoblast, but also for bone regeneration by differential induction of hMSCs, thus mimicking the commonly used biochemical inducers like BMP-2 (human bone morphogenic protein).

3) Increased attention on global health has allowed vaccines to develop and to become a fundamental opportunity for human care. Vaccines represent a valuable modality for immunization against human pathogens and treatment of diseases. Although several systems are currently available in the market, vaccines delivered through skin patches as “needle-free” devices offer remarkable advantages in form of avoiding injection for easy application and lack of painful sensation, efficacy and low toxicity, possibility for a prolonged delivery and increased patient compliance, especially for the young and elderly. However all these factors are not sufficient to guarantee the success of vaccination, owing to the presence of a physiological barrier in form of uppermost layer of the epidermis called stratum corneum, which represents the primary obstacle to the transport of hydrophilic bioactive molecules of high molecular weight.

The aligned, solid supported nanorods made up of ZnO can be functionalized with vaccines and used as a therapeutic skin patch for their transdermal delivery, whereby the vaccines along with nanorods will be able to penetrate across the stratum corneum and will be delivered to the targets in the epidermis.

2.2 Objectives

On the basis of the three main aspects considered as the rationale of this thesis, we propose the following specific objectives:

- To functionalize SWCNTs and MWCNTs with appropriate functional groups to improve their water dispersibility, decrease their tendency to aggregate and simultaneously characterize their biocompatibility and cytotoxicity in terms of evaluation of several parameters such as 1) sidewall functionalization; 2) concentration; 3) degree of dispersibility; 4) length and 5) purity.
- To prepare compact and uniform thin film of PEG functionalized carbon nanotubes having nanometric irregularities as a biocompatible scaffold, which can provide suitable microenvironment for growth, proliferation and specific differentiation of hMSCs into osteogenic lineages, without the need of any additional biochemical inducer to the osteogenic medium.
- To carry out a preliminary study of transdermal delivery of a vaccine prototype using aligned ZnO nanorods grown successfully on silicon chip as part of a future platform for transdermal delivery of therapeutics including pertussis, tetanus and influenza vaccines.

Chapter 3

Functionalization, characterization and cytotoxicity profiles of carbon nanotubes towards promising biomedical applications

3.1 INTRODUCTION

Carbon-based nanostructures, such as carbon nanotubes (CNTs) represent a fascinating example of nanomaterials that are attracting increasing attention (Lin, Taylor et al. 2004; Bianco, Kostarelos et al. 2005) for several biotechnology and biomedical applications. CNTs embody a recently discovered pseudo-one-dimensional carbon allotrope, with high aspect ratio, wide surface area, and excellent material properties such as excellent electrical and thermal conductivities (Ajayan 1999; Dai 2001; Lu, Gu et al. 2009). Generally they exist as a macro-molecule of carbon atoms, deriving from one or more layers of graphene sheets rolled up in to a cylinder and sealed by hemispherical "caps". Depending on such rolling, CNTs have been divided into three main kinds, namely 'armchair', 'zigzag' and 'chiral' types (Wildoer, Venema et al. 1998), which mainly differ in terms of electric properties (metallic or semiconducting). Despite being light (Collins and Avouris 2000), flexible (Yu, Lourie et al. 2000; Demczyk, Wang et al. 2002), thermally stable(Thostenson, Li et al. 2005) and chemical inert (Ajayan 1999; Niyogi, Hamon et al. 2002), they present a very robust arrangement, which results in a material a hundred times as strong as steel (Chang, Hsu et al. 2010).

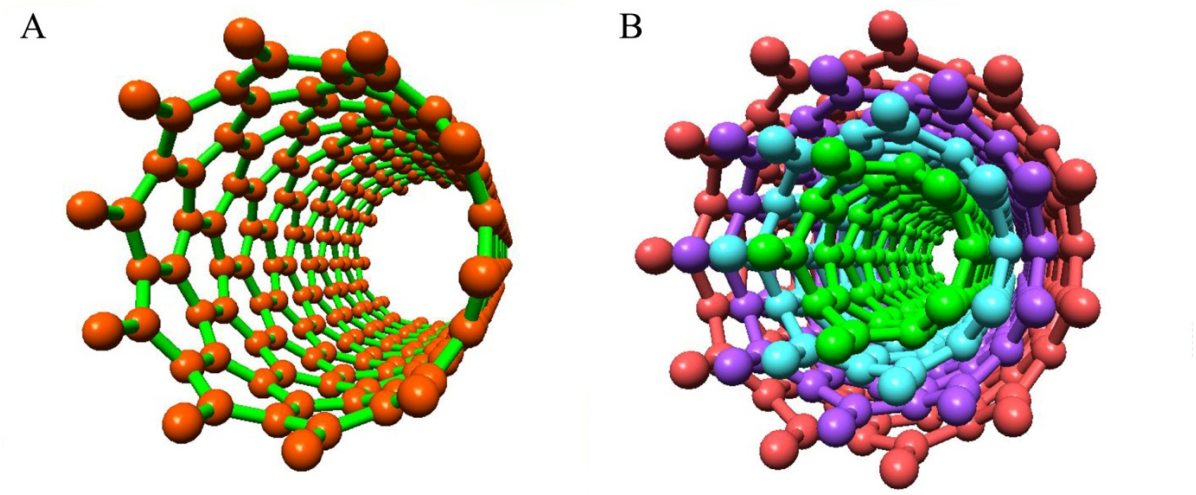

Figure 3.1: A) Single-walled carbon nanotubes (SWCNTs), B) Multi-walled carbon nanotubes (MWCNTs). Images have been generated from the program ***Nanaotube Modeller*** (http://jcrystal.com/products/wincnt/).

On the basis of the number of concentrical layers inside the tubes, there are two main types of CNTs (**Figure 3.1**): (i) the single-walled carbon nanotubes (SWCNTs), which are made up of a single graphene layer wrapped into a cylindrical structure, and (ii) multi-walled carbon nanotubes (MWCNTs), with a central tube of nanometric diameter, surrounded by several graphitic layers spaced by a distance of about 0.34 nm (Iijima 1991). Most commonly, the diameter range of CNTs varies between 0.4 and 2 nm for SWCNTs and between 1.4 and 100 nm for MWCNTs (Haddon 2002), while the length for both can be as long as several microns. Typically, SWCNTs exist as bundles of 10–30 nm in diameter because of strong van der Waals interactions, resulting in ropes (Dai 2002; Pastorin, Kostarelos et al. 2005), which are tangled with one another.

There are three main methods to synthesize CNTs, which include arc-discharge, laser ablation and chemical vapor deposition (Dai 2001). The first two employ solid-state carbon precursors to provide carbon sources needed for nanotube growth and involve carbon vaporization at high temperatures (thousands of degrees Celsius). These methods are well established in producing high-quality and nearly perfect nanotubes structures, despite large amounts of by-products (amorphous carbon, graphitic particles and catalyst remains) associated with them. Chemical vapour deposition (CVD) utilizes hydrocarbons gases as sources for carbon atoms and metal catalysts particles as "seeds" for nanotubes growth that takes place at relatively lower temperatures (500-1000ºC). A subcategory of this CVD synthesis procedure known as High-Pressure CO Conversion process (HiPCO) being widely used because it can be easily scaled-up to industrial production affording long length, controllable diameter and acceptable CNT purity (Nikolaev, Bronikowski et al. 1999). However, as-prepared nanotubes typically contain up to 30% of metal catalyst (mainly iron and nickel particles) and some amorphous carbon and nanoparticles residual of the production procedure (Klumpp, Kostarelos et al. 2006). Therefore, further

purification is always needed before using this material. One of the most commonly employed techniques for the purification and eventual solubilisation of CNTs is the tubes' oxidation using strongly acidic treatments, which permit removal of a large part of the metallic impurities. Nevertheless, this methodology is not devoid of consequences for the tubes. Indeed, strong acidic conditions cut the tubes in shorter pieces and generate carboxylate functions at the tips and around the sidewalls where the curvatures of the tubes present a higher strain. To avoid this, alternative methods have been explored including gel permeation chromatography (GPC), chromatographic separation, centrifugation, filtration or other chemical derivatization techniques (Niyogi, Hu et al. 2001; Zhao, Hu et al. 2001; Georgakilas, Voulgaris et al. 2002; Arnold, Stupp et al. 2005; Dyke, Stewart et al. 2005). These purification techniques increase also the nanotubes' solubility, making them easier to separate from the insoluble impurities.

3.1.1 Limitations of pristine nanotubes

Production of structurally and chemically reproducible batches of CNTs with identical characteristics, high quality control and minimal impurities is still a challenge to the pharmaceutical and clinical application of these nanomaterials. In addition to that, severe limitations persist as the pristine (as prepared, non-functionalised) CNTs are inherently hydrophobic, therefore the main obstacle in the utilisation of CNTs in biology and medicinal chemistry is their lack of solubility in most solvents compatible with the biological milieu (aqueous based). Several attempts have been made to overcome this problem, mainly focusing on modification of the surface of CNTs (functionalization) with different molecules and chains, which will render them more hydrophilic. Through such modifications, the water solubility of CNTs is improved and their biocompatibility profile remarkably enhanced (Lacerda, Bianco et al. 2006).

Simultaneously, CNTs' toxicological profile is not yet well elucidated, since research has shown contradictory results. Cui *et al*. (2005) (Cui, Tian et al. 2005) found that pristine SWCNTs inhibited HEK293 cell proliferation, decreased cell adhesive ability, in a dose and time dependent manner. On the contrary, Davoren *et al*. (2007) (Davoren, Herzog et al. 2007) reported that exposure of A549 cells to a wide dose range of pristine SWCNTs (1.56-800 μg/ml) for 24 hour displayed very low toxicity. The disparity could be attributed to different cell viability methods, cell lines and sources of CNTs. CNTs might also reveal unusual toxicological properties because their shape belongs to both fibres and nanoparticles (Donaldson and Tran 2002; Bernstein, Castranova et al. 2005; Poland, Duffin et al. 2008), and they often contain metallic residues such as iron even after their purification (Takagi, Hirose et al. 2008).

A comparative study on the cytoxicity of pristine *versus* oxidized MWCNTs onto human Jurkat T leukemia cells has shown that the latter were more toxic (Bottini, Bruckner et al. 2006). CNTs tend to aggregate in ropes, decreasing their aqueous solubility and increasing the cytotoxicity. The type of nanotubes used in such studies is therefore extremely important. Another report on cytotoxicity induced by different carbon allotropes in alveolar macrophages showed that SWCNTs provoked the highest toxic effect, followed by MWCNTs, quartz and fullerenes (Jia, Wang et al. 2005). A study on the effect of CNTs' length on cytotoxicity showed that the inflammatory response was higher for CNTs of 825 nm in comparison to those of 220 nm (Sato, Yokoyama et al. 2005). CNTs may lead to toxicological side-effects in case of biological and biomedical applications, however up to this date this seems mainly the case for non-fuctionalized, insoluble material. Finally, it has been previously shown that cytotoxicity of water-soluble fullerene derivatives is improved as the degree of surface modification is

increased (Sayes, Liang et al. 2006). Thus, it is reasonable to anticipate that functionalized and water-soluble nanotubes will be less cytotoxic.

3.1.2 Functionalization of Carbon nanotubes to improve solubility

Although the dispersion of CNTs in a specific medium is strongly dependent on (a) the method of their production, (b) the tubes' concentration and (c) their tendency to aggregate into bundles and/or precipitate, there are a few techniques to improve their dispersibility, such as sonication and functionalization of CNTs. Sonication improves the dispersion of nanotubes in water by shortening the tubes through the application of ultrasonic energy. Shorter tubes are proposed to entangle less easily and they are also less likely to form aggregates (Hilding, Grulke et al. 2003). However, prolonged sonication can decrease the aspect ratio of CNTs, which is a desirable physicochemical property of CNTs (Hilding, Grulke et al. 2003). In view of these limitations, the functionalization method seems more promising. There are at least two main strategies to increase their solubility. One procedure consists of the non-covalent functionalization of CNTs with surfactants, nucleic acids, peptides, polymers and oligomers (Islam, Rojas et al. 2003; Moore, Strano et al. 2003; Richard 2003; Wang, Humphreys et al. 2003; Zheng, Jagota et al. 2003; Shvartzman-Cohen, Nativ-Roth et al. 2004; Sinani, Gheith et al. 2005; Noguchi, Ishibashi et al. 2006; Meuer, Braun et al. 2009; Liu, Chipot et al. 2010). The second procedure is based on CNTs' covalent functionalization with dispersing agents (Hirsch 2002; Tagmatarchis and Prato 2004).

3.1.2.1 Non-covalent functionalization of carbon nanotubes

This methodology shows the advantage to preserve the aromatic structure of the nanotubes and thus their electronic characteristics. Hydrophobic interactions and favourable π–π interactions (or ''π–π stacking'') in water between absorbates and carbon

nanotubes (sometimes with electrostatic interactions between ionic adsorbents) and supramolecular inclusions are the most frequently suggested mechanisms for non-covalent stabilization (Lin, Taylor et al. 2004). Nowadays, three classes of molecules are mainly used for non-covalent modification of CNTs: (a) surfactants (b) organic polymers (c) biopolymers (nucleic acids and peptides) (**Table 3.1**).

Type of CNT	Type of Solubilizing molecules	References	Solubility (mg/mL)
SWCNTs	1-pyrenebutanoic succinimidyl ester	(Chen, Zhang et al. 2001)	0.7 (H_2O)
SWCNTs	Poly(m-phenylenevinylene) ester	(Star, Stoddart et al. 2001)	0.5 (DMF or $CHCl_3$)
SWCNTs	α-Helical amphipathic peptide	(Dieckmann, Dalton et al. 2003)	0.7 (H_2O)
SWCNTs	Nucleic acids	(Zheng, Jagota et al. 2003)	-
SWCNTs	Surfactants: Tween 20	(Chen, Bangsaruntip et al. 2003)	0.05 (H_2O)
	Triton X100	(Chen, Bangsaruntip et al. 2003)	≤0.5 (H_2O)
	SDS	(Moore, Strano et al. 2003)	≤0.1 (H_2O)
SWCNTs	Surfactants+Polymer(PEG)	(Bandow, Rao et al. 1997; Shim, Kam et al. 2002)	-
	Starch	(Star, Steuerman et al. 2002)	0.5 (H_2O)

Table 3 1: Methods for CNTs solubilization and dispersion based on non-covalent functionalization (Pastorin, Kostarelos et al. 2005).

3.1.2.1.1 Surfactants

A series of anionic, cationic and non-ionic surfactants have been already proposed to disperse nanotubes. Sodium dodecyl sulphate (SDS) and Triton X-100 were used to

obtain CNT suspensions up to 0.1 and 0.5 mg/mL, respectively (Islam, Rojas et al. 2003). However, the stability of this suspension was no longer than 1 week. A better result was obtained by using sodium dodecylbenzene sulfonate (SDBS), which was able to provide stability over one month reaching 10 mg/mL concentration of the suspension (Moore, Strano et al. 2003). The combination of π–π interactions of aromatic moieties between CNTs and SDBS and the long lipid chains of the SDBS increase the stability of the tubes. Atomic force microscopy (AFM) and transmission electron microscopy (TEM) studies of SDBS/CNT dispersions showed that CNTs were mainly present as individual tubes uniformly covered by the surfactant (Moore, Strano et al. 2003). The types of amphiphilic molecules with long lipid chains have shown to be able to form a half-cylinder perpendicular or tilted around the tubes in a micelle-like arrangement (Richard 2003). Triton-X instead mainly interacts by π-stacking. Another approach for the adsorption/dispersion of CNTs via π interaction resides on the use of 1-pyrenebutanoic acid activated as succinimidyl ester, which promptly reacts with the amino groups present in the proteins like ferritin or streptavidin(Chen, Zhang et al. 2001). The solubility of CNTs was between 0.1 and 0.7 mg/mL, which is rather low but acceptable for biological use. Although surfactants may be efficient in the solubilisation of CNTs, they are known to permeabilize plasma membranes and they seem responsible for intrinsic toxicity (Liwarska-Bizukojc, Miksch et al. 2005; Dong, Joseph et al. 2008). Therefore, the implications stemming from use of surfactants interacting with biological systems can limit the possible biomedical applications of such surfactant-stabilized CNT complexes.

3.1.2.1.2 Polymers

Polymers are widely used for example as molecular carriers for drug delivery (Minko 2005). In the solubilisation of CNTs, they represent a good alternative to

surfactants although they do not have better dispersion efficiency (Moore, Strano et al. 2003). The mechanism of dispersion is based in this case on wrapping of the polymer around the tubes. Star *et al.* (Star, Stoddart et al. 2001) have used for example a substituted poly(metaphenylenevinylene) to suspend SWCNTs in organic solvents. The driving force of the tubes' dispersion is likely to be the steric repulsion of the polymer. More precisely, once the polymer is attached to the surface of the nanotubes, it offers a sufficient repulsive potential among the tubes, thus stabilizing the dispersion (Shvartzman-Cohen, Nativ-Roth et al. 2004). In the case of non-ionic polymers, based on poly(oxyehtylene) co-polymers, the efficiency of the dispersion is instead due to their hydrophilic counterpart. For particularly high molecular weight polymers, the suspendibility is enhanced as the steric stabilization is increased by a wider coverage of the surface (Moore, Strano et al. 2003). In another approach, using charge repulsion, CNTs were dispersed by using cationic copolymers (Sinani, Gheith et al. 2005). The nanotubes were covered by the hydrophobic backbone of the polymer, while the positive tetraalkylammonium groups were exposed at the surface to display water solubility. In another instance Poly (vinylpyrrolidone) was conjugated with fluorescent dyes and the resulting fluorescent polymers were used to suspend CNT in 1% SDS to form supramolecular complexes, which were found to have potential applications as new molecular probes. These types of fluorescent polymers have also been employed to study the interaction with mammalian cells (Didenko, Moore et al. 2005).

3.1.2.1.3 Biopolymers

The solubilisation of CNTs with biological components is certainly more appropriate towards integration of this new type of material with living systems. Self-assembly processes similar to π–π interactions (typical of double-stranded DNA) can be

for example exploited to disperse the nanotubes. Nucleic acids are certainly ideal candidates to form supramolecular complexes based on π-stacking between the aromatic bases and the CNT surface (Klumpp, Kostarelos et al. 2006). Indeed, Zheng *et al.* (Zheng, Jagota et al. 2003; Zheng, Jagota et al. 2003) have described an easy way to solubilize carbon nanotubes by simple sonication in the presence of a single-stranded (ss)DNA. A molecular modelling study was performed to explain the mechanism underneath DNA wrapping and subsequent CNT debundling. The DNA–nanotube complexes displayed solubility in the range of mg/mL, and their good stability enabled the purification using ion-exchange chromatography. Amphiphilic peptides belong to another class of biopolymers that efficiently disperse CNTs (Dieckmann, Dalton et al. 2003). The presence of amino acids like tryptophan, phenylalanine, tyrosine and histidine in the peptide sequence plays a key role on the solubilisation process in water. These peptides could be selected from phage-display peptide libraries (Wang, Humphreys et al. 2003) or by design (Dieckmann, Dalton et al. 2003; Dalton, Ortiz-Acevedo et al. 2004; Zorbas, Ortiz-Acevedo et al. 2004). The design of highly specific peptides able to wrap around the nanotubes represents an interesting way to assure solubility and may even provide a useful tool for size separation. More recently, cyclic peptides were also proven to have similar capabilities (Ortiz-Acevedo, Xie et al. 2005).

In addition, CNTs could have open ends and functionalized surfaces, which would improve their interaction with molecular components abundant in living organisms, including carbohydrates, DNA and proteins. Starch, for example, is a natural carbohydrate that wraps itself helically around small molecules and can transport CNTs into aqueous solutions (Star, Steuerman et al. 2002).

Another interesting aspect is that a wide variety of proteins can bind the CNTs surface via nonspecific adsorption, especially if they can be inserted into the tubular space of open-ended MWCNTs (Davis, Green et al. 1998). The mechanism responsible for such binding seems to be more complicated than the well-known hydrophobic interaction. It was observed that the adsorption of proteins on CNTs is insensitive to their isoelectric point, and strongly influenced by the affinity of nanotubes to amino groups (Kong and Dai 2001). In the same context, peptide-nanotubes represent a useful model for protein-nanotube interactions, suggesting that aromatic, flexible and eventually amphiphilic peptides contribute to the observed affinity.

Carbon nanotubes also have been modified with mucin mimics (glycosylated polymers designed to mimic natural cell-surface mucins) making them water soluble, resistant to non-specific binding of protein and linking specific molecules via receptor-ligand interactions (Chen, Zhang et al. 2001).

3.1.2.2 Covalent functionalization

The alternative way to render CNTs soluble into a wide range of solvents is the modification of their sidewalls and tips by covalent functionalization (Hirsch 2002; Dyke and Tour 2004; Tagmatarchis and Prato 2004; Balasubramanian and Burghard 2005). The aqueous solubility can be assured for example by a covalent attachment of hydrophilic moieties. The chemical functionalization of CNTs is based on two main approaches (**Table 3.2**): (i) esterification or amidation of oxidized tubes (Hamon, Chen et al. 1999; Ziegler, Gu et al. 2005) and (ii) sidewall covalent attachment of functional groups (Holzinger, Vostrowsky et al. 2001; Tagmatarchis, Georgakilas et al. 2002; Holzinger, Abraham et al. 2003; Stevens, Huang et al. 2003; Strano, Dyke et al. 2003; Dyke and

Tour 2004; Heald, Wildgoose et al. 2004; Hudson, Casavant et al. 2004; Liang, Sadana et al. 2004; Tagmatarchis and Prato 2004; Dyke, Stewart et al. 2005).

Type of CNTs	Type of Solubilizing molecules	Reference	Solubility (mg/mL)
SWCNTs/ MWCNTs	Oxidation process (HNO_3/H_2SO_4)	(Hamon, Chen et al. 1999)	1.77 (H_2O)
SWCNTs/ MWCNTs	Nitrenes	(Holzinger, Vostrowsky et al. 2001; Holzinger, Abraham et al. 2003)	1.2 (DMSO or TCE)
	Carbenes	(Holzinger, Vostrowsky et al. 2001)	- (DMSO)
	Radicals	(Holzinger, Vostrowsky et al. 2001)	-(TCE)
SWCNTs	Solvent-free functionalization	(Dyke and Tour 2004)	0.8-0.7 (DMF, THF, $CHCl_3$)
	Fluorination/Amination	(Stevens, Huang et al. 2003)	-(Ethanol)
	Reduction of diazonium salts	(Strano, Dyke et al. 2003)	-(H_2O)
	Electrophilic addition	(Tagmatarchis, Georgakilas et al. 2002)	- (Toluene, $CHCl_3$, CH_2Cl_2)
SWCNTs/ MWCNTs	1,3-Dipolar cycloaddition	(Georgakilas, Kordatos et al. 2002)	20 (H_2O)

Table 3 2: Methods for CNTs solubilization and dispersion based on covalent functionalization (Pastorin, Kostarelos et al. 2005).

Concerning the first approach, the oxidation process is conducted under strong acidic conditions. This treatment provokes the opening of CNTs endcaps, generating carboxylic groups suitable for further derivatization (Hamon, Chen et al. 1999). On the other hand, the direct sidewall functionalization of CNTs with organic groups is possible by using reactive species such as nitrenes, carbenes and radicals (Holzinger, Vostrowsky et al. 2001). To this end, alkyl azides, dipyridyl imidazolium salts and perfluoroalkyl radicals were employed, respectively, as efficient reagents (Holzinger, Abraham et al.

2003). The high solubility of the resulting adducts can be explained through mutual, electrostatic repulsion of the tubes.

Recently, the sidewall functionalization of SWCNTs and MWCNTs has been developed, through the 1,3-dipolar cycloaddition of azomethine ylides, a reaction successfully applied to fullerenes (Maggini, Scorrano et al. 1993). The easiest way for the preparation of such derivatives consists on the decarboxylation of immonium salts obtained by the reaction of an amino acid with an aldehyde (Georgakilas, Kordatos et al. 2002). In particular, a glycine modified at the N-terminus with an N-Boc-protected-triethylene glycol chain was proposed because of its high solubilizing power after removal of the Boc group. Both SWCNTs and MWCNTs with the free amino function have become extremely soluble in aqueous solvents and ready for further derivatization (Tagmatarchis and Prato 2004; Pastorin, Kostarelos et al. 2005).

3.2 OBJECTIVE

The main aim and objectives of this chapter was to functionalize and characterize CNTs to render them suitable for biomedical applications. To that purpose, we chemically modified both SWCNTs and MWCNTs by introducing solubilising chains, which improved their water solubility and decreased their tendency to aggregate. Simultaneously we systematically evaluated several parameters (e.g. surface/sidewall functionalization, concentration, degree of solubility, length and purity) that are potentially associated with CNTs' cytoxicity.

3.3 MATERIALS

3.3.1 Chemicals

Carbon nanotubes: SWCNTs (containing a certain amount of double-walled nanotubes) with diameters of <2 nm, length of 5-15 μm, and a purity of ≥90% (code L.SWNTs) and MWCNTs with diameters of ≤ 10 nm, length of 1-2 μm, and a purity of ≥95% (code S.MWNTs-10), were purchased from NTP (Shenzhen Nanotech Port Co. Ltd, China). Ultrapure-MWCNTs were kindly provided by Professor Ramaprabhu (Nano-Functional Materials Technology Centre (NFMTC), Indian Institute of Technology, Chennai, India).

All the reagents used in the experiment were purchased from Sigma Aldrich, with the exception of Dimethylsulfoxide (DMSO), Nitric Acid (HNO_3) 65%, and Sulphuric Acid (H_2SO_4) 98 %, which were procured from Merck; HPLC grade Dimethylformamide (DMF) from Fisher Scientific; HPLC grade Tetrahydrofuran (THF) from Reagent Chemical Industry Ltd.; Methanol from Tedia; FMOC-NH-PEG-SCM (Succinimidyl Carboxy Methyl ester: SCM), MW5000 from Laysan Bio, Inc.

3.3.2 Cell lines & culture medium

Human mammary gland adenocarcinoma epithelial cells (MCF-7, HTB-22), passage 3 and human mesenchymal stem cells (hMSCs), Passage 2 courtesy of Assistant Professor Rachel Ee of Department of Pharmacy, National University of Singapore, Human promyelocytic leukemia cells (HL-60, CCL-240), passage 5, courtesy Assistant Professor Gigi Chiu of Department of Pharmacy, National University of Singapore were used for the purpose.

While RPMI-1640 media (GIBCO) was used to grow MCF-7 (10% FBS) cells, IMDM media (Sigma Aldrich) was used for HL-60 (20%FBS) cells. The DMEM media (10% FBS) added with NEAA and sodium Pyruvate was used to grow hMSCs.

Several cytotoxicity data involving carbon nanotubes are already available in literature with respect to tumoral cell lines like A549, Caco-2 and HeLa cells. Similarly MCF-7 cells have also been used in many cases (Lu, Moore et al. 2004; Bianco, Kostarelos et al. 2005; Ali-Boucetta, Al-Jamal et al. 2008; Chiaretti, Mazzanti et al. 2008), not only for cytotoxicity regarding various functionalized CNTs and nanoparticles, but also for drug delivery experiments. Therefore we have decided to use MCF-7 cells for the purpose. In comparison to MCF-7 cells (adherent cells), we have used HL-60 cells, which are suspension cells, to investigate whether the type of cells is also a factor responsible for biocompatibility of CNTs. Living aside these tumoral cell lines we have also evaluated the interaction of CNTs with normal human mesenchymal stem cells (hMSCs).

3.4 METHODS

3.4.1 Functionalization of Carbon nanotubes

Samples were synthesized following the procedure reported in **Figure 3.2** (Wu, Wieckowski et al. 2005).

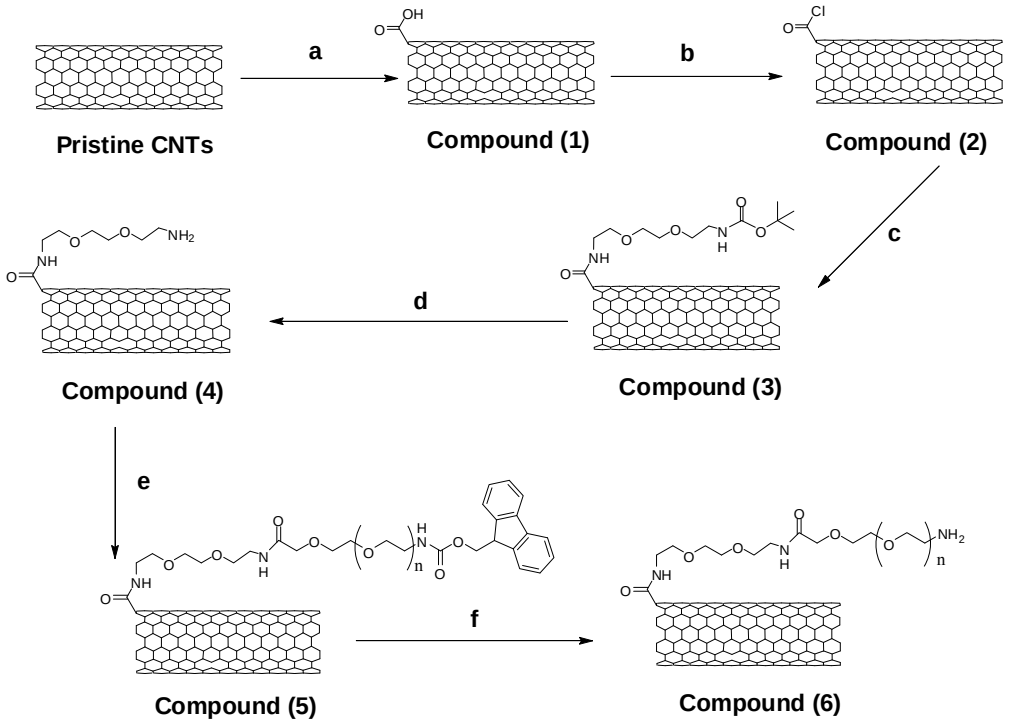

Figure 3.2: synthetic procedure of the samples: **(a)** HNO_3/H_2SO_4 (v/v, 1:3), Sonication 3h, 6h, 9h, 12h, 24h for MWCNTs or 4h for SWCNTs **(b)** $(COCl)_2$ **(c)** monoBOC-TEG, THF, DIPEA, reflux **(d)** HCl 4M in dioxane **(e)** FMOC-NH-PEG-SCM (MW5000), THF, DIPEA, reflux **(f)** 50% piperidine in DMF. n =103.

Synthesis of compound 1: *CNT-COOH*

Pristine CNTs (raw CNTs) were oxidized by sonicating them in the presence of an acidic mixture consisting of 95% sulphuric acid and 65% nitric acid in a 3:1 ratio. All the samples (both SWCNTs and MWCNTs) underwent 3, 6, 9, 12 and 24 hours of sonication (Ney-Ultrasonik 28H with sonication power of 230W). We also oxidised one sample of SWCNTs for 4 hours to have approximately similar length range with respect to MWCNTs oxidised for 6 hours, both of which were utilised for further functionalization. The CNTs acid mixture was then diluted by rinsing with distilled water and centrifuged

for at least 4 times at 13,000 g (15 mins per cycle) until the contents showed neutral pH. A small amount of water was added to the product that underwent lyophilization to provide *compound 1* in dry and powdered form.

Synthesis of compound 2: *CNT-COCl*

The suspension of *compound 1* (SWCNTs sonicated for 4 hours and MWCNTs sonicated for 6 hours) in oxalyl chloride (10 mg of *compound 1* required 4 ml of oxalyl chloride) was stirred at 62ºC for 24 hours under nitrogen. After 24 hours, excess of oxalyl chloride was evaporated under vacuum leaving behind dry *compound 2* (11.3 mg of SWCNTs and 10.7 mg of MWCNTs, respectively).

Synthesis of compound 3: *CNT-TEG-monoBOC*

Compound 2 (10 mg of SWCNTs and 10 mg of MWCNTs, respectively) was then derivatized with BOC-TEG-NH_2 (Boc-mono-protected diaminotriethylene glycol) (120 mg, 484 μmol) by a 48 hour reflux in Tetrahydrofuran (THF) with the presence of N,N-di-isopropyl ethylamine (DIPEA, 90 μl, 532 μmol). After cooling at room temperature, excess of Boc-mono-protected diaminotriethylene glycol was removed by washing with methanol several times using 0.22 μm PTFE membrane. The resulting *compound 3* (7.4 mg of SWCNTs and 8.2 mg of MWCNTs, respectively) was dried at room temperature under vacuum and lyophilized.

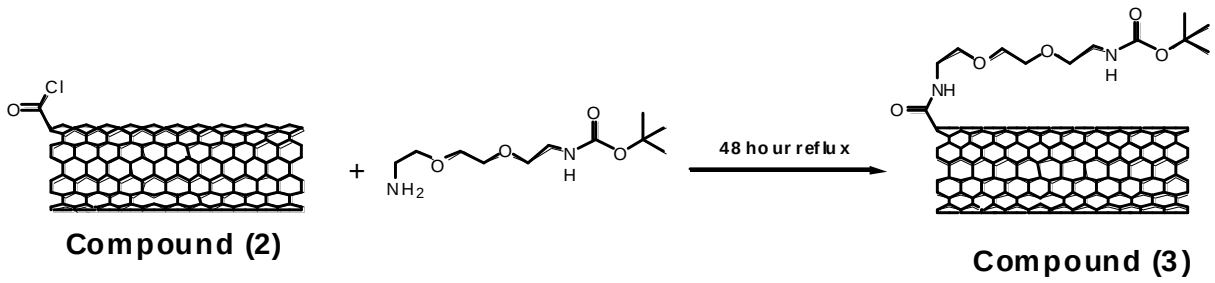

Figure 3.3: Schematic representation of derivatization of ***compound 2*** with mono-Boc-protected diaminotriethylene glycol.

Synthesis of compound 4: *CNT-TEG*

The protective BOC group was subsequently cleaved via the addition of 4 mL of hydrogen chloride 4.0 M solution in 1,4 Dioxane to result in *compound 4*. The solvent was evaporated in the presence of saturated $NaHCO_3$ solution and the product was washed with diethyl ether several times, using a 0.22 μm PTFE membrane, and finally lyophilized to get a dry powder. Amount of μmol of amino groups per gram of sample (loading) was calculated through quantitative Kaiser Test (Sarin, Kent et al. 1981). SWCNTs: 198 μmol/g and MWCNTs: 233 μmol/g.

A small additional complex (*CNT-TEG–NH-Ac*) was obtained by treating the free-amino-TEG-CNT sample with acetic anhydride, in order to study the influence of the charges in further cytotoxicity assays (data not shown).

Synthesis of compound 5: *CNT-PEG-Fmoc*

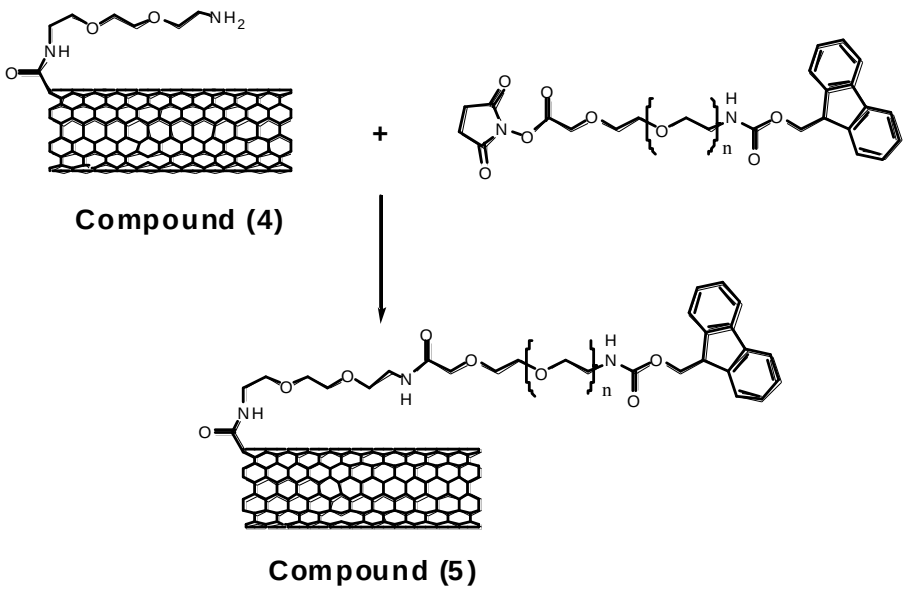

Figure 3.4: Schematic representation of derivatization of ***compound 4*** with FMOC-NH-PEG-SCM. .

CNTs conjugated with triethylene glycol (*compound 4*, 4mg each for SWCNTs and MWCNTs) were further functionalized with 4.04 mg (0.80 μmol) and 4.75mg (1.11 μmol) of Fmoc-NH-PEG-SCM (Fluorenylmethyloxycarbonyl-NH-polyethylene glycol-Succinimidyl Carboxy Methyl ester) (MW5,000), respectively, to form *compound 5* by a 48 hour reflux in THF with the presence of DIPEA **(**3 μl, 17.6 μmol**).** After which, vacuum was applied until the content was nearly dry. The excess of Fmoc-NH-PEG-SCM was removed by washing with methanol several times. The resulting product was lyophilized to get a dry powder

Synthesis of compound 6: *CNT-PEG*

Subsequent removal of Fmoc from *compound 5* (3.1 mg of SWCNTs and 3.3 mg of MWCNTs, respectively) was achieved by reaction with 50% piperidine in DMF by stirring at room temperature for 3 hours to form *compound 6* (2.4 mg of SWCNTs and 2.5 mg of MWCNTs, respectively). Dichloromethane (CH_2Cl_2) was added to the contents and filtered using Nylon 66 membrane. The filtrate of CNTs was rinsed with methanol, then with diethyl ether. Finally the product was lyophilized from water.

The amount of functional groups around the tips and sidewalls of the CNTs can be quantified using different techniques, such as absorption spectroscopy, calorimetric analyses, etc. In our experiments, when free amino groups are present on the CNT surface, the Kaiser test is extremely useful for quantitative evaluations (Georgakilas, Voulgaris et al. 2002; Pantarotto, Partidos et al. 2003). The exact procedure is reported in the following paragraph, and the amount of μmol of amino groups per gram of sample (loading) through quantitative Kaiser Test resulted as follows: SWCNTs: 198.00 μmol/g and MWCNTs: 231.00 μmol/g.

3.4.2 Quantitative Kaiser Test

Quantitative Kaiser Test was subsequently carried out to verify the successful functionalization of CNTs. The extent of functionalization which can be termed as "loading" indicates the amount of functional group (free amino groups) present in one gram of CNTs. Loading allows determination of the degree of functionalization (Sayes, Liang et al. 2006), which in turn is related to cytotoxicity and dispersibility of *f*-CNTs.

3.4.2.1 Chemicals

(a) Ethanol (60%):- 66.66 ml of 90% ethanol was mixed with 34.34 ml of water in a 100 ml beaker to get 60% ethanol (ETOH).

(b) Phenol in ethanol:- 40 g of phenol was weighed and added to 10 ml of 90% ETOH.

(c) 1.0 g of Ninhydrin was mixed by sonication with 20 ml of ETOH (95%) and stored at 4ºC in amber coloured glass bottle to protect from light.

(d) KCN solution in pyridine:- 65 mg of KCN were weighed inside a bottle and 10 ml of water were added to get a 100mM solution. The spatula used for the purpose was bleached with sodium hypochlorite to neutralize KCN, which is a poison. The 100mM KCN solution was further diluted with water to get 1mM KCN solution. Finally, 400µl of KCN solution was added with 19.6 ml of pyridine and stored in a closed bottle at 4ºC.

3.4.2.2 Procedure

The Ninhydrin reagent (75µL of phenol solution, 100µL of KCN solution and 75µL of Ninhydrin solution) was added to 100µg of functionalized CNTs (*f*-CNTs) in a 5 mL test tube. The contents were heated for 7 minutes using a water bath at constant 100 ºC. Immediately after heating, the contents were diluted with 60% ethanol to a final volume

of 5mL and the absorbance at λ = 570.0 nm was measured. A negative control (containing all the reagents but without CNTs) was used as baseline. The presence of free amino groups is indicated by a violet coloration of the solution, whereas their absence is indicated by a yellow coloration of the solution comparable to that of the control.

3.4.2.3 Calculation

$$\text{Loading (Number of mmol of } NH_2 \text{ groups Present per g of sample)} = \frac{[\text{Abs sample-Abs blank}] \times [\text{dilution (ml)}] \times 10^6}{(\text{Extinction coefficient} = 15000) \times [f\text{-CNTs weight } (\mu g)]}$$

3.4.3 Microscopy

Transmission electron microscopy (TEM):

Original pristine CNTs and functionalized-CNTs (*f*-CNTs) *(compounds 1, 4,* and *6)* were examined by transmission electron microscopy (TEM) using a JEOL JEM 2010F microscope. The samples were prepared on 200 mesh copper grids coated with formvar. Length and diameter measurement calculations, based on microscopic scale, were performed using Image J software (U.S. National Institute of Health).

Raman analysis:

Raman spectrometric measurements were carried out with WiTec GmbH confocal Raman microscope using argon ion laser having an excitation wavelength of 514.5 nm laser and using FT-Raman spectrometer (FRA 106 Bruker) excited by a 1064 nm laser.

Energy Dispersive X-ray Spectroscopy (EDS):

JEOL JSM-6701F Scanning electron microscope (field-emission) equipped with JEOL JED-2300 EDS system was used for quantitative elemental analysis of different

CNT samples. The powdered and well dried CNT samples were mounted on the sample holder using carbon tape. The excess amounts of powders were blown away. Further the mounted samples were introduced into the SEM sample chamber for EDS. The collection and quantification of spectra was computer controlled with integrated software.

3.4.4 Dispersibility Test

Dispersibility of functionalized CNTs (*f*-CNTs) was determined using DMSO and milliQ water. Range of weights of *f*-CNTs employed in the dispersibility test was 10 µg to 5 mg. Each sample of CNTs was added with 1 ml of milliQ water in a 2 ml microcentrifuge tube. Sufficient DMSO was introduced to this tube to keep its concentration at maximum 1%. Tubes were further sonicated for 1 hour (Ney-Ultrasonik 28H with sonication power of 230W) to aid in dispersion of CNTs in water.

Samples were considered dispersible if they did not show precipitation for a period exceeding 48 hours after sonication, in order to avoid precipitation during cell incubation for the cytotoxicity studies. Ultrapure-MWCNTs formed suspensions without DMSO and they were stable for a period exceeding 4 months.

3.4.5 MTT assays

Cell culture:

Cells were grown in required media supplemented with specific amount of Fetal Bovine Serum (FBS HyClone) and 1% Penicillin/Streptomycin (PAA The Cell Culture Company) in a humidified jacketed incubator (Binder), with a temperature of 37°C, 5% CO_2. Media was changed every two days. The cells were allowed to grow to near confluence before being used. Cells at passages 4-9 were used in this study. Prior to the seeding of the cells in a 96-well plate, the cells were rinsed with PBS (Phosphate Buffer

Solution) and trypsinised. The number of viable cells were then determined using Trypan blue dye exclusion assay. By using the information obtained from the Trypan blue assay, cells were seeded at a density of 1 x 10^5 viable cells/ml (200 µl per well) in 96-well plates, and incubated for 24 hours prior to treatment with CNTs. All the experiments were performed in triplicates (n = 3).

The CNTs used in the experiments included the following: Pristine CNTs, *compound 1*, *compound 4*, *compound 6* and ultrapure MWCNTs. The concentrations of CNTs that were employed in these experiments usually ranged between 10-50 µg/mL. These concentrations were chosen based on several literature reports (Dumortier, Lacotte et al. 2006; Sayes, Liang et al. 2006; Wick, Manser et al. 2007) and on the results from our dispersibility test. In order to prepare those concentrations, 50 to 250 µg of CNTs were weighed out and added to three separate centrifuge tubes that contained 12.5 µl of DMSO and 37.5 µl of media each. The presence of DMSO and the sonication process helped in the dispersion of CNTs. These represented the standard solutions and from each of them, 10 µl were extracted and added to 990 µl of RPMI-media to form a final volume of 1 ml of each of the three concentrations. The mixtures were then sonicated for a few minutes to obtain a homogenous dispersion of *f*-CNTs before incubation with cells. DMSO in the final concentration was 0.25%: we on purpose minimized this concentration, since from previous experiments we identified that values beyond 0.5% deeply affected cell viability.

Assay procedure:

Untreated control cells, which were added to culture medium without any CNTs, served as a negative control. 0.25% DMSO, which was used to aid the dispersion of *f*-CNTs, was added to cells to investigate whether it had any effect on cell viability. 1%

sodium dodecyl sulphate (SDS) was added to cells as a positive control to induce cell death. 100 µl of each of the five concentrations of *f*-CNTs dispersion was introduced into each well. Cells were then incubated for 24 hours in a jacketed incubator at 37°C, 5% CO_2. The number of surviving cells treated with CNTs was then compared to the control groups.

Assessment of cell viability was determined using a metabolic activity assay, MTT, 3-(4, 5-Dimethylthiazol-2-yl)-2, 5-Diphenyltetrazolium Bromide (Duchefa Biochemie) or CyQUANT test. In the first case, the test principle is based on the reduction of the tetrazolium salt from yellow color to purple color by the mitochondria in viable cells (Mosmann 1983).

After the 24 hour interval, the contents in each well were pipetted out and PBS was added to wash the cells. 100 µl of tetrazolium salt (0.1 mg/mL) were added to each well and allowed to incubate for 4 hours in the jacketed incubator. After 4 hours, the contents in each well were pipetted out and DMSO was added to lyse the cells and to solubilize the insoluble formazan dye.

The plate was shaken for 3 minutes to ensure homogeneity of color and aid solubilisation of the dye prior to measure absorbance. The absorbance was recorded using the Benchmark Plus micro plate Spectrophotometer (Bio-Rad Laboratories) at 590 nm. The absorbance recorded is directly proportional to the number of viable cells present. All the experiments were repeated in triplicate and the results were expressed as the mean value.

$$\% \text{ Cell viability} = \frac{\text{Absorbance of test sample} - \text{Absorbance of blank (PBS)}}{\text{Absorbance of the control} - \text{Absorbance of Blank (PBS)}} \times 100$$

3.4.6 CyQUANT assays

Since the MTT assay is a colorimetric assay and we used CNTs (which are black in color and might have interfered in the assay), we compared our results with those carried out with CyQUANT assay (Blaheta, Franz et al. 1991) (which is a fluorescence based assay) to confirm the results. The CyQUANT (Invitrogen) Cell Proliferation Assay kit consists of two components: a green fluorescent nucleic acid dye and a background suppression dye. The nucleic acid dye is a live cell-permeable reagent that mainly concentrates in the nucleus of mammalian cells and exhibits strong fluorescence enhancement when bound to nucleic acid. The suppression dye is impermeable in live cells and suppresses "green" fluorescence, emanating due to nucleic acid dye that has not penetrated the cells. In other words any fluorescence resulting due to binding of nucleic acid dye to residual CNTs will be suppressed by suppression dye which eliminates potential interference in fluorescence readouts. Over all, combinations of these two components result in an assay based on both DNA content and membrane integrity. As part of the assay frozen cells are simply thawed and lysed by addition of a buffer containing the CyQUANT GR dye. Fluorescence is then directly measured and compared with control (untreated cells).

Assay procedure:

A concentrated cell suspension ideally at a density of about $1x10^6$ viable cells/mL was prepared using Trypan blue with the help of haemocytometer. This cell suspension was further diluted and cells were seeded at a density of 1×10^5 viable cells/mL (200 µl per well) in 96-well plates, and incubated for 24 hours prior to treatment with CNTs. All the experiments were performed in triplicates (n = 3). The samples of different concentration of CNTs in 0.25% DMSO (preparation described previously) were used for

the purpose including 1%SDS in culture medium treated cells as negative control and 0.25% DMSO in culture medium treated cells as positive control. The well plates were further kept in incubator for 24 hours. Finally in case of adherent cell lines the media was removed carefully from each well without disturbing the cells and frozen at -80ºC. In case of suspension cells, the well plates were subjected to centrifugation for 5 minutes at 200 x g. The supernatant was carefully removed without disturbing the cell pellets and then the well plates were frozen at -80ºC. After 24 hrs the well plates were taken out from freeze and cell pellets were thawed at room temperature. 200µl of the CyQUANT GR dye/cell-lysis buffer were added to each well. The cells in the wells were suspended by vortexing briefly. The fluorescence intensity of each test wells were measured using a fluorescence micro plate reader (Infinite 200) set up with 480 nm excitation maximum and 520 nm emission maximum filters and compared with fluorescence intensity of control wells to determine percentage cell viability.

Presentation of Data Obtained in MTT and CyQUANT Assays:

We chose a linear regression model to present the data obtained in the MTT or CyQUANT assays. For each plot, r^2 (coefficient of determination) values were obtained. By adopting the linear regression model, we assumed that the relationship between cell viability and concentration can be represented with a straight line and not a curve.

We also carried out Student t-test to calculate p-value. If the p-value was found to be less than the threshold (0.05) chosen for statistical significance, then the null hypothesis (which states that the two groups do not differ) was rejected in favor of an alternative hypothesis, which states that the groups do differ significantly.

3.5 RESULTS

3.5.1 Physicochemical characterization of *f*-CNTs

Syntheses of functionalized carbon nanotubes (*f*-CNTs) (***compounds 1*** to ***6***) were successfully accomplished and the products were characterized using TEM, Raman spectroscopy and EDS as appropriate. Also, comparisons of the various *f*-CNTs were carried out using the Kaiser tests as well as studies on their water dispersibility.

3.5.1.1 Characterization by TEM

We oxidized tubes (both SWCNTs and MWCNTs) at different times (3, 6, 9, 12 and 24 hours), since it is known that sonication of CNTs in mixtures of sulphuric and nitric acids can cut the cylindrical structure into fragments, whose lengths are inversely proportional to the oxidation time (Mawhinney, Naumenko et al. 2000; Hu, Bhowmik et al. 2001). In other words, the longer the treatment, the shorter the length of the tubes, as confirmed by our pictures obtained under Transmission Electron Microscopy (TEM) (**Figure 3.5, 3.6**) and reported in **Table 3.3**.

Time of Sonication(h)	Length of MWCNTs (nm)	Length of SWCNTs (nm)
0	1,000-2,000	5,000-15,000
3	600-800	700-1000
6	250-350	150-200
9	150-250	50-100
12	100-150	-
24	50-100	-

Table 3.3: Length of different CNTs oxidized by treatment with strong acids and sonication for different time intervals

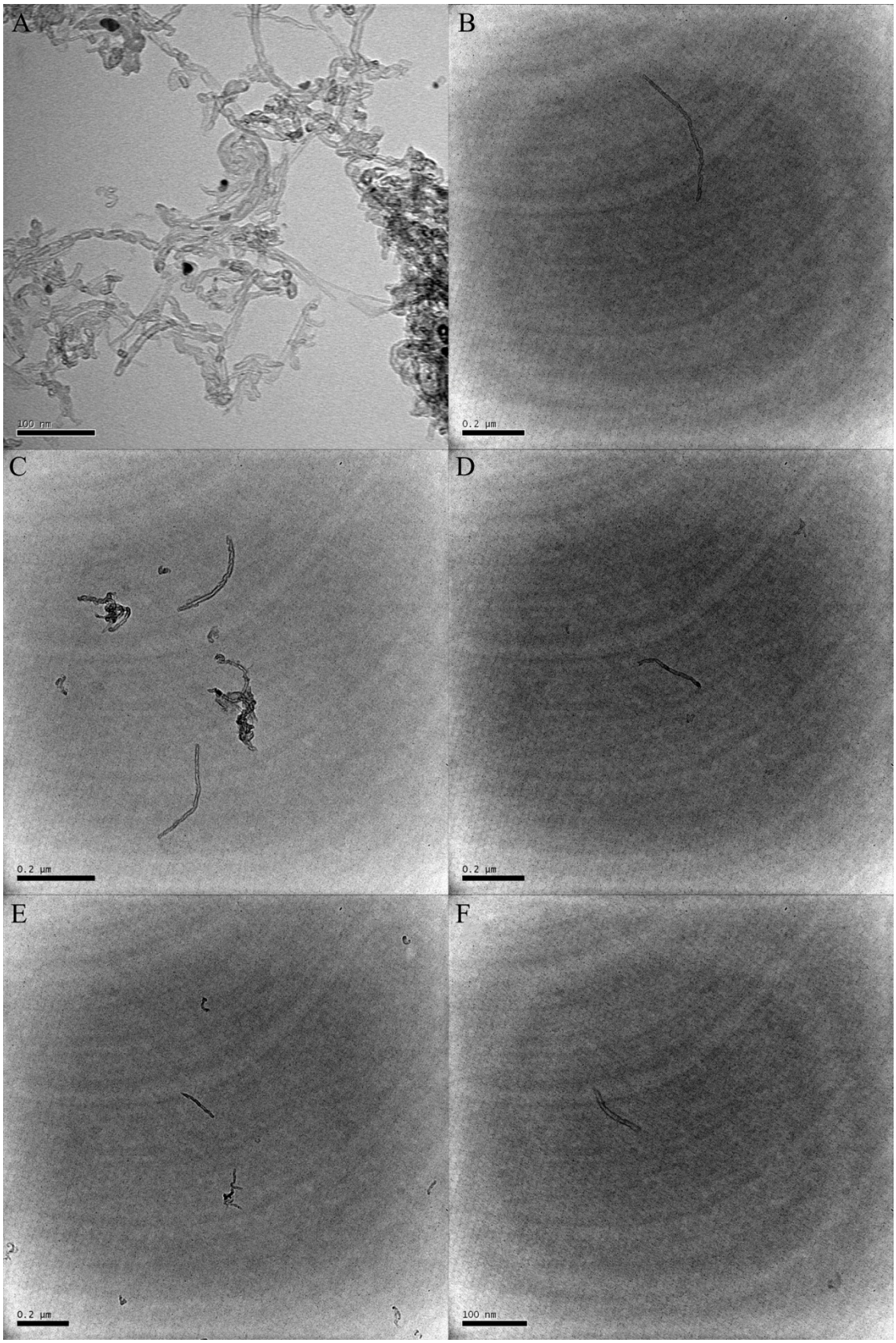

Figure 3.5: Images under TEM on the length of 20 µg/ml **MWCNTs** oxidized for different time period. **MWCNTs** oxidized for different time period **(A)** Non-oxidized pristine CNTs, **(B)** 3 hr, **(C)** 6 hr, **(D)** 9 hr, **(E)** 12 hr, **(F)** 24 hr. In case of B, C, D, E the scale is 200 nm, while for A and F the scale is 100 nm.

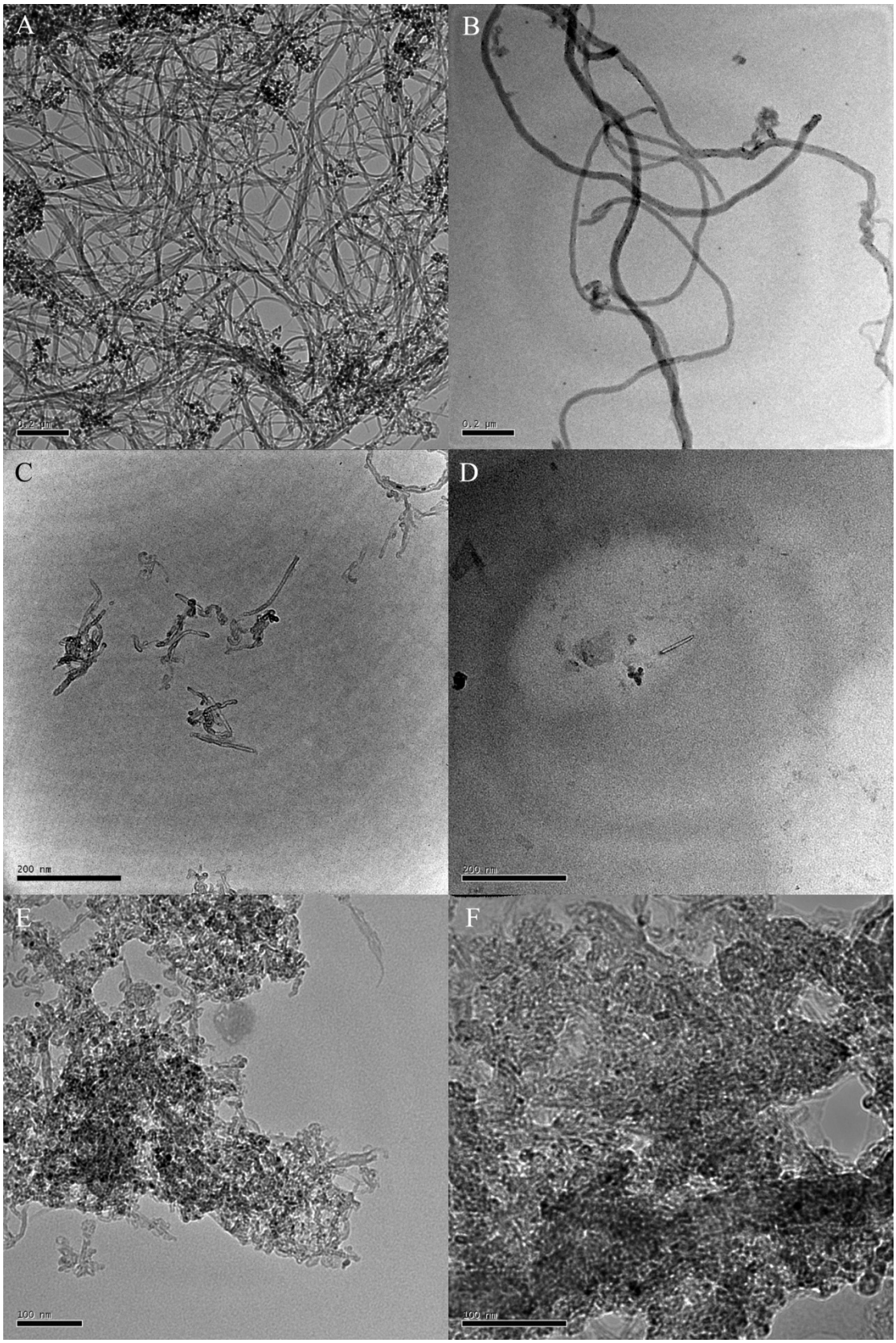

Figure 3.6: Images under TEM on the length of 20 µg/ml **SWCNTs** oxidized for different time period. **SWCNTs** oxidized for different time period **(A)** Non-oxidized pristine CNTs, **(B)** 3 hr, **(C)** 6 hr, **(D)** 9 hr, **(E)** 12 hr, **(F)** 24 hr. In case of A, B, C, D the scale is 200 nm, while for E and F the scale is 100 nm.

It can be seen, from **Figure 3.5, 3.6 and Table 3.3** that the exposure of CNTs to these oxidative conditions cut the tubes within precise ranges, which were comparable to those reported in literature (Wu, Wieckowski et al. 2005); in addition, it generated surfaces which in turn provided abundant sites for carboxylation and further chain functionalization along the side walls. Since sonication deeply affected the structure of SWCNTs, while preserved the tubular shape of MWCNTs for longer time, therefore we adopted 4-hour and 6-hour sonication as optimal treatment of SWCNTs and MWCNTs, respectively, in all the remaining experiments.

An important factor to consider is that temperature associated with extensive sonication might play a synergistic effect in altering the final structure of the tubes; more precisely, the bath temperature in the sonicator would have increased proportionally with the duration of the oxidation process, thus confounding our results. For that reason, and in order to prevent excessive cutting, we maintained the water bath in the sonicator at temperature below 35º C (Hilding, Grulke et al. 2003), which has indicated to have minimal influence on the tubes' constitution.

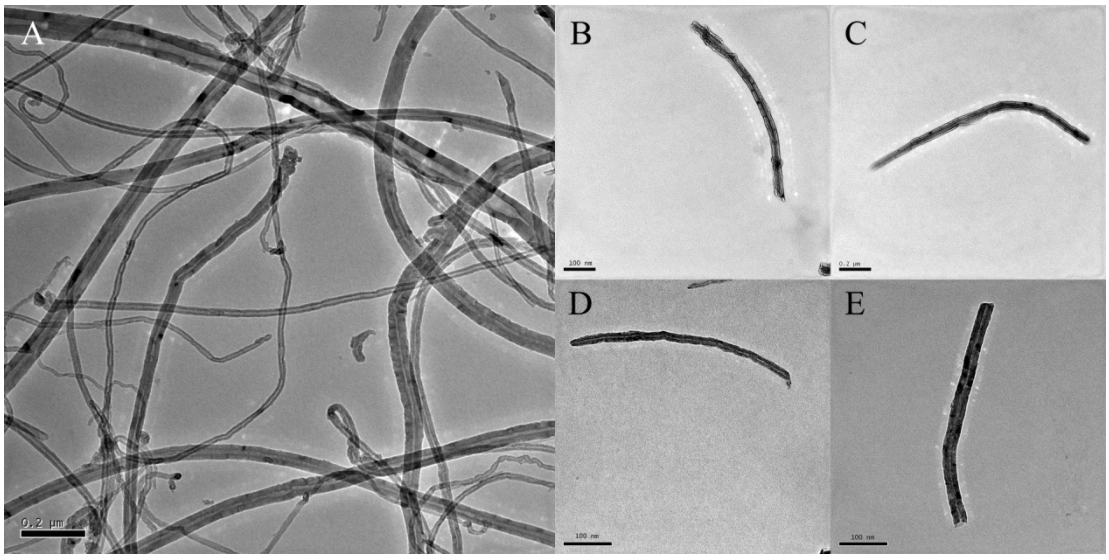

Figure 3.7: TEM images of (A) pristine and (B–E) oxidized (6 hr) ultrapure MWCNTs. The scale for (A) is 200 nm and the scale for (B–E) is 100 nm.

According to **Figure 3.7**, pristine ultrapure **MWCNTs** appear as long, continuous tubes whereas oxidized MWCNTs are truncated to approximately 400 to 700 nm in length. The ultrapure MWCNTs (**Figure 3.7)** were used as such without any chemical modifications for biological characterization.

3.5.1.2 Kaiser Test results and Loading

The Kaiser Test is reliable as a qualitative method to characterize *f*-CNTs by indicating the presence or absence of free primary amino functional groups in the tubes. Those *f*-CNTs with no free amino groups (***compounds 1, 2, 3*** and ***5***) were all tested negative for Kaiser Test, producing the same yellow color in the Ninhydrin reagent as the negative control. On the other side, *f*-CNTs with free amino groups (***compounds 4*** and ***6)*** gave a positive Kaiser Test result, producing a purple coloration in the Ninhydrin reagent **(Table 3.4).** Kaiser Test can also be used to monitor the progress of functionalization at each step if free amino groups are involved. For example, ***compound 3*** shows a negative Kaiser Test result. Upon successful synthesis to form ***compound 4***, it gives positive Kaiser Test. Further successful functionalization to ***compound 5*** (which has no free amino groups) yields a negative Kaiser Test result. ***Compound 6***, synthesized from ***compound 5***, involves addition of a molecule with free amino groups, giving a positive Kaiser Test again.

The loading values of all *f*-CNTs that showed positive Kaiser Test have been listed in **Table 3.4**. This was used to calculate the minimum amount of reagent, Fmoc-NH-PEG-SCM required for further functionalization from ***compound 4.*** The negative Kaiser Test result in ***compound 5*** shows the success of functionalization and the usefulness of the loading values to ensure that an adequate amount of reagent was added in the synthesis of ***compound 5*** starting from ***compound 4***.

Compound No	*f*-CNTs	Kaiser test results and loading (µmols/g)
Compound 1	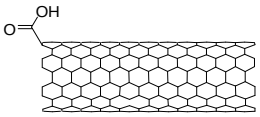	Negative
Compound 2	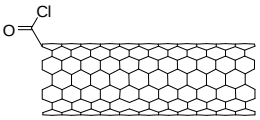	Negative
Compound 3	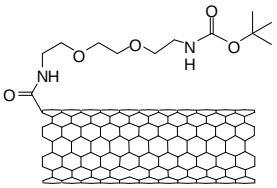	Negative
Compound 4	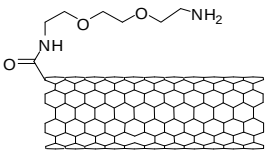	SWCNTs- 198.00 MWCNTs- 233.00
Compound 5	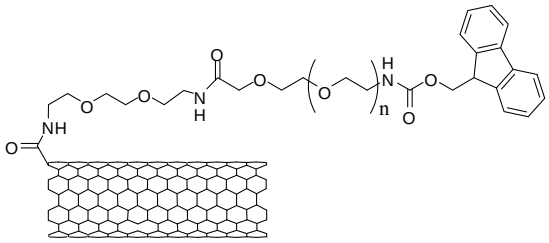	Negative
Compound 6	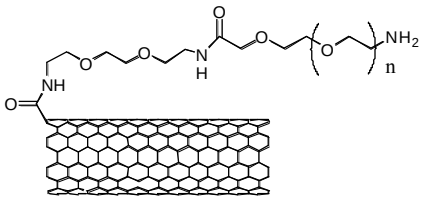	SWCNTs- 198.00 MWCNTs- 231.00

Table 3.4: Kaiser Test results and loading of all the functionalized CNTs

3.5.1.3 CNTs' dispersibility

In our experiments on dispersibility, the use of organic solvent (DMSO) was standardized at a final concentration of 1%; hence, dispersibility of the various *f*-CNTs

was determined using DMSO and milliQ water, while short sonication was also applied to aid their dispersion in water.

Sample	Type of CNTs	Dispersibility (μg/ml)
Pristine CNTs	SWCNTs	≤1.25
	MWCNTs	1.25
Compound 1	SWCNTs	1.25
	MWCNTs	5
Compound 2	SWCNTs	1.25
	MWCNTs	4.0
Compound 4	SWCNTs	2.5
	MWCNTs	25
Compound 6	SWCNTs	5
	MWCNTs	≥25
Ultra-Pure MWCNTs	MWCNTs	≤3mg/ml

Table 3.5: Dispersibility of *f*-CNTs in water containing DMSO (less than 1% v/v).

As reported in **Table 3.5**, due to different functionalization, our samples showed either similar or increased water dispersibility in comparison with pristine carbon nanotubes. In general, pristine CNTs were hardly soluble in any of the usual solvents (ethyl acetate, ethanol, DMF etc.). Conversely, oxidation of the pristine CNTs to form *f*-CNTs (***compound 1*****)** slightly enhanced their suspendibility. This was in agreement with the order of polarity of *f*-CNTs, which increased as follows: **Pristine CNTs ≤ Oxidized CNTs (*compound 1*) ≤ TEG–CNTs (*compound 4*) ≤ PEG–CNTs (*compound 6*).**

In particular, derivatization of CNTs with polar chains such as tri(ethylene glycol) (***compound 4*****)** resulted in further increase in their water suspendibility, which surpassed that of pristine CNTs by a factor of 2 in SWCNTs and by a factor of more than 5 in MWCNTs, respectively. Functionalization of CNTs with longer chains such as poly(ethylene glycol) (***compound 6*****)** resulted in dramatic improvement in CNT dispersibility in water by a factor of 5 in case of SWCNTs and a factor of 25 in case of MWCNTs. A point to note is that, although dispersibility in water generally improved

through the incorporation of hydrophilic chains, the number of carbon atoms involved in such functionalization was still quite low in comparison to the rest of the tubes. In other words, these *f*-CNTs were expected to retain some form of hydrophobicity as not all of the carbons on the CNTs' surface underwent these reactions (Kam, Jessop et al. 2004). Overall, MWCNTs seemed to be better dispersible than SWCNTs in water.

In the special case of ultrapure MWCNT samples, suspensions in water (without DMSO) were stable, until a maximum concentration of 3 mg/ml, for a period longer than 4 months.

3.5.1.4 Raman Spectroscopy for MWCNTs

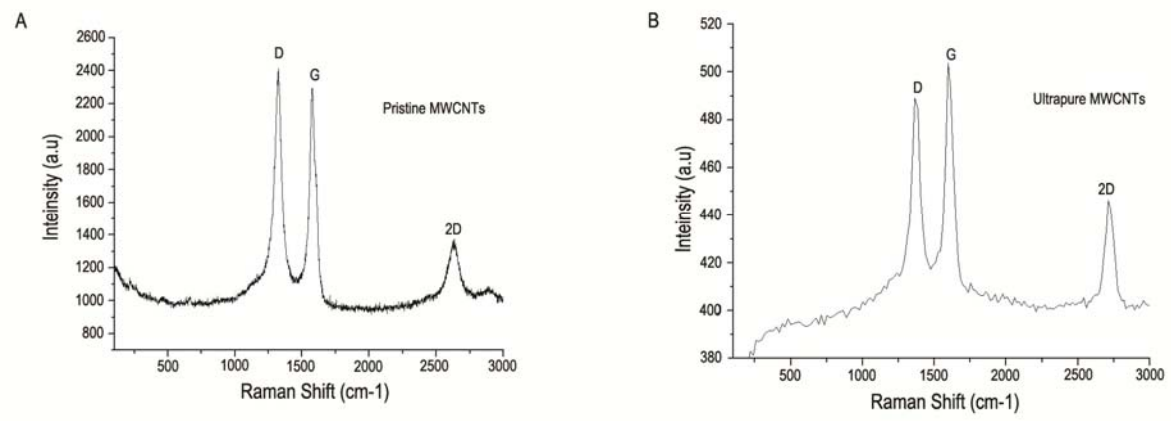

Figure 3.8: Raman analysis of MWCNTs from different sources, showing low **(A)** and high **(B)** purity.

Raman analysis was also employed to evaluate how impurities could affect the characteristic bands of carbon nanotubes and especially to compare between pure and ultrapure sample (hence it was limited to MWCNTs commercially available *versus* those obtained after ultrapurification procedures by our collaborator). In fact CNTs usually show tangential bands (G-band) at 1,500-1,600 cm^{-1}, as well as broad bands (D-band) at approximately 1,350 cm^{-1} (Karachevtsev, Glamazda et al. 2006; Kawamoto, Uchida et al. 2006; Kawamoto, Uchida et al. 2006). It has been shown that D-bands of impure carbon

nanotubes are generally much broader than those of the typical nanotube, so that an indication of the CNTs purity level may be obtained by simply examining the line-width of the D-band (Li, Biris et al. 2007). In addition, ratio of intensities of D-band (I_D) to G-band (I_G) is often used as an estimation of carbonaceous impurity content and defect-site density (Dillon, Yudasaka et al. 2004). A high I_D/I_G ratio would mean that there are more defects inside the carbon layers (Fraczek, Menaszek et al. 2008). In our case, bands were not affected in width, but in commercial pristine CNTs, D-band was higher than G-band (therefore high I_D/I_G ratio), and this is usually observed when side walls are not uniform or some amorphous carbon is still present (**Figure 3.8A**). Conversely, the ultra-pure samples showed D-band smaller than G band (therefore low I_D/I_G ratio), thus indicating that fewer impurities were present on the surface of these tubes (**Figure 3.8B**).

3.5.1.5 EDS

The EDS involves the basic principles used for determining chemical composition of any conducting samples on the micro meter scale using SEM or TEM (Goldstein, Newbury et al. 2003). The X-rays emitted from a specimen bombarded with the finely focused electron beam of scanning electron microscope, are sorted by energy levels, and a spectrum of X-ray energy vs. counts is plotted, which is indicative of the element present and of the concentration of each element present (**Table 3.6**). The quantitative elemental analysis of CNT samples from different sources by EDS revealed the presence of iron and cobalt in the commercially available SWCNTs, cobalt, molybdenum and traces of iron in the commercially available MWCNTs; however, ultrapure MWCNTs were free from these catalytic elements (**Figure 3.9, 3.10, 3.11 and Table 3.6**).

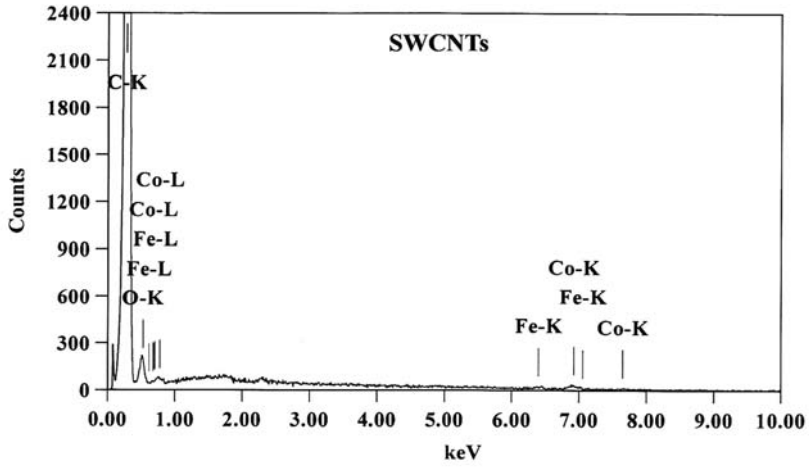

Figure 3.9: Energy dispersive x-ray spectrum of commercially available **SWCNTs**

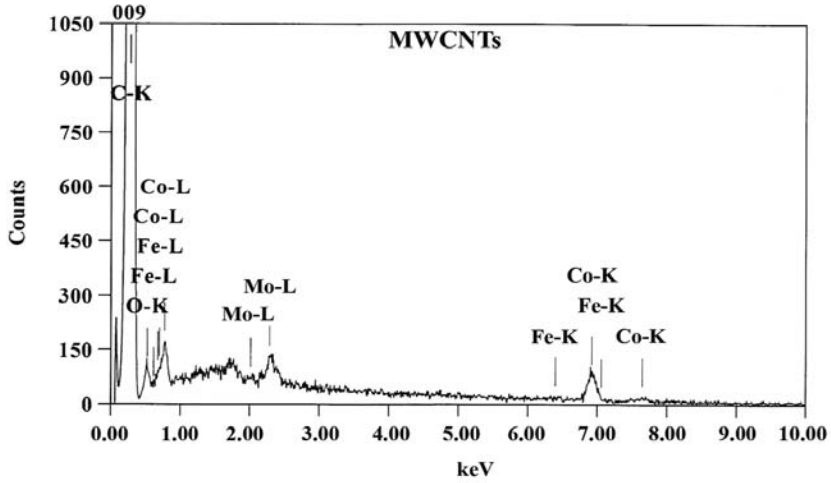

Figure 3.10: Energy dispersive x-ray spectrum of commercially available **MWCNTs**

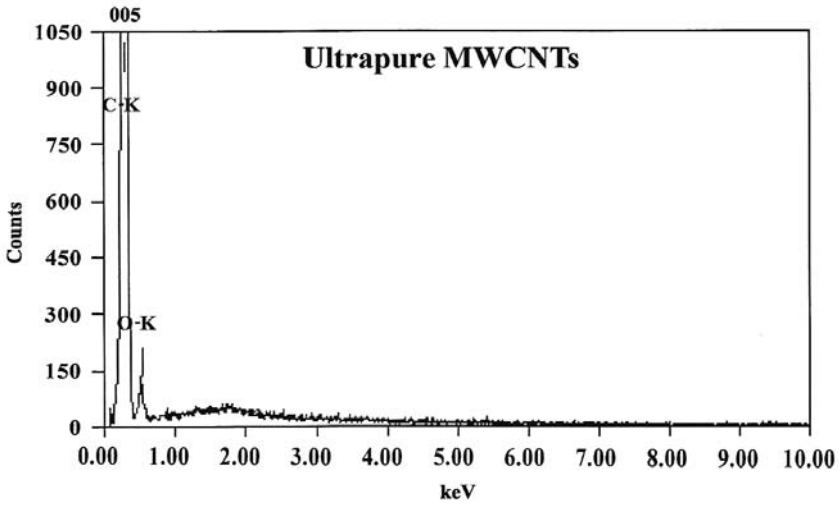

Figure 3.11: Energy dispersive x-ray spectrum of ultrapure **MWCNTs**.

Mass%	MWCNTs	SWCNTs	Ultrapure MWCNTs
C	86.51	85.98	**97.31**
O	4.75	10.91	**2.69**
Fe	0.20	1.02	**0.00**
Co	7.03	2.09	**0.00**
Mo	1.52	0.00	**0.00**
Total	**100**	**100**	**100**

Table 3.6: Mass % of elements present in different CNT samples derived from quantitative elemental analysis by EDS.

3.5.2 Biological characterizations

The functionalized carbon nanotubes (*f*-CNTs) including ultrapure MWCNTs were characterized for cytotoxicity and biocompatibility using MTT assay. Several parameters potentially influencing CNTs' cytotoxicity like surface/sidewall functionalization, concentration, degree of solubility, length and purity were evaluated. A great care was taken to wash out all the CNTs (black in color) which may lead to false positive result during the MTT assay (a colorimetric assay). To exclude this false positive result, in few cases CyQUANT assay was also performed to confirm the MTT assay data.

3.5.2.1 Sidewall functionalization of CNTs

Carbon nanotubes underwent several chemical modifications in order to introduce suitable functional groups on their surface. Although functionalization of CNTs is associated with the loss of their aromaticity (Sayes, Liang et al. 2006), with an eventual reduction of their aspect ratio (Hilding, Grulke et al. 2003) and with possible inter-CNTs coupling (which could result in further CNTs agglomeration (Smart, Cassady et al.

2006)), in our case we made use of amino-protecting groups (e.g. BOC and Fmoc) that ensured that each water soluble chain could react with an activated carboxylic group only on one side, while the other part remained unavailable to any further reaction until the protective group was cleaved. Pristine, non-functionalized CNTs were either used directly as control or subjected to chemical functionalization to incorporate several moieties. The samples were subsequently incubated within different cell lines in concentrations ranging from 10 to 50 μg/ml. MTT assay results showed that CNTs, once functionalized, were less cytotoxic and thus caused less cell loss in comparison to their pristine counterparts (**Figure 3.12** for SWCNTs and **Figure 3.13** for MWCNTs). CNTs were considered cytotoxic when cell viability was lower than 60% at the incubated dose.

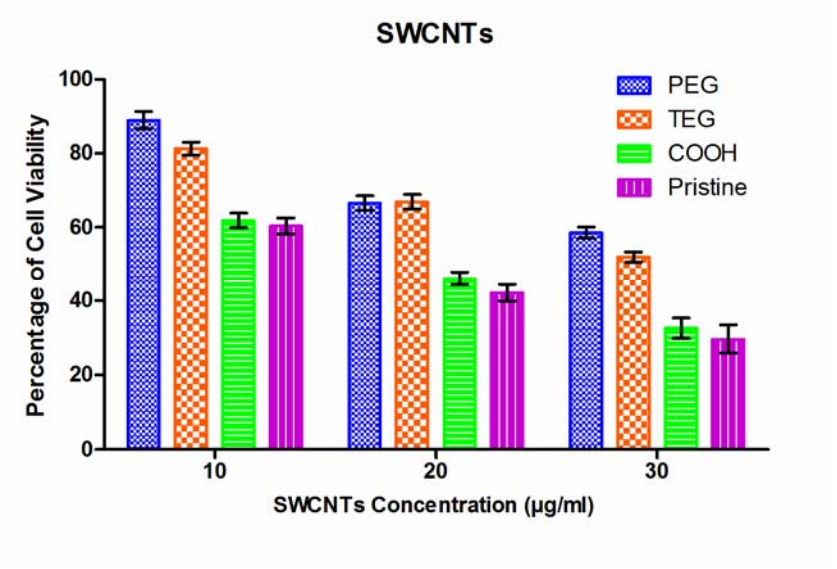

Figure 3.12: Percentage of cell viability of MCF-7 cells after 24 hours exposure to **Pristine, oxidized, TEG and PEG SWCNTs** at three concentrations: 10μg/ml, 20μg/ml and 30μg/ml. Dose–dependent cytotoxic effect was observed for all the samples.

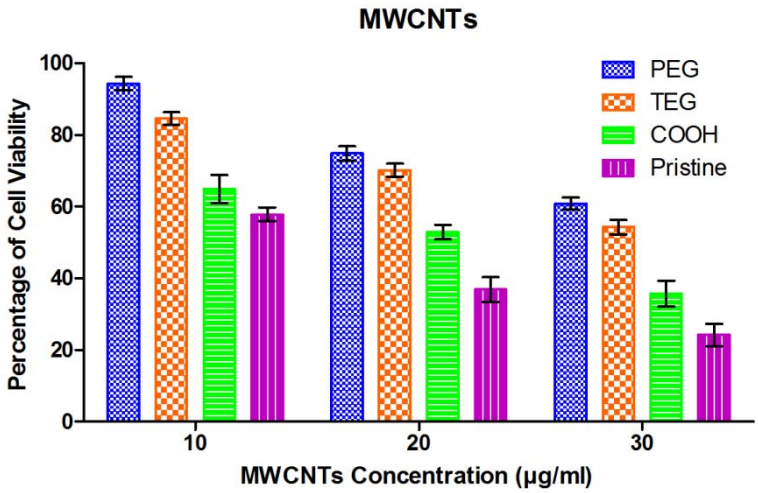

Figure 3.13: Percentage of cell viability of MCF-7 cells after 24 hours exposure to **Pristine, oxidized, TEG and PEG MWCNTs** at three concentrations: 10µg/ml, 20µg/ml and 30µg/ml. Dose–dependent cytotoxic effect was observed for all the samples.

Pristine CNTs, without chains attached on their surface, showed the worst profile even at 10 µg/ml, while cell viability improved in those tubes bearing a tri(ethylene glycol) (TEG) chain (more than 80% at doses of 10 µg/ml) and it reached its maximum (more than 94% for MWCNTs at concentrations of 10 µg/ml) with a long poly(ethylene glycol) (PEG) chain (MW 5,000) (Fig. **13**).

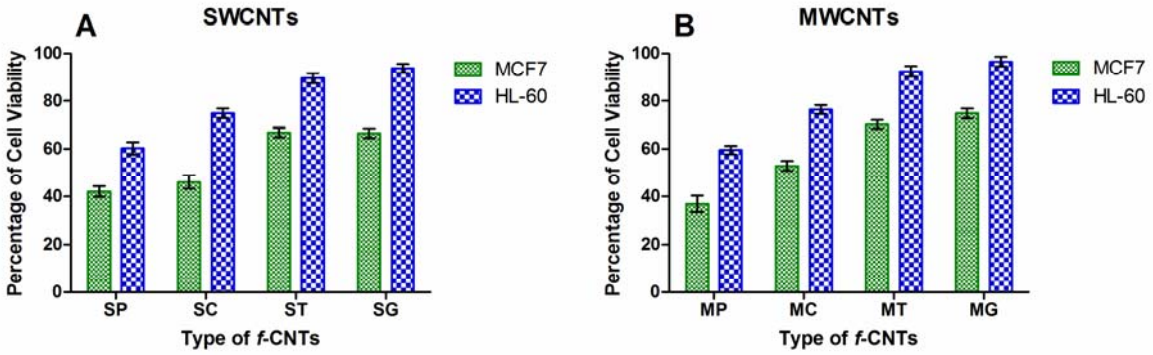

Figure 3.14: Percentage of cell viability of **MCF-7** and **HL-60** cells after 24 hours exposure to 20 µg/ml of **Pristine (SP** and **MP), oxidized (SC** and **MC), TEG (ST** and **MT)** and **PEG (SG** and **MG) functionalized CNTs.** While **(A) SWCNTs** were oxidized and sonicated for 4 hours**, (B) MWCNTs** were oxidized and sonicated for 6 hours.

Similarly, we also compared the effects of different functionalizations (pristine tubes, oxidized and with hydrophilic chains) between MCF7 and HL60 cells to determine cell viability pattern for both adherent and suspension cells. The concentration of the different samples of CNTs was kept constant at 20 µg/ml. From Figure **3.14**, it can be seen that HL60 cells showed a better cell viability than MCF7 cells ($p<0.05$) for all the different functionalizations including the pristine CNTs. The above result is also proportional to the order of enhanced dispersibility (**Table 3.5**) due to extent of the hydrophilic chains incorporated onto the tubes' surface for both suspension and adherent cells.

3.5.2.2 CNTs' concentration

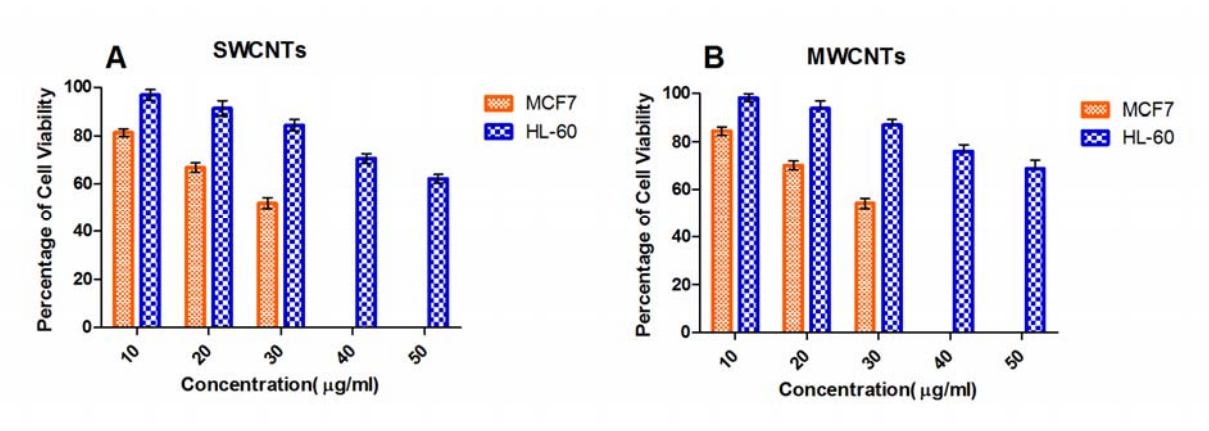

Figure 3.15: Percentage of cell viability of **MCF-7** and **HL-60** cells after 24 hours exposure to (A) SWCNT-TEG and (B) MWCNT-TEG (*compound 4*) at 5 concentrations: 10µg/ml, 20µg/ml, 30µg/ml, 40 µg/ml, and 50 µg/ml ($p<0.05$). Dose–dependent cytotoxic effect was observed for all the samples.

From **Figure 3.15** it can be seen that the percentage of cell viability of MCF 7 cells for TEG-conjugated SWCNTs and TEG-conjugated MWCNTs (***Compound 4*** (CNT-TEG)) at 30 µg/ml concentration is 52% and 54%, respectively. On the other hand, the percentage of cell viability of HL60 cells for SWCNTs and MWCNTs at higher doses (50 µg/ml) is 62% and 68%, respectively. Through this observation we concluded that HL60 cells, even at a concentration of 50 µg/ml, show a better cell viability ($p<0.05$) than what

MCF7 cells demonstrated at 30 μg/ml. This may be due to sedimentation of *f*-CNTs during the period of the experiment, increasing their virtual concentration at the bottom of the well plate where adherent cells (MCF-7) cells grow. Inversely any reduction in *f*-CNT concentration in the medium helps in cell viability of suspension cells like HL60 cells. So this difference in cell viability between adherent and suspension cells can only be corroborated if the *f*-CNTs could be made completely soluble in the medium.

For all the samples tested in case of above MTT assays of MCF7 and HL60 cells, higher doses (30 μg/ml) of CNTs resulted in a lower cell viability compared to a lower dose (10 μg/ml) (**Figure 3.12, 3.13, 3.15**). In other words, dose dependent cytotoxic effect was observed for all the samples.

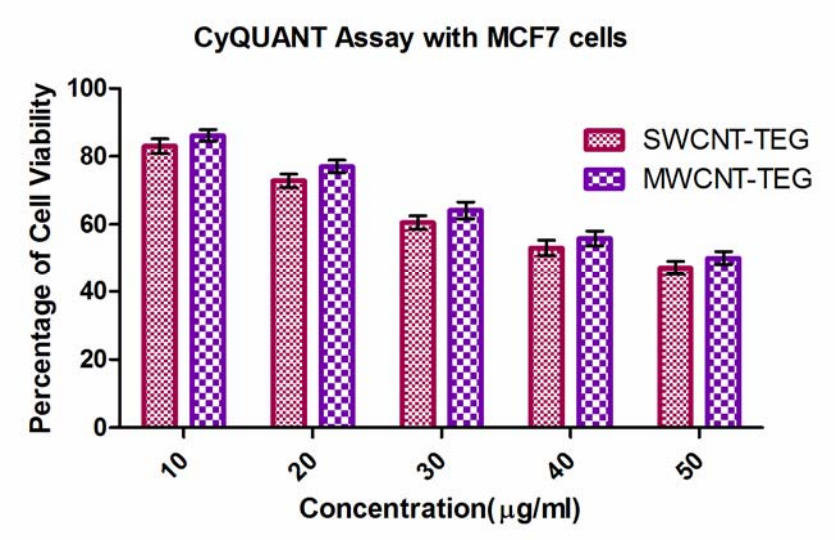

Figure 3.16: CyQUANT cell viability assay of MCF-7 cells after 24 hours exposure to **CNT-TEG** at five concentrations: 10μg/ml, 20μg/ml, 30μg/ml, 40μg/ml and 50μg/ml. The results were comparable to MTT assay result of CNT-TEG ($p>0.05$).

To confirm the above result, CyQUANT assay was carried out with **MCF-7** cells (**Figure 3.16**) using ***Compound 4*** (CNT-TEG), which followed similar pattern of cell viability seen in case of MTT assay. Although for each concentration, CyQUANT assay

showed better cell viability compared to MTT assay result, the difference was not significant ($p>0.05$).

3.5.2.3 CNTs' Length

We also investigated the influence of the tubes' length on cell viability, while concentration was maintained fixed at 20 μg/ml. For that purpose, we used tubes (both SWCNTs and MWCNTs) oxidized for different time period (3, 6, 9, 12 and 24 hours) as mentioned in **Figure 3.5**, **3.6** and **Table 3.3**.

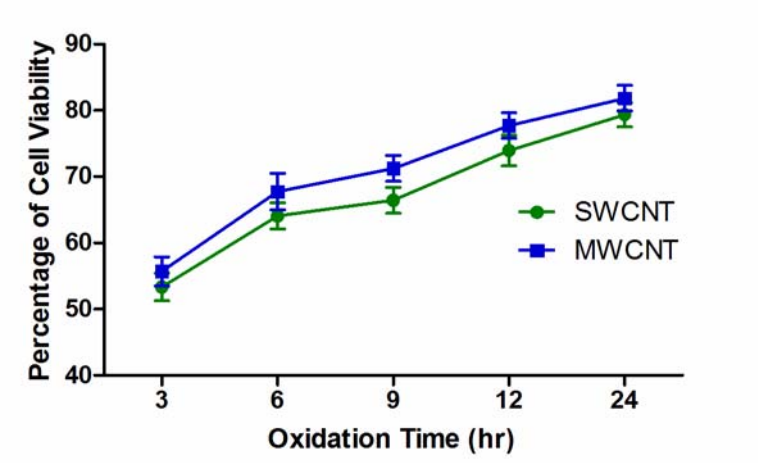

Figure 3.17: Percentage of cell viability of MCF-7 cells after 24 hour exposure to CNTs (20 μg/ml) oxidized for different time period: 3 hrs, 6 hrs, 9 hrs, 12 hrs and 24 hrs ($p<0.05$).

From **Figure 3.17,** it can be seen that CNTs subjected to longer oxidation time showed better ($p<0.05$) cell viability than the CNTs oxidised for shorter oxidation time. This was confirmed with both SWCNTs and MWCNTs but there was no significant difference ($p>0.05$) in percentage of cell viability between SWCNTs and MWCNTs oxidised for the same time period.

3.5.2.4 Purity

In our experiments, we used SWCNTs and MWCNTs with an initial purity of ≥ 90% and ≥ 95%, respectively. These pristine CNTs were not subjected to any purification process and they were most likely to contain the highest percentage of metallic catalysts

since the subsequent samples were all derived from CNTs treated with acids. Cell viability of MCF-7 cells decreased when concentration of pristine CNTs was increased from 10 μg/ml to 30 μg/ml. Even after oxidation, which is a known procedure aimed to increase their water dispersibility, the cytotoxic profile did not improve: cell viability was never above 65%, thus suggesting that CNTs without any long chain attached on their sidewalls, showed a remarkably negative effect (**Figure 3.12, 3.13**).

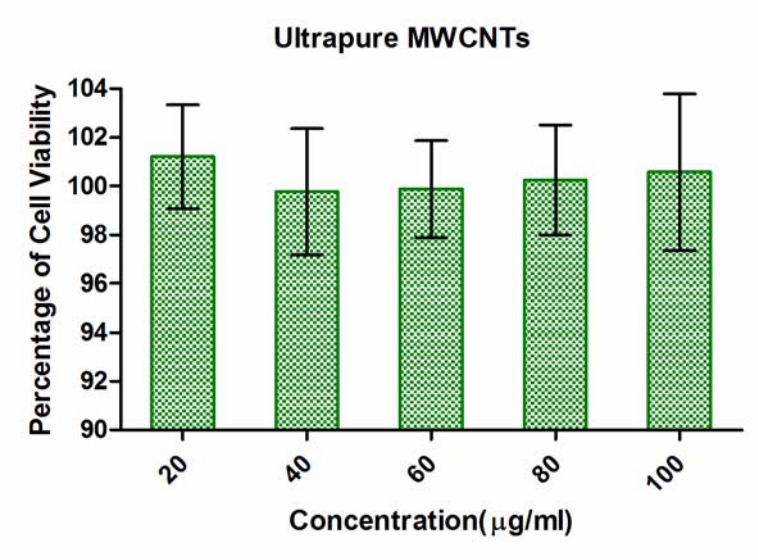

Figure 3.18: Percentage of cell viability as obtained by MTT assay of MCF-7 cells after 24 hours exposure to **Ultrapure MWCNTs** at the following concentrations: 20μg/ml, 40μg/ml, 60 μg/ml, 80μg/ml and 100μg/ml (P~1).

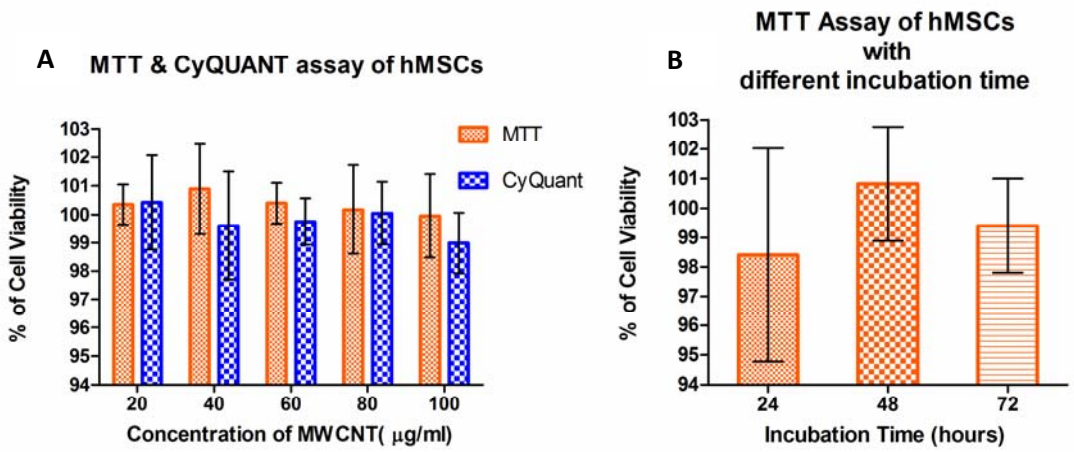

Figure 3.19: A) Percentage of cell viability as obtained by MTT and CyQUANT assays of hMSCs after 24 hours exposure to Ultrapure MWCNTs at the following concentrations: 20μg/ml, 40μg/ml, 60 μg/ml, 80μg/ml and 100μg/ml (p~1). **B)** MTT assay at different time frames (24, 48 and 72 hours) of hMSCs incubated at the highest dose (100μg/ml.). No cytotoxicity was observed in the range of incubation time period used for the purpose (p~1).

We also investigated cytotoxicity of ultrapure MWCNTs. As can be seen from the **Figure 3.18** and **3.19(A)**, the MTT assay of MCF-7 and hMSCs did not reveal any cytotoxicity in case of ultrapure-MWCNTs until a concentration of 100µg/ml; statistically negligible difference (p ~1) was detected in such range. To confirm the above result we did CyQUANT assay of ultrapure MWCNTs for hMSCs at the same range of concentrations used for above MTT assays. From **Figure 3.19 (A)**, it can be seen that the result is comparable to MTT assay results as no cytotoxicity was observed until 100µg/ml.

To further confirm this finding and to determine the cytotoxicity of Ultrapure MWCNTs with regard to different incubation times, we introduced ultrapure MWCNTs to hMSCs, 24, 48 and 72 hour prior to executing the MTT assay. The concentration of ultrapure MWCNTs used for the purpose was maintained at 100µg/ml for different incubation time periods. As can be seen from the **Figure 3.19 (B)**, there is no change in cell viability and hence no cytotoxicity is observed with hMSCs even at 72 hourr incubation with ultrapure MWCNTs.

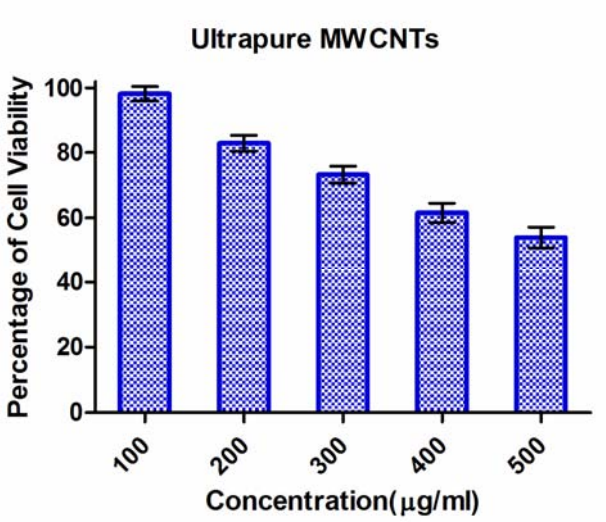

Figure 3.20: Cytotoxic profile of **ultrapure MWCNTs** after 24 hour exposure to MCF-7 cells at doses of 100, 200, 300, 400 and 500 µg/ml.

Due to the lack of toxicity for ultrapure-MWCNTs (Figs. **18, 19**), doses between 100 and 500 μg/ml were subsequently evaluated (Fig. **20**), with regard to MTT assay of MCF-7. It can be seen from Fig. **20**, that even at a concentration 15 times higher than the range 10-50 μg/ml of the other samples, the cytotoxic profile was improved: no sign of cell loss were detectable until 150μg/ml. Cell viability was below 60% only at doses above 400 μg/ml of ultrapure nanotubes.

On the whole, the combination of MTT and CyQUANT assays, Raman and EDS analyses clearly indicated the extent of purity of the different batches of CNTs, confirming that the presence of catalyst is the most influencing component affecting the quality of the samples. Hence, from the obtained results, we confirmed the promising exploitation of ultra-pure MWCNTs for biomedical applications.

3.6 DISCUSSION

CNTs are classified as "synthetic graphite" by the National Occupational Safety and Health Administration on the basis of the same hexagonal/honeycomb pattern (http://www.osha.gov/dts/chemicalsampling/data/CH_244000.html). However, they show physicochemical properties different from graphite and dependent on size, chemical composition, solubility, and aggregation (Donaldson, Aitken et al. 2006). These parameters can modify cellular uptake, protein binding and cause tissue damage. Many studies have assessed that CNTs are toxic, proposing some valuable reasons: small dimensions (which allow them to escape from normal phagocytic defences), hydrophobic nature (incompatible with biological fluids), impurities (difficult to remove even after their manipulation) and differences in CNTs dispersion (which might form sediments on the cell culture and therefore reduce cell viability) (Sato, Yokoyama et al. 2005; Garibaldi, Brunelli et al. 2006; Lacerda, Ali-Boucettal et al. 2008).

However, in the most of the cases, data showing toxicity had been obtained from non-functionalized samples, rather than ultrapure or chemically-modified nanotubes; therefore, we investigated both pristine tubes and samples subjected to further treatments of purification, functionalization, dispersibility and length control.

3.6.1 Surface and sidewall functionalization of CNTs

In the present study, we evaluated both surface charges and covalent functionalization on the tubes. In fact cationic liposomes demonstrated to improve cell uptake while lowering toxicity (De Rosa, De Stefano et al. 2008); in contrast, surface charges might alter blood-brain-barrier integrity, with concomitant modulation of toxic effects (Lockman, Koziara et al. 2004). In agreement with earlier studies done in this regard (Dumortier, Lacotte et al. 2006), we demonstrated that carbon nanotubes, once functionalized covalently, caused less cell damage. No remarkable effects were observed for the presence of charges on the surface (data not shown); on the contrary, toxicity inversely correlated with the length of water-soluble chains (e.g. PEG) attached (**Figure 3.12** and **3.13**), since PEG reduces the hydrophobic interactions among CNTs and favours their water dispersibility. Another factor that may have helped in water dispersibility of the functionalized CNTs is oxidation by sonication under strong acid condition, which not only narrows the tube's ranges in terms of length, but also helps in further purification of pristine CNT samples from residual metals and amorphous carbon during the extensive washing and filtration process associated with it.

Interestingly, pristine SWCNTs displayed higher cell viability than MWCNTs, but such difference became less obvious after oxidation ($p>0.05$) and it even reversed with hydrophilic chains; hence, PEG-CNTs showed a better profile than TEG-CNTs ($p<0.05$) and PEG-MWCNTs displayed less cell loss than PEG-SWCNTs ($p>0.05$) (Fig. **12** and

Fig. **13**). Therefore, as the number of ethylene-oxide groups increased, cell viability showed a better correlation with water dispersibility. Conversely, pristine CNTs, being the most hydrophobic, had the worst toxicological profile. This result is in accordance with the previous observation pertaining to more hydrophobic molecules leading to greater cell toxicity due to their higher propensity to interact with the hydrophobic membrane (Nimmagadda, Thurston et al. 2006).

3.6.2 CNTs' concentration

In agreement with other studies (Magrez, Kasas et al. 2006; Nimmagadda, Thurston et al. 2006; Sayes, Liang et al. 2006), incubation at different concentrations showed a direct correlation between cell loss and doses used. However, with ultrapure-CNTs we assisted to an incredible effect: no appreciable difference ($p\sim1$) was observed between a dose of 10μg/ml and that of 100μg/ml (**Figure 3.18, 3.19**). This impressive result induced us to increase the concentrations till toxicity was observed: for that purpose, we investigated the effect until 500μg/ml, and the results have been discussed in the paragraph of purity.

3.6.3 CNTs' dispersibility

Any cell evaluation needs a medium to dissolve the sample. Physiological solutions are the most appropriate, but sometimes the low solubility of carbon material requires organic solvents. It has already been reported that human keratinocytes, once exposed to nanotubes, displayed cell death (Manna, Sarkar et al. 2005). This was attributed to oxidative stress within cells and to activation of NF-*k*B factor. However in that particular case dimethylformamide was used to dissolve the samples and it might have induced some alterations, since it is a toxic solvent, which should be avoided in cell manipulation. In our experiments we used DMSO and maintained its' concentration as low as 1% (v/v)

to avoid any deceptive result. DMSO, together with CNTs' functionalization, improved the tubes' dispersibility, indicating the maximum weight of nanotubes that could be added with minimal formation of aggregates (**Table 3.5**). As aggregates of *f*-CNTs may also result in cell death (Raja, Connolley et al. 2007) leading to decrease in cell viability, therefore extreme care was taken to avoid formation of aggregates.

Moreover, better dispersibility and loading were observed for *f*-MWCNTs in comparison with *f*-SWCNTs, suggesting that further sidewall functionalization caused an increase in *f*-CNTs concentration that could form stable suspensions.

3.6.4 Length

In addition to the above-mentioned factors, length could influence the toxicity of CNTs. It has been previously demonstrated that shorter CNTs (220 nm) displayed lower inflammation compared to longer CNTs (825 nm) (Sato, Yokoyama et al. 2005).

Therefore, CNTs were subjected to strong acidic conditions to generate tubes with lengths inversely proportional to the oxidizing times (**Table 3.3**). It is worth mentioning that for TEM analysis (**Figure 3.5**), we on purpose focused on MWCNTs, since a long sonication time in strong acidic environment might result in excessive cutting, leading to loss of tubular structure of SWCNTs (Colomer, Piedigrosso et al. 1998; Kam, Jessop et al. 2004). In fact images on SWCNTs treated beyond 9 hours (**Figure 3.6D**) resulted in too small fragments, comparable to those reported after 24-hour oxidation of MWCNTs (**Figure 3.5F**).

As indicated in **Figure 3.5**, **3.6, 3.17**, the longer the incubation time, the shorter the tube length and the higher the cell viability. Surprisingly, there was no remarkable difference between cytotoxicity of SWCNTs and MWCNTs, even though their structure was much different after 9 hours. This result suggests that high aspect-ratio is not a

favourable parameter in enhancing cell viability, since cells demonstrated to prefer fragmented tubes.

In previous studies it was reported that MWCNTs with diameters of 60-100 nm, induced more serious cytotoxicity on alveolar macrophages in comparison to smaller diameters (<60 nm)(Bai, Wang et al. 2007). Conversely, toxicity of SWCNTs with a mean diameter of 1.4 nm was much higher than MWCNTs of 10-20 nm, with serious damage of alveolar macrophages at doses as low as 0.38μg/ml (Jia, Wang et al. 2005). In our case there was no clear indication of the effect of the diameter on cell viability (**Figure 3.17**), as there was no significant difference in cell viability between MWCNTs and SWCNTs. Hence we conclude that tubes' diameter does not play a crucial role in the cytotoxic profile.

3.6.5 Purity

Methods of CNTs production involve the use of metals as catalysts (Flahaut, Durrieu et al. 2006) which, if present in high amount, enhance toxicity (Jia, Wang et al. 2005). An example of a commonly used metallic catalyst, iron results in oxidative stress to the cells (Kagan, Tyurina et al. 2006).

Studies were performed with SWCNTs and MWCNTs with initial purity ≥ 90% and ≥ 95%, respectively. When compared with MWCNTs, pristine SWCNTs exhibited a better toxicological profile as indicated by the higher cell viability for each tested concentration, but after oxidation the corresponding values were totally comparable, perhaps because of a slight improvement in the dispersibility of oxidized-MWCNTs ($0.05<p<0.1$).

Interestingly, one of our samples (so called ultrapure MWCNTs), without catalysts (the initial $MmNi_3$ was not detected once subjected to thermo gravimetric analysis) and negligible amorphous carbon (Rakhi, Sethupathi et al. 2008), showed no sign of toxicity (**Figure 3.18, 3.19**) in case of both tumoral cell line (MCF-7) and normal cell line (hMSCs); for that reason, doses were increased, and the first evidence of toxicity was detected only at concentrations above 150 μg/ml (**Figure 3.20**).

Recently, it has also been proposed Raman spectroscopy to evaluate the purity of CNTs, whose characteristic bands show deviation from common values in case of impurities (Kawamoto, Uchida et al. 2006). In our samples, MWCNTs showed slight changes, while ultrapure-MWCNTs were not affected, thus confirming the absence of either metal catalysts or amorphous carbon inside the tubes (**Figure 3.11**). This was further confirmed by the quantitative elemental analysis of these CNT samples by EDS: ultrapure MWCNTs were completely devoid of catalytic elements, while the same was not true with regard to commercial CNTs (**Figure 3. 9, 3.10)**. The x-ray spectra showed presence of iron, cobalt and molybdenum, thus confirming a lower purity of these samples (**Table 3.6**).

To our knowledge, very less information is available in the literature with regard to toxicological profiles testing such high doses, analogue compatibility with cells *in vitro* and high purity by Raman analysis and EDS, suggesting that further functionalizations could be introduced in the "ultrapure" sample for a better cell targeting but without harmful consequences. This result not only allowed us to identify the sample's purity as the most crucial parameter that is responsible for the toxicity of CNTs, but it also encourages further application of these non-toxic nanomaterials in the field of nanomedicine.

3.7 CONCLUSIONS

Even though in the last decade carbon nanotubes have shown exquisite properties and encouraging results, they still present a fundamental aspect that has limited their widespread applications: none among their characteristics in term of structure, size and composition can be ascertained with unquestionable certainty. Manufactured samples present huge differences and their further modification, through chemical procedures, enhances their diversity. Therefore, it becomes extremely important to identify the dependence from a particular property, in order to obtain more reproducible results. This chapter of the thesis offers an overview on the latest findings derived from *in vitro* studies of pristine or functionalized carbon nanotubes. In particular, it emphasizes the major factors responsible for their toxicity, such as CNTs' length, functionalization, purity and dispersibility. Different samples, cell lines, cell viability methods, and polar chains have also been evaluated and compared with the data reported in literature. The results from our study have shown that when the surface chemistry of CNTs is modified via attachment of water soluble chains, there is an improvement in the toxicological profile. In addition, it has emerged that the purity of the sample represents the most crucial parameter that is able to guarantee a safe application of this material in biology and medicine. For those samples that did not present any sign of toxicity, we increased concentrations until doses that have been hardly ever documented. That strengthens the importance of our results and offers new opportunities of functionalization for a selective cell targeting.

In conclusion, it has emerged that for the safe application of CNTs, ultra-pure material should be employed and, in any case, human and environmental health evaluations of different carbon nanomaterials must be considered in depth.

Chapter 4

Application of Carbon Nanotubes as Suitable Scaffold Material for Osteoblast Proliferation and Bone formation

4.1 INTRODUCTION

Tissue engineering is an emerging multidisciplinary field involving biology, medicine, and engineering. It is likely to revolutionize the ways to improve the health and quality of life for millions of people worldwide by restoring, maintaining or enhancing tissue and organ functions (NIH, USA). It is associated with interesting therapeutic applications, where the tissue is either grown inside a patient's body or built outside the patient and subsequently transplanted. Alternatively, tissue engineering can be exploited in terms of diagnostic applications, where the tissue is grown *in vitro* and used for testing drug metabolism and uptake, toxicity, and pathogenicity.

4.1.1 Bone Tissue Engineering

Every year, millions of people are suffering from bone defects arising from trauma, tumor or bone related diseases and the lack of suitable bone tissue is responsible for a not-negligible increase in morbidity and even mortality (Murugan and Ramakrishna 2004). Current therapies for critical-sized bone defects such as hip fracture, malignant bone lesions, bone trauma and congenital defects, or bone substitutes include autologous bone (from the patient), allogeneic bone (from a donor), demineralised bone matrices, and metal implants (Swetha, Sahithi et al. 2010). Although improving life expectancy remarkably, these approaches are still facing many limitations and problems.

Since the late 1980s, the use of autologous bone grafts has been the preferential choice for bone repair and regeneration (de Boer 1988; Damien and Parsons 1991; Coombes and Meikle 1994; Yaszemski, Payne et al. 1996). A patient's own bone lacks immunogenicity and provides bone-forming cells, which are directly delivered at the implant site. Moreover, autologous bone grafts recruit mesenchymal cells and induce

them to differentiate into osteogenic cells through exposure to osteoinductive growth factors (Urist 1965; Brown and Cruess 1982; Damien and Parsons 1991; Lane, Tomin et al. 1999). Although there are many advantages deriving from the use of autologous bone, there are major drawbacks especially in the harvesting procedures: not only there are limited sites where bone may be harvested without loss of function (Enneking, Eady et al. 1980; Brown and Cruess 1982), but also the extra surgery involved in harvesting autologous bone causes morbidity at the donor site (Brown and Cruess 1982; Damien and Parsons 1991; Koole 1994; Lane, Tomin et al. 1999), post-operative continuous pain (Cowley and Anderson 1983; Prolo and Rodrigo 1985; Damien and Parsons 1991; Arrington, Smith et al. 1996), hypersensitivity (Damien and Parsons 1991), pelvic instability (Coventry and Tapper 1972; Cowley and Anderson 1983; Arrington, Smith et al. 1996), infection (Arrington, Smith et al. 1996; Lane, Tomin et al. 1999), and paraesthesia (Damien and Parsons 1991; Lane, Tomin et al. 1999). These complications affect 10% to 30% of the patients (Arrington, Smith et al. 1996). Moreover, the amount of bone that can be collected is limited. Hence there has been a search for alternatives for several decades.

A possible solution is represented by the use of allografts (from human to human), which eliminates the harvesting of tissue from patient and the quantity of available tissue is no longer an issue. Nevertheless, the quality of allografts is worse than that of autologous grafts. Allografts have a poor degree of cellularity, less revascularisation, and a higher resorption rate compared to autologous grafts (Lane, Tomin et al. 1999), resulting in a slower rate of new bone tissue formation, as observed in several studies (Oikarinen and Korhonen 1979; Prolo and Rodrigo 1985; Oklund, Prolo et al. 1986; Anderson, Dhert et al. 1999). In addition, the immunogenic potential of these allografts

and the risks of virus transmission to the recipient are serious disadvantages (Oikarinen and Korhonen 1979; Coombes and Meikle 1994; Strong, Friedlaender et al. 1996).

Although processing techniques such as demineralisation, freeze-drying, and irradiation have been shown to reduce the patient's immune response, these procedures also alter the structure of the graft and reduce the potential to induce bone healing (osteoinductivity), while the occurrence of disease transmission still remains (Damien and Parsons 1991). Similarly, metals such as iron, cobalt and titanium may be permanently implanted in bone to fill a defect and provide internal fixation. However, fatigue, corrosion, tissue infections, poor implant-tissue interface and stress-shielding effects create many problems for patients (Bobyn, Mortimer et al. 1992; Mistry and Mikos 2005). To overcome these drawbacks of the current graft materials and metal implants, new bone tissue engineering approaches have been suggested as promising techniques for reconstructing bone defects.

Bone tissue engineering aims to control and guide bone regeneration in order to restore structure and function of a defect by utilizing the body's natural healing response. It may provide functional substitutes of native tissues, to serve not only as grafts for implantation (Langer and Vacanti 1993), but also as physiologically relevant models for controlled studies of cell function and bone development (Freed and Vunjak-Novakovic 2000). Three essential elements in bone tissue engineering are:

1. **Cells**: They constitute the living tissue in bone and are responsible for mineral deposition. They can be exploited by (a) developing methodologies for the proliferation and their differentiation; (b) their acquisition from appropriate source (such as autologous cells, allogeneic cells, xenogeneic cells, stem cells, genetically engineered cells) and (c) their immunological manipulation.

2. **Biomolecules**: They comprise of angiogenic factors, growth factors (dexamethasone, L-glutamine and ascorbic acid etc.), osteoinductive and osteogenic proteins e.g. BMP-2, which help in accelerating cell differentiation into osteoblastic lineage and osteoblast functions.

3. **Biomaterials & scaffolds**: They provide the optimal microenvironment conducive for bone growth (Langer and Vacanti 1993; Meinel, Karageorgiou et al. 2004). These novel biomaterials need to be designed to direct the organization, growth, and differentiation of cells in the process of forming functional bone tissue by providing both physical and chemical cues.

4.1.1.1 Stem Cells in Bone Tissue Engineering

Modern tissue engineering strategies tend to combine scaffold materials with living cells to develop biological substitutes that can restore tissue functions (Sittinger, Bujia et al. 1996; Vacanti and Langer 1999; Khademhosseini, Vacanti et al. 2009). The cells are important to build new tissue through extracellular matrix synthesis (Bonassar and Vacanti 1998). While proliferating, they fill up the scaffold and grow into a three-dimensional tissue (Schultz, Sittinger et al. 2000; Moroni, de Wijn et al. 2008).

Generally tissue specific cell types are not always available in sufficient amounts to guarantee complete recovery of damaged tissue; therefore stem cells (**Figure 4.1**) embody a striking alternative for tissue engineering. Embryonic stem cells or the reprogrammed induced pluripotent stem cells (iPS) are pluripotent, but they are also prone to tumour formation. Until now, adult stem cells, such as mesenchymal stem cells (MSCs) (**Figure 4.2**), are considered to be the most promising, since they have a high differentiation

potential (**Figure 4.3**) in to diversified lineages without being tumorigenic (Zippel, Schulze et al. 2010)

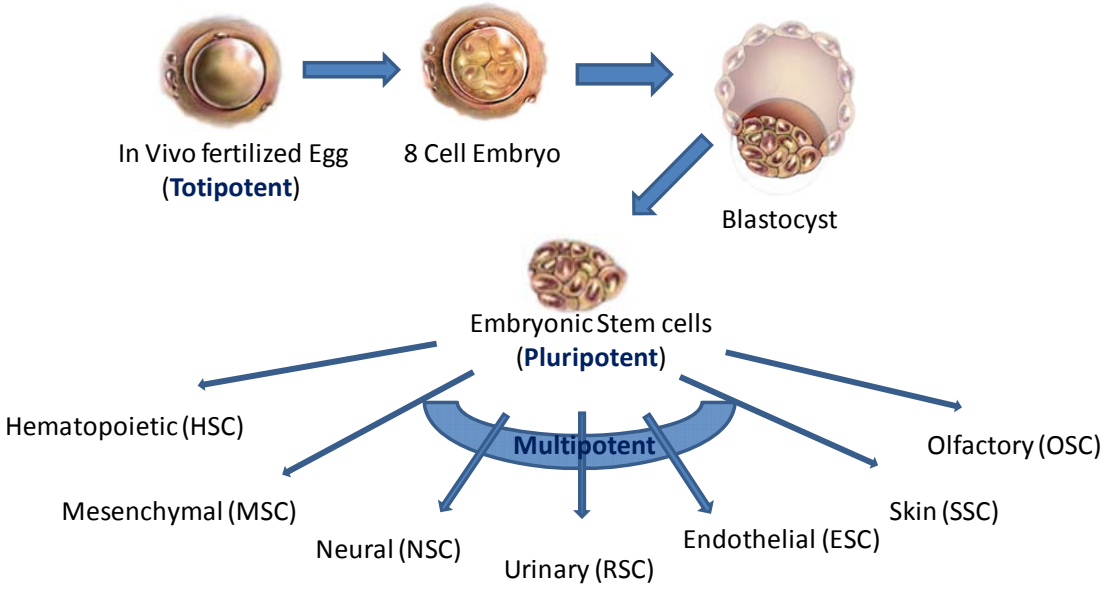

Figure 4.1: Schematic diagram of generation and fate of different kind of stem cells.

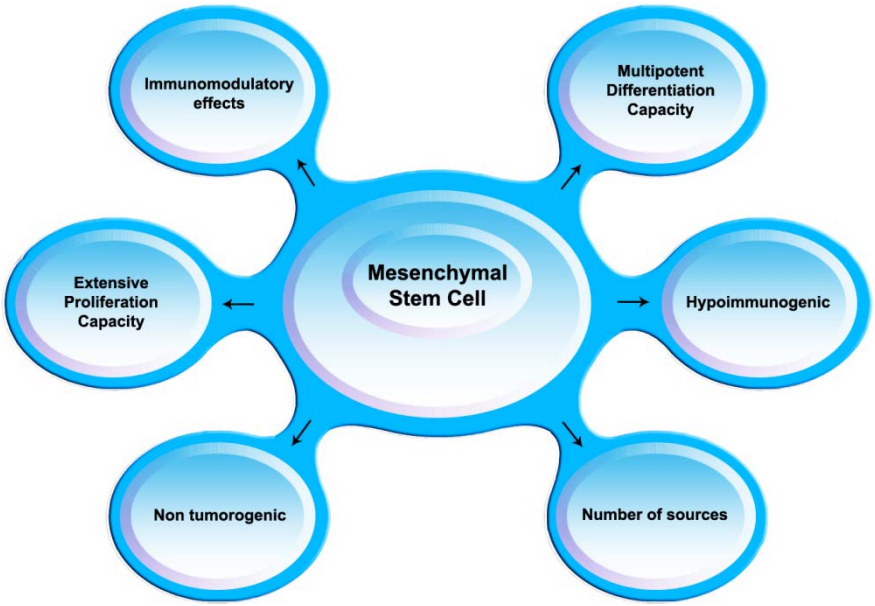

Figure 4.2: Therapeutically significant properties of MSCs. MSCs can be isolated from a number of sources and they are capable of *in vitro* expansion, differentiation and transdifferentiation. They do not express MHC class II and co-stimulatory molecules (CD40, CD80 and CD86) preventing immune response upon transplant and inhibit immune cell (B cells, T cells, natural killer cells and dendritic cells) proliferation and activation. Their ability to respond to damage signals such as chemokines aids in homing to the injured sites, and enhance tissue repair by facilitating recruitment of endothelial cells and macrophages by secretion of angiogenic and chemotactic factors (Satija, Singh et al. 2009).

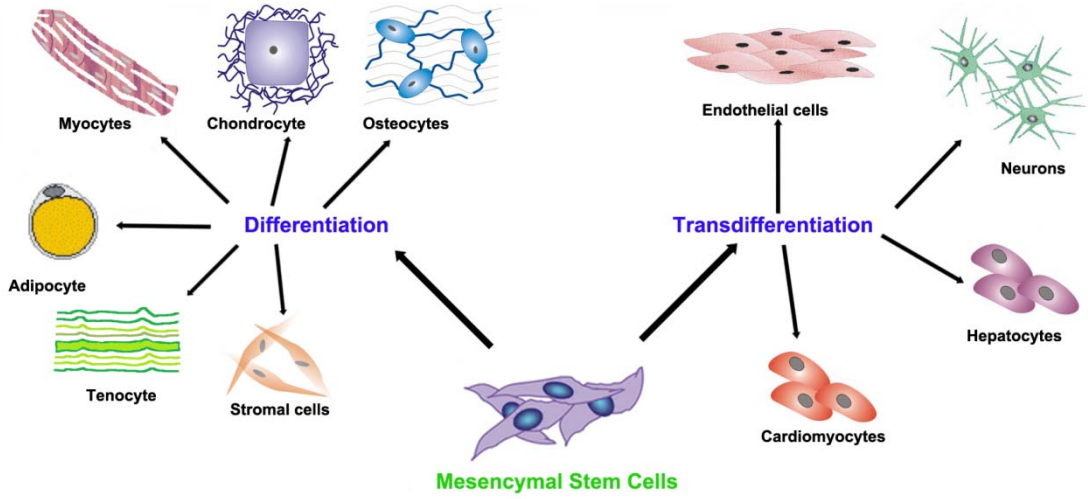

Fig. 4.3: Differentiation and trans-differentiation capability of MSCs to various cell lineages (Satija, Singh et al. 2009).

Bone marrow harbours cells of haematopoietic and non-haematopoietic lineages and their precursors, known as stem/progenitor cells. The non-haematopoietic stem/progenitor cell compartment contains mesenchymal stem cells (MSCs), which are involved in remodelling of the mesenchymal tissues throughout adult life. Although generally isolated from the bone marrow (Pittenger, Mackay et al. 1999), these multi-potent cells have also been isolated from peripheral blood (Zvaifler, Marinova-Mutafchieva et al. 2000), periosteum (De Bari, Dell'Accio et al. 2001), umbilical cord blood (Lee, Kuo et al. 2004), synovial membrane (De Bari, Dell'Accio et al. 2001), trabecular bone (Tuli, Tuli et al. 2003), adipose tissue (Boquest, Shahdadfar et al. 2005), limbal stroma (Polisetty, Fatima et al. 2008), amniotic fluid (in 'tAnker, Scherjon et al. 2003), lung (Martin, Helm et al. 2008), dermis and muscle (Young, Steele et al. 2001). Due to lack of specific markers, these isolated MSCs can only be functionally characterized on the basis of their ability to differentiate and transdifferentiate into different cell types (**Figure 4.3**) such as

osteoblasts, chondrocytes, adipocytes, cardiomyocytes, hepatocytes, endothelial cells and neuronal cells in culture upon induction with specific medium (da Silva Meirelles, Caplan et al. 2008). However, phenotypically they are defined as positive for CD105, CD73, CD90, CD166 and CD44, and negative for haematopoietic markers like CD34, CD45, CD11b and CD19 (Dominici, Le Blanc et al. 2006). Such immense differentiation potential or plasticity, coupled with their ability to modulate the activity of immune cells, makes them attractive for stem cell-based therapy aimed at treating previously incurable disorders (Satija, Singh et al. 2009). Capitalizing on the extraordinary properties of MSCs to differentiate into osteocytes, several experimental and preclinical studies have been undertaken to evaluate their potential for bone tissue engineering.

4.1.1.2 Growth and Differentiation Factors in Bone Tissue Engineering

For bone regeneration therapy to be successful, adequate mesenchymal precursor cells must be either recruited or implanted directly to the damaged sites, and these cells must be given appropriate signals to replicate, differentiate (MSC→Preosteoblast→Osteoblast) and accomplish normal osteoblastic functions (adhesion, proliferation, mineralization, etc.) in a controlled manner (Dee and Bizios 1996; Atala, Lanza et al. 2008). For in-vivo bone formation, recruitment, replication, differentiation, and regulation of osteoblastic cells are mediated by circulating (systemic) and locally produced growth factors and osteogenic inducers (Dee and Bizios 1996). But for in-vitro bone formation on a predetermined scaffold as in case of bone tissue engineering, these biochemical agents must be provided in appropriate concentration to imitate the in-vivo microenvironment. There are a number of bone-related growth/differentiation factors, including insulin-like growth factor, acidic and basic fibroblast growth factor, platelet derived growth factor, and the members of the

transforming growth factor-β (TGFβ) superfamily, which regulate osteoblast functions (Mohan and Baylink 1991; Baylink, Finkelman et al. 1993; Mundy 1993).

The bone morphogenetic proteins (BMPs) are members of the transforming growth factor-β superfamily, which consists of a group of related peptide growth factors. More than 40 related members of this family have been identified, including 15 BMPs (de Caestecker 2004). They are further divided into subfamilies according to their amino acid sequence similarities. BMPs consist of dimers that are interconnected by seven disulfide bonds. This dimerization is essential for bone induction. BMPs are active both as homodimers that consist of two identical chains, and as heterodimers consisting of two different chains (Granjeiro, Oliveira et al. 2005). Compared to other known BMPs, BMP-2 (Boyne, Lilly et al. 2005) and BMP-7 (Vaccaro, Patel et al. 2005) have the most robust osteoinductive activity as observed in both preclinical animal studies and in human trials. They have received much attention due to their ability to promote bone formation both in vitro and in vivo (Atala, Lanza et al. 2008). Additionally they also stimulate alkaline phosphatase activity and collagen synthesis by osteoblastic cells in vitro and promote chondroblastic and osteoblastic differentiation including formation of mineralized matrix by osteoblast (Dee and Bizios 1996).

4.1.1.3 Biomaterials for bone tissue engineering

Biomaterials play a pivotal role in the success of tissue engineering approaches; as they guide the shape and structure of developing tissues, provide mechanical stability and present opportunities to deliver inductive molecules to transplanted or migrating cells (Davis and Leach 2008). Therefore, the selection of the appropriate biomaterial can have a profound impact on the quality of newly formed tissue. But the fact that very few

biomaterials possess all the characteristics necessary to perform ideally, the identification of materials capable of promoting the desired cellular and tissue behaviour is still a major challenge facing the field of tissue engineering. To alleviate this problem engineers and clinicians alike have been pursuing the development of hybrid or composite biomaterials to synergize the beneficial properties of multiple materials in to a superior matrix. Particularly the combination of natural and synthetic polymers with various other materials has demonstrated the ability to enhance cellular interaction, encourage integration into host tissues, and provide tuneable material properties and degradation kinetics (Davis and Leach 2008). In this chapter of my thesis we have selected and utilized polyethylene glycol (PEG) conjugated multiwall carbon nanotubes (MWCNTs) as a composite biomaterial to promote the osteogenic differentiation of human mesenchymal stem cells (hMSCs) and simultaneous bone matrix mineralization.

Currently, most artificial scaffolds used in bone implants are made of polymers and peptide fibres. However, these materials have relatively low strength and are often susceptible to immune rejection (Veetil and Ye 2009). The discovery of carbon nanotubes (CNTs) and their extraordinary physical and chemical properties have fuelled intense research and paved way for recent developments of CNT-based tissue engineering. There are several unique properties of CNTs that make them suitable materials for bone scaffolds. Although having density similar to that of graphite, which is much lower than steel or other metal implants, CNTs are the strongest known material on earth (Yu, Files et al. 2000). Coupled with their excellent flexibility and elasticity, CNTs can potentially improve the mechanical properties of bone implants and may find a permanent mechanical role in bone regeneration. Besides, having a one-dimensional thread-like structure, CNTs are ideal materials for the manufacturing of composite scaffolds

(Zanello, Zhao et al. 2006). Hence, CNTs can be incorporated to enhance the mechanical properties of some biomaterials that are currently used in bone regeneration: an example is polymethyl methacrylate (PMMA), a common polymer material for bone cement and dental prostheses. Researchers have found that the incorporation of MWCNTs favourably alters the static and fatigue mechanical properties of this acrylic bone cement. It is also discovered that augmentation of the bone cement with CNTs offers thermal benefits and improves the longevity of the implants. Usually, the temperature in the bone-cement interface inside the body is elevated leading to hyperthermia based destruction of bone adjacent to cement mantle. The presence of MWCNTs in the bone cement can significantly reduce the high temperatures at cement-bone interfaces during *in vivo* polymerization. This can be attributed to the high thermal conductivity of CNTs (Marrs, Andrews et al. 2006).

On top of that, it has been found that the elevated surface roughness of scaffold constructs, due to the presence of CNTs, can lead to greater protein adsorption and enhanced cell adhesion, which may be responsible for increased osteoblast proliferation and differentiation (Hatano, Inoue et al. 1999; Khang, Kim et al. 2007).

Studies on a CNT-reinforced porous polyurethane nanocomposite scaffold have revealed another promising aspects – apart from improving the physical properties, due to the changes in surface chemistries and nanoscale architectures, it was found that there is an increased level of production of vascular endothelial growth factor—a potent angiogenic factor—in proportion to the CNT loading in the scaffold (Jell, Verdejo et al. 2008). This may signify more favourable cell growth in engineered tissues using CNT as scaffold, provided that angiogenesis is not implicated in any pathologic consequence.

Similarly PEG in form hydrogels was found to enhance cell viability of hMSCs (Jongpaiboonkit, King et al. 2009) and stem cells photoencapsulated with PEG hydrogels have shown homogeneous deposition of neocartilage when induced for chondrogenic differentiation (Elisseeff, Puleo et al. 2005). Furthermore, Briggs et al. (Briggs, Treiser et al. 2009) observed up regulation of osteogenic markers as demonstrated by alkaline phosphatase activity and ostocalcin expression when hMSCs were grown on polycarbonates copolymerized with 3% PEG. Therefore in this chapter of my thesis we have selected and utilized PEG-conjugated multiwall carbon nanotubes (MWCNTs) as a composite biomaterial to assess the osteogenic differentiation of human mesenchymal stem cells (hMSCs) and the eventual bone matrix mineralization.

4.2 OBJECTIVE

The aim and objective of this study was to prepare biocompatible scaffolds in the form of thin films of pegylated, ultrapure carbon nanotubes to support hMSCs growth, proliferation and specific differentiation into bone forming osteoblast cells. Furthermore, we intended to demonstrate that a compact and uniform thin film of PEG functionalized carbon nanotubes having nanometric irregularities can provide suitable microenvironment for differentiation of hMSCs into osteogenic lineage, without the need of any additional growth factor.

4.3 MATERIALS

4.3.1 Chemicals

Ultrapure-MWCNTs were kindly provided by Professor Ramaprabhu (Nano-Functional Materials Technology Centre (NFMTC), Indian Institute of Technology, Chennai, India). Unless otherwise mentioned, all chemicals and reagents were obtained from Sigma-Aldrich as the highest available grades.

4.3.2 Cell lines & culture medium

Human mesenchymal stem cells (hMSCs), passage 1 were obtained courtesy of Assistant Professor Rachel Ee of Department of Pharmacy, National University of Singapore.

4.3.2.1 Preparation of medium for hMSCs

Low-glucose Dulbecco's modified eagles' medium (powder, Sigma) along with 3.706g of sodium bicarbonate was dissolved in 700ml of MilliQ water. The volume was made up to 870ml using MilliQ water (produced using Millipore's Synergy water purification system with cartridge Simpak2) and filtered through 0.2 μm membrane (Millipore). This was added with 10 ml of sterile solution of non-essential amino acids, sodium pyruvate and penicillin/streptomycin (GIBCO) each and 100 ml of sterile fetal bovine serum (Invitrogen) to make 1 litre of medium. The whole medium was stored at 4 ºC for further use.

4.3.2.2 Preparation of osteogenic medium

The osteogenic medium was prepared following known procedure (Im, Shin et al. 2005) and according to the formula depicted below (**Table 4.1**). BMP-2 (150 ng/ml) was

added to the medium whenever required according to the experiment. The following stock solutions of essential reagents were made to formulate the osteogenic medium.

Dexamethasone: About 3.92mg of dexamethasone were dissolved in 10 ml of ethanol to make a 10^{-3} M solution.10^{-3} M dexamethasone solution was diluted 1:100 times with PBS to make stock of 10^{-5} M solution. Finally it was filtered and stored at -20ºC as single use aliquots.

Ascorbic acid: 10mg of ascorbic acid powder was dissolved in 2 ml PBS. It was then filtered and stored at -20ºC away from light.

Beta-glycerophosphate: About 0.612 g of beta-glycerophosphate was dissolved in 10 ml PBS. It was then filtered and stored at -20ºC.

BMP-2 (Invitrogen): 10 µg (1 vial) of lyophilized powder was added to filtered PBS solution containing 4mM HCl and 0.1% BSA.

Materials	**Volume (ml)**	**Stock Concentration**	**Final Concentration**
DMEM+10% FBS+1% pen/strep	9.2	-	-
L-glutamine	0.1	100x	-
Ascorbic acid	0.1	5 mg/ml	50 µg/ml
Beta-glycerophosphate	0.5	0.2M	10mM
Dexamethasone	0.1	10^{-5}M	10^{-7}M

Table 4.1: Preparation of Osteogenic induction medium

4.3.3 Antibodies & markers

Goat anti mouse antibody conjugated with FITC was purchased from Biolegend, San Diego, California (USA). Markers (osteocalcin and CD44) were purchased from Acris Antibodies GmbH (Germany).

4.4 METHODS

4.4.1 Functionalization of MWCNTs and characterization

Ultrapure multiwalled carbon nanotubes (MWCNTs) were functionalized following the procedure reported elsewhere (Zhao, Hu et al. 2005) and illustrated in **Figure 4.4**. The extent of oxidation of MWCNTs, loading with PEG and dispersibility were determined by transmission electron microscopy (TEM), thermogravimetric analysis (TGA) and dispersibility study, respectively.

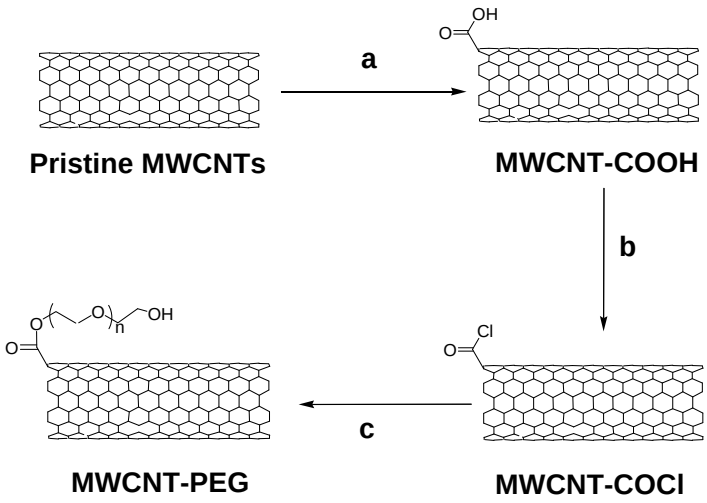

Figure 4.4: Schematic representation of the synthesis of MWCNT-PEG from pristine MWCNT. **(a)** HNO_3/H_2SO_4 (v/v, 1:3), sonication for 6 hrs, **(b)** $(COCl)_2$ (2hrs at 0ºC, 2 hrs at rt, 17 hrs at 70ºC), **(c)** PEG (100 ºC, 5 days).

4.4.1.1 Synthesis of oxidized-CNTs (MWCNT-COOH)

Ultrapure MWCNTs (500 mg) were oxidized following the procedure mentioned in **chapter 3** (**Section 3.4.1**, page number **37**), as already reported by Wu *et al* (Wu, Wieckowski et al. 2005).

4.4.1.2 Synthesis of MWCNT-COCl

500 mg of oxidized MWCNT powder were sonicated in 170 ml of Dimethylformamide (DMF, Fisher Scientific) for 2 hrs. 20 ml of oxalyl chloride were added drop wise to the suspension at 0°C under N_2 and the mixture was stirred at 0°C for 2 hrs and then at room temperature for another 2 hrs. The temperature was then raised to 70 °C, and the mixture was stirred overnight, after which the excess of oxalyl chloride was removed by evaporation under vacuum.

4.4.1.3 Synthesis of MWCNT-PEG

5 g of polyethylene glycol (PEG, MW = 600, 1.128 g/ml, 8.47mmols) were added to the suspension of 500 mg of MWCNT-COCl in 500 ml of DMF and the mixture was stirred at 100 °C for 5 days. After cooling to room temperature, the mixture was filtered through a 0.2 μm pore-size PTFE filter membrane (Millipore) and washed thoroughly with ethyl alcohol and finally distilled water. A black solid – PEGylated MWCNTs collected on the membrane was dried overnight under vacuum.

4.4.2 Transmission electron microscopy

Functionalized-MWCNTs (*f*-MWCNTs) were examined under transmission electron microscopy (TEM) using a JEOL JEM 2010F microscope (**Figure 3.7** in **chapter 3**). The samples were prepared on 200 mesh copper grids coated with formvar.

Length and diameter measurement calculations, based on microscopic scale, were performed using Image J software (U.S. National Institute of Health).

4.4.3 Extent of functionalization of *f*-MWCNTs

The extent of oxidation of MWCNTs and loading with PEG were determined by thermogravimetric analysis (TGA). From the obtained data, the initial weight percentage of metal residue was 4.2%, indicating the high purity of our starting material. After oxidation, such content further decreased to 2.4% for MWCNT-COOH, and 1.7% for MWCNT-PEG. On the basis of these values, the loading and the fraction of carbon atoms in the samples that became functionalized with PEG chain in the MWCNT-PEG complex were estimated. We estimated the loading of MWCNTs in MWCNT-PEG to be about 70.3%. Since the molecular weight of PEG used in this work was about 600, the degree of functionality in MWCNT-PEG in terms of molar functionality was equal to (29.7/600)/ (70.3/12) = 0.8%.

4.4.4 Dispersibility study

MWCNT-COOH and MWCNT-PEG samples of varying concentrations (ranging from 5μg/ml to 25 mg/ml) were prepared in 1.5 ml microcentrifuge tubes and subjected to 2 hrs of sonication. Samples were allowed to stand at room temperature. At 1 hr, 5 hrs and 24 hrs, samples were checked for any sedimentation, which indicated the eventual instability of the dispersion at particular concentrations.

4.4.5 Coating of cover slips and their characterization

4.4.5.1 Coating of cover slips with PEG-functionalized CNTs

Lyophilized samples of PEG-functionalized (MWCNT-PEG) and oxidized nanotubes (MWCNT-COOH), along with only PEG sample were individually sonicated in milliQ water to obtain a 10 mg/ml suspension. The suspension was sprayed with an airbrush (Badger^{TM} 100LG model) onto round glass cover slips (12 mm diameter, Electron Microscopy Sciences), which had been previously heated up to 160°C to allow the fabrication of uniform films (Malarkey, Fisher et al. 2009) (**Figure 4.5**). Coated cover slips were allowed to dry in air and were used for cell culture after sterilization with UV irradiation overnight.

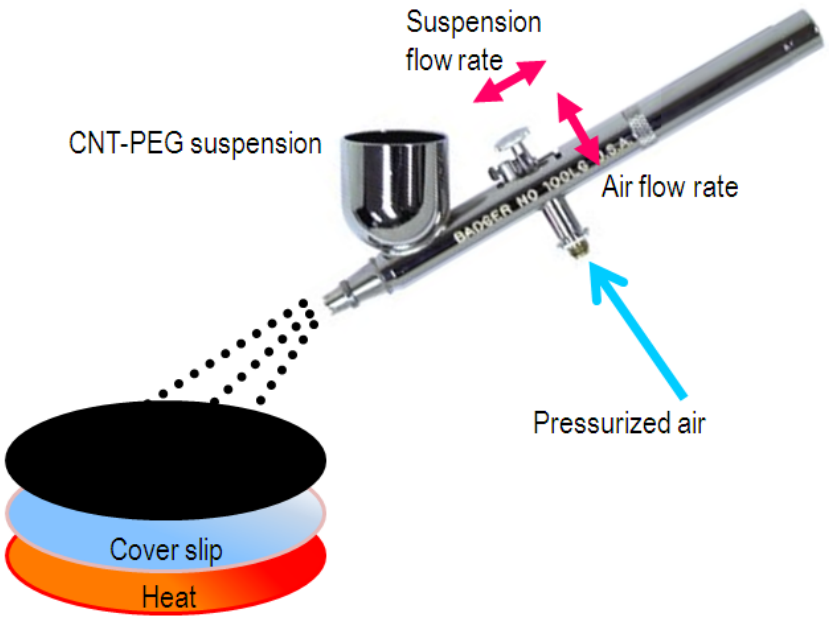

Figure 4.5: Schematic representation of coating procedure of functionalized CNTs on pre-heated cover slips.

4.4.5.2 Optical microscopy

Optical pictures (**Figure 4.7**) of coverslips coated with *f*-CNTs were taken to visualize any cracks in the coating visible under microscope (Nikon AZ-100).

4.4.5.3 Atomic Force Microscopy (AFM)

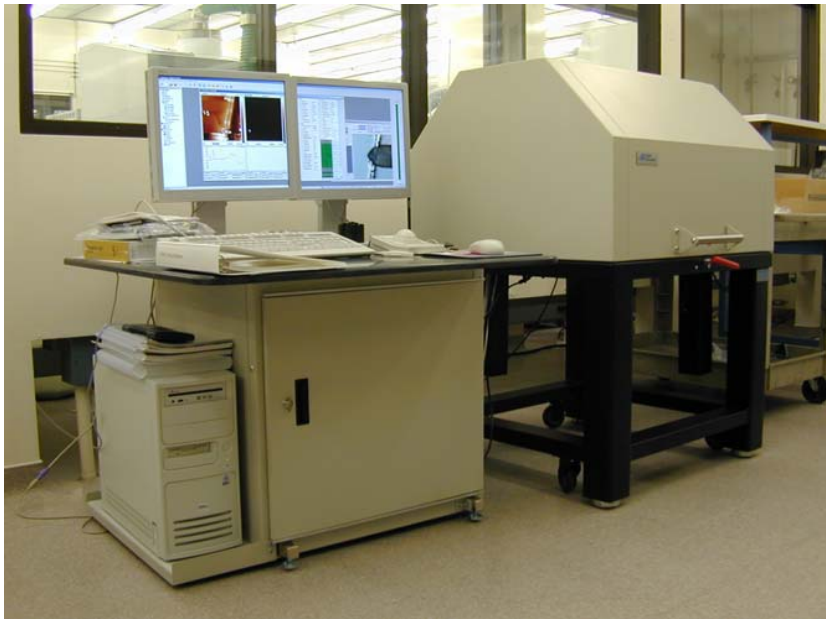

Figure 4.6: Image showing setup of Veeco Dimension 3100 Atomic force microscope

Atomic force microscopy (AFM, Veeco dimension 3100, USA, **Figure 4.6**) was done to determine the roughness of cover slips coated with different *f*-CNTs. The scanning was done in tapping mode using a silicon nitride probe. The roughness was calculated in terms of the average deviation (3 images for each sample) from the mean plain of surface. Root mean square (RMS) values and peak-to-peak ratios were also calculated to compare the roughness between different surfaces. AFM images of the samples were obtained by spraying the dispersions of *f*-MWCNTs (10 mg/ml) with an airbrush onto round cover slips (12 mm in diameter) heated to 160°C.

4.4.5.4 Durability study

To determine the strength of the different *f*-CNTs coating on the cover slips, the fully coated cover slips were kept inside small petri plates filled with MilliQ water and shacked on a gyro-rocker (Stuart, SSL3) at 30 rpm. The shaking was continued till the coatings on the cover slips coated with different f-CNTs were completely destroyed.

4.4.6 Covalent immobilization of BMP-2 on MWCNT-COOH coated cover slips

Some of the sterile MWCNT-COOH coated cover slips were subjected to covalent attachment of the osteogenic inducer (bone morphogenetic protein or BMP-2) following the procedure mentioned elsewhere (Asuri, Karajanagi et al. 2006). Briefly, ten MWCNT-COOH fully-coated cover slips were taken and kept inside wells of a 24-well plate. 1 ml of MES (2-(N-Morpholino) ethanesulfonic acid) buffer (50 mM, pH 6.2) and 1ml of 400 mM N-hydroxysuccinimide (NHS) in MES buffer were added to each well and kept for 1 hour. 20 mM EDC (1-ethyl-3-(3-dimethylaminopropyl) carbodiimide) was added to initiate the activation of the carboxylic groups on the MWCNT-COOH. After 1 hour all the reagents were removed from MWCNT-COOH coated cover slips, which were then rinsed carefully to remove the excess of NHS and EDC. BMP-2 (150 ng, 15µl) in 50 mM acetate buffer (pH 4.5) was added to each well and kept for 2 hr at room temperature. After that the cover slips were washed carefully with acetate buffer and 1% Tween 20 to remove any BMP-2 bound nonspecifically. Finally the cover slips were air dried inside laminar hood and kept in a controlled air container at 4ºC for future use. The value of BMP-2 required for this experiment was calculated through the procedure reported in the following paragraph and **Appendix I**.

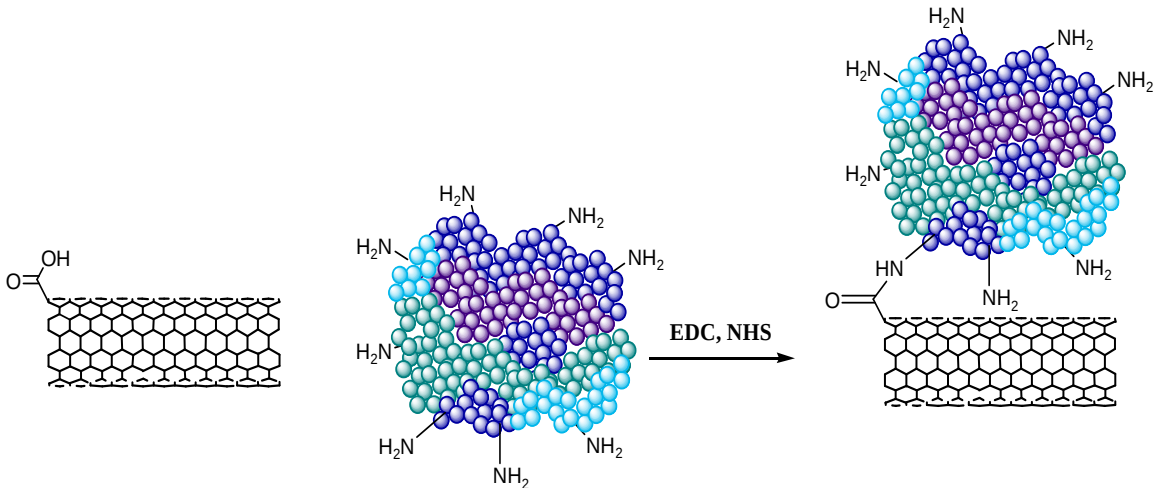

Figure 4.7: Schematic Representation of synthesis of MWCNT-BMP2 through covalent bond.

4.4.7 Determination of BMP-2 loaded onto MWCNT-COOH coated cover slips

To determine the amount of BMP-2 covalently immobilized onto MWCNT-COOH, three coated cover slips were taken and the coating was scrapped out and kept separately in two different 2 ml microcentrifuge tubes. The centrifuge tubes were further added with 1 ml milliQ water and sonicated to get a dispersed mixture. 50 µl of each sample were transferred into separate centrifuge tubes and 400µl of BCA (Pierce, Thermo Scientific) working reagent were added to each centrifuge tube. The contents of the tubes were mixed thoroughly and shaken for 30 seconds. The initial solution became coloured due to the presence of BMP-2 and it was kept at room temperature to help CNTs settle down completely. 25 µl of the solution at the top of the tube (supernatant) were taken out and put into separate wells of a 96-well plate. Absorbance of the coloured solution was recorded through a micro plate reader (Tecan, Infiite 200) at 562 nm. The quantity of BMP-2 on each cover slip was calculated using previously prepared BCA protein standard curve of BMP-2 (**Appendix II**) through the same procedure.

4.4.8 Stem cells growth and culture

The hMSCs were cultured in T75 culture flasks using normal stem cell medium mentioned above. The medium was refreshed every 3-4 days till the cells reached 80-90% confluence (12-14 days). Trypan blue dye exclusion assay was used to count viable cells for all experimental purpose.

4.4.8.1 Subculture

The medium of the above mentioned culture flasks were removed and cells were washed using PBS solution. Trypsin-EDTA (3 ml) was added to the culture flask and incubated for 3-5 minutes in 37ºC incubator. Without removing the trypsin, 7-10 ml of fresh medium were added to the flask. Then this cell suspension was transferred to a 15 ml centrifuge tube and centrifuged at 1,500 rpm for 4 minutes (room temperature). The supernatant was removed and fresh medium was added to disperse the cells from the cells pellet. The cells suspension was distributed into 2-3 new flasks and added with fresh medium to make up the volume up to 10 ml. The flasks were swirled gently and put inside the incubator. The medium was refreshed every 3-4 days till the cells reached 80-90% confluence (12-14 days) and ready for future experiments.

4.4.8.2 Cytotoxicity assays

To determine the cytotoxicity of ultrapure MWCNTs towards hMSCs, MTT (3-(4,5-Dimethylthiazol-2-yl)-2,5-diphenyltetrazolium bromide) and CyQUANT (Invitrogen) assays were performed according to the known procedures(Mosmann 1983; Blaheta, Franz et al. 1991) as mentioned in chapter 3.

4.4.8.3 Fluorescence microscopy

Cover slips coated with different substrates (MWCNT-COOH, MWCNT-PEG and only PEG) along with uncoated (used as control) cover slips were put individually into wells of a 24 well plate (Greiner bio-one, Germany). hMSCs were seeded (5,000 cells/well) onto these wells and cultured as mentioned above. Post confluence, the medium was aspirated out of the wells and all the cover slips having cells growing on them were transferred into a new 24 well plate. Cells in each cover slip were washed carefully with 1 ml PBS for 3 times. Further 1 ml of PBS was added to each well followed by 5 µl of calcein AM (1mM). The well plates were incubated for 30 min at room temperature in the dark. Finally all the cover slips were washed 3-4 times with PBS and were inverted onto glass slides mounted with 70% glycerol and visualized under fluorescence microscope (Nikon AZ-100 multipurpose microscope). The experiment was repeated a few times to have proper representation of images.

4.4.8.4 Calcein AM cell viability assay

Similar procedure as mentioned above was followed with respect to staining of cells with calcein acetoxymethyl ester (AM). After washing all the cover slips 3-4 times with PBS, 1 ml of PBS was left on each well along with the wells having no cells as control. Fluorescence signal pertaining to excitation wavelength of 490 nm and emission wavelength of 520 nm was read using a micro well plate reader (Infinite 200). The number of viable cells was obtained for all the cover slips by comparing the fluorescence signals with a previously prepared calcein AM cell viability standard curve (**Appendix III**) obtained using a known number of viable cells (2,000-20,000) and utilizing the same procedure.

4.4.8.5 Scanning electron microscopy

Cells (hMSCs) growing on MWCNT-PEG coated cover slips were subjected to critical point drying according to a known procedure (Minqin, van Kan et al. 2007). Briefly the culture medium was completely removed and the cells growing on the MWCNT-PEG coated cover slips were given a quick wash with phosphate buffer (PB) (0.1 M pH 7.4). Cells were then fixed with 3% glutaraldehyde (prepared in 0.1 M PB pH 7.4) for 1 hour. The fixative was then removed and cells washed with PB for 5 minutes (3X). The cells were then passed through a series ethanol: 25%-3 min, 50%-3min, 75%-3 min, 100%-5 min, 100%-5min. The coated cover slips having cells on them were then transferred into the critical point dryer (BAL-TEC CPD 030) (Minquin et al., 2007) and dried for about 1 hour (samples were placed in small porous containers to ensure they were not damaged during the drying process). The pressure was released slowly after drying to avoid disturbing the coating on the cover slips. Finally the cells on the MWCNT-PEG coated cover slips were observed under field-emission scanning electron microscope (SEM) (JEOL JSM-6701F, Tokyo, Japan).

The growth of hMSCs on MWCNT-COOH coated cover slips could not be visualized by SEM as the coating was unstable during the process of critical point drying.

4.4.9 Osteogenic induction and differentiation

hMSCs at 5,000 cells per well were seeded into a 24 well plate having both uncoated and MWCNT-coated cover slips. The well plate was left overnight inside the incubator at 37 ºC for cells to adhere to the surface of tissue culture plates. After 24 hrs, osteogenesis was induced by replacing original medium in selected wells with osteogenic medium. BMP-2 (150ng/ml) was added to osteogenic medium depending upon the

purpose of the experiments. The osteogenic medium was replaced every 3 days till confluence (12-14 days) was reached. Osteoinduced cells were compared with non-induced cells on both uncoated and coated cover slips. Post confluence alizarin red quantification, immunofluorescence and qPCRwere performed on the cell samples.

4.4.9.1 Alizarin red quantification

Alizarin red quantification was performed according to previously established procedure (Tataria, Quarto et al. 2006) to assess extracellular matrix (ECM) mineralization after 14 days in osteogenic media with or without BMP-2. This was done by fixing cells with 100% ethanol for 15 min and then staining with 0.2% alizarin red solution with a pH between 6.36 and 6.4 at room temperature for 1 hr. After 1 hr, un-bound alizarin red was aspirated and bound alizarin red was quantified using 20% methanol (Tedia) and 10% acetic acid in water. After 15 min, the methanolic mixture for each sample was transferred to a 96 well plate (200 µl/well) and performed in triplicates. The quantity of alizarin red was read on the micro plate reader at 450 nm, and normalized to protein content using BCA protein assay done using same alizarin red samples.

4.4.9.2 Immunofluorescence

Osteoinduction without BMP-2 was done for hMSCs growing on cover slips coated with different substrates (plain cover slips, cover slips coated with MWCNT-PEG and PEG alone), according to the procedure already mentioned before.

Post confluence, cells growing on cover slips were taken out from the wells and put into a newly marked 24 well plate. The cells on all the cover slips were fixed by treating with ice cold 50%/50% methanol/acetone. After 5 minutes, methanol/acetone solution was removed and the cover slips were left open inside the laminar hood to be air dried.

After the cover slips were completely dried, the fixed cells were treated with 10% FBS in PBS (blocking agent) for 20 minutes. The blocking agent was aspirated and 5 µl of different primary antibodies to cellular markers (CD44 for hMSCs and osteocalcin for osteoblasts) were put onto different cover slips coated with each type of substrates (including plain cover slips used as a control) and incubated at room temperature. After 1 hour, the cells on the cover slips were extensively washed with milliQ water for 5 minutes and then rinsed in PBS for 5 minutes. After that, 100 µl of diluted (1/100) secondary antibody (goat antimouse antibody) conjugated with a fluorescent dye (FITC) was added onto each cover slip (both coated and uncoated) and incubated at room temperature. After 30 minutes the cover slips having cells were washed with milliQ water and were inverted onto glass slides mounted with vectashield with the fluorescent dye 4',6-diamidino-2-phenylindole (DAPI, H 1200, Vector labs) and visualized under fluorescence microscope (Nikon AZ-100 multipurpose microscope). The pictures were taken separately at the same positions using both green fluorescent protein (GFP) and DAPI filter to capture both the fluorescence due to FITC conjugated secondary antibody staining the marker proteins and DAPI staining the nucleus of each cell. Subsequently, images were merged using Nikon elements BR 3.1 image processing software.

4.4.9.3 Quantitative RT-PCR

Q-PCR was done by Miss Phua Lee Cheng in Dr Ho Han Kiat's Lab. Approximately one million cells from each BMP-2-treated and control experiment were harvested for RNA isolation using mirVana miRNA isolation kit (Ambion, Austin, TX), according to manufacturer's instructions. Total RNA was quantified and the quality was ascertained (OD260/280 within 1.9-2.1) using NanoDrop (Thermo, Wilmington, DE). cDNAs of respective samples were synthesized from 0.3 - 1 µg of total RNA using

SuperScript III reverse transcriptase (Invitrogen, Carlsbad, CA), according to manufacturer's instructions. Quantitative real-time-PCR was performed using Applied Biosystems 7500 Fast Real-Time PCR System with Fast SYBR Green master mix and primers (1^{st} BASE) for *osteopontin (OPN)* (NM_001040058; F: 5'-ACG CCG ACC AAG GAA AAC TC-3'; R: 5'-GTC CAT AAA CCA CAC TAT CAC CTC G-3'). *18S* RNA (NR_003286; F: 5'-CGG CTT AAT TTG ACT CAA CAC G-3'; R: 5'-TTA GCA TGC CAG AGT CTC GTT C-3') were quantified as housekeeping control. The thermal cycling condition comprised an initial denaturation at 95 ^{o}C (20 s), followed by 40 cycles at 95 ^{o}C (3 s) and 60 ^{o}C (30 s). Melting curves were generated at the end of 40 cycles to verify the purity of the PCR product. The samples were prepared in triplicates with 4 μL of 10 fold-prediluted cDNA. Data were obtained as average C_T values, and normalized against housekeeping control as ΔC_T. Expression changes in *OPN* transcripts in various samples were measured as fold change with respect to cells grown on cover slip in the absence of BMP-2 stimulation using $2^{\Delta\Delta CT}$ ($\Delta\Delta C_T$ = ΔC_T of test sample– ΔC_T of control cells).

4.4.10 Statistical analysis of the data

All the data from cell cytotoxicity assays, viability assays, alizarin red quantification and qPCR were subjected to student *t*-test to calculate *p*-value. If the *p*-value was found to be less than the threshold (0.05) chosen for statistical significance, then the null hypothesis (which states that the two groups do not differ) was rejected in favor of an alternative hypothesis, which indicates that the groups do differ significantly.

4.5 RESULTS

4.5.1 Functionalization of MWCNTs and characterization

Ultrapure multi-walled carbon nanotubes (MWCNTs) were functionalized following the procedure reported elsewhere(Zhao, Hu et al. 2005) and they were confirmed by TEM and TGA measurements. The dispersibility of MWCNT-COOH and MWCNT-PEG in water was determined in order to know minimum amount of these *f*-CNTs required to make the solution for coating of coverslips with these *f*-CNTs. Simultaneously MTT and CyQUANT cytotoxicity assay of pristine ultrapure MWCNTs were also done to determine biocompatibility with regard to human mesenchymal stem cells.

Characterization through TEM (**Figure 3.7** in **Chapter 3**) showed that acidic treatment and sonication for 6 hours shortened ultrapure MWCNTs in comparison to pristine tubes, while their diameters remained intact. In other words pristine ultrapure MWCNTs appear as long, continuous tubes whereas oxidized MWCNTs (MWCNT-COOH) were truncated to approximately 500 to 1000 nm in length.

The extent of oxidation of MWCNTs and loading with PEG were also determined by TGA. As can be seen from **Figure 4.8**, the initial weight percentage of metal residue in pristine ultrapure MWCNTs was 4.2%, indicating the high purity of our starting material. After oxidation, such content further decreased to 2.4% for MWCNT-COOH (990°C) and 1.7% for MWCNT-PEG (990°C). On the basis of these values, the loading and the fraction of carbon atoms in the samples that became functionalized with PEG chain in the MWCNT-PEG complex were estimated. We estimated the loading of MWCNTs in MWCNT-PEG to be about 70.8%. Since the molecular weight of PEG used

in this work was about 600, the degree of functionality in MWNT-PEG in terms of molar functionality was equal to (100-7.8/600)/ (70.8/12) = 0.8%. In addition, TGA graphs (Figure 4.8) showed distinct derivative curves of pristine MWCNTs, oxidized nanotubes (MWCNT-COOH) and MWCNT-PEG complexes, which was in agreement with the work performed by Zhao and collaborators (Zhao, Hu et al. 2005).

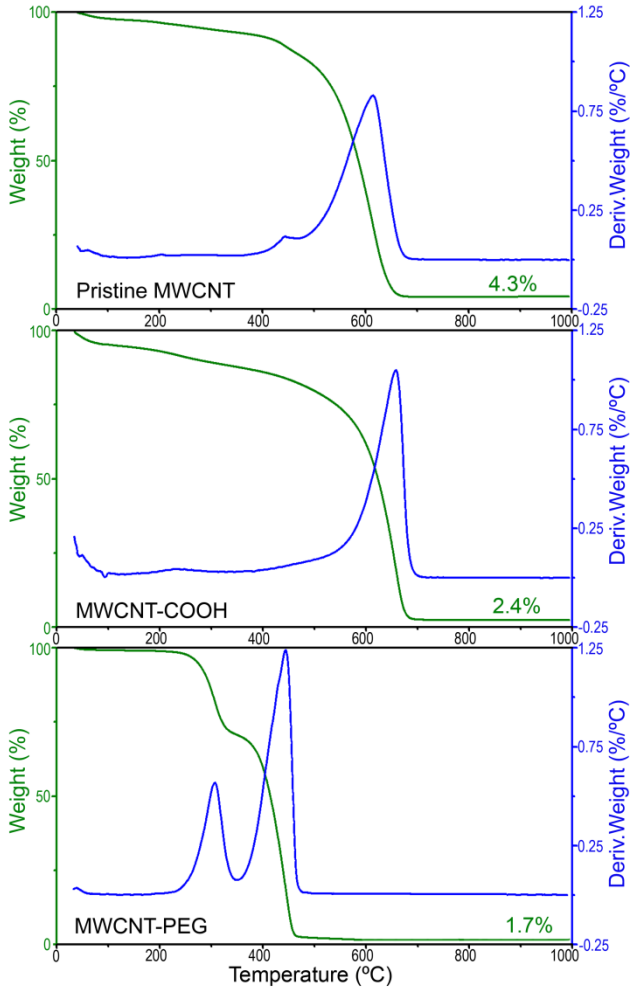

Figure 4.8 TGA graphs and derivative curves of MWCNT samples. The TGA graphs are labelled with the wt% of metal residue after ramping the sample to 1000 °C.

	MWCNT-COOH			MWCNT-PEG		
Time / Conc (mg/ml)	1 h	5 h	24 h	1 h	5 h	24 h
0.005	✓	✓	✓	✓	✓	✓
0.05	✓	✓	✓	✓	✓	✓
0.5	✓	✓	✓	✓	✓	✓
1	✓	✓	✓	✓	✓	✓
2.5	✓	✓	✓	✓	✓	✓
5	✓	✓	×	✓	✓	✓
7.5	✓	×	×	✓	✓	✓
10	✓	×	×	✓	✓	×
15	×	×	×	✓	×	×
20	×	×	×	×	×	×
25	×	×	×	×	×	×

Table 4.2 Dispersibility study of MWCNT-COOH and MWCNT-PEG of varying concentrations at specific standing time. Tick (✓) indicates stable dispersion whereas cross (×) indicates partial sedimentation.

From **Table 4.2**, it can be seen that at 24 hours MWCNT-COOH had dispersibility of 2.5 mg/ml, whereas MWCNT-PEG showed dispersibility of 7.5 mg/ml. Similarly at 1 hour, MWCNT-COOH showed dispersibility of 10 mg/ml, while MWCNT-PEG showed dispersibility of 15 mg/ml. So for every time period tested for dispersibility, MWCNT-PEG showed better dispersibility profile in comparison to MWCNT-COOH. Although as time lapsed the dispersions of both MWCNT-COOH and MWCNT-PEG became increasingly unstable and sedimentation occurred, the rate of sedimentation for MWCNT-COOH was faster than the MWCNT-PEG. Since MWCNT-COOH showed dispersibility of 10 mg/ml at one hour, which is lower than the dispersibility of MWCNT-PEG at the same time-frame, we used this particular concentration of functionalized CNTs to coat the cover slips to get a uniform and smooth coating.

The cytotoxicity profile of hMSCs with regard to ultrapure MWCNTs has already been discussed in **Chapter 3**. Briefly, the MTT assay of hMSCs did not reveal any cytotoxicity in the case of ultrapure-MWCNTs at concentrations up to 100μg/ml (**Figure 3.19A**) and incubation periods up to 72 hours (**Figure 3.19B**); a statistically negligible difference (p ~1) was detected in such range. To exclude the possibility that black carbon nanotubes interfered with the result of the MTT assay, we also performed a CyQUANT assay of ultrapure MWCNTs for hMSCs at the same range of concentrations used for the above reported MTT assays. As expected, the result was comparable to that of the MTT assay, as no cytotoxicity was observed until 100μg/ml.

4.5.2 Characterization of *f*-MWCNT coated coverslips

Coverslips coated with *f*-MWCNTs (MWCNT-COOH and MWCNT-PEG) along with only PEG were subjected to characterization by optical microscopy, atomic force microscopy and durability study.

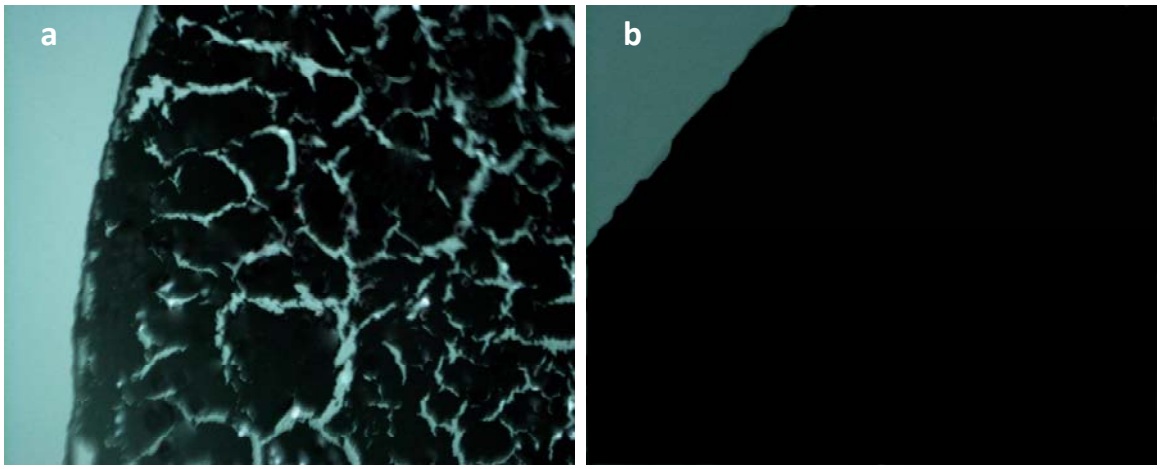

Figure 4.9 Optical images of cover slip coated with different functionalized MWCNTs. (a) Cover slip coated with MWCNT-COOH, (b) Cover slip coated with MWCNT-PEG.

Figure 4.9 shows optical images of MWCNT-COOH and MWCNT-PEG coatings on the coverslips. While **Figure 4.9(a)** representing MWCNT-COOH coating shows

cracks visible under microscope, **Figure 4.9(b),** representing MWCNT-PEG, presents a quite uniform coating without any noticeable cracks. Similarly, in the durability study, the MWCNT-COOH coating was destroyed within the first two hours of shaking, while the MWCNT-PEG coating remained intact for one week, after which it detached from the cover slip but it did not undergo destruction till the third week.

In order to characterize the roughness properties of different *f*-MWCNT coatings on coverslips, surface topographies were recorded under Atomic Force Microscope (AFM) over scanned areas of 2 μm x 2 μm**.** To quantify micro-roughness, the arithmetic roughness (R_a), the root mean square (RMS) of the surface height variations and the peak-valley height difference (R_t) were determined (**Table 4.3).** A Typical top-view image of (**a**) MWCNT-COOH and (**b**) MWCNT-PEG coatings is displayed in **Figure 4.10**. To explore the consistency of the surface roughness, several different locations on the same sample were imaged and the above mentioned parameters were analyzed and compared.

Samples	Average (R_a) (nm)	RMS (nm)	Peak to Peak (R_t) (nm)
MWCNT-COOH	41.4	54.6	433
MWCNT-PEG	18.3	23.9	270

Table 4.3 AFM data showing average, root mean square and peak to peak deviation of surface roughness between surfaces of cover slips coated with MWCNT-COOH and MWCNT-PEG.

It can be seen from the **Table 4.3** and **Figure 4.10**, that both the MWCNT-COOH and MWCNT-PEG coatings formed rough surface. However, MWCNT-PEG thin films, with a R_a of 18.3 nm and R_t of 23.9 nm, showed comparatively smoother surfaces than MWCNT-COOH coatings, with an average roughness of 41.4 nm. Likewise, MWCNT-COOH thin film surface also showed higher peak-to-peak deviation of roughness compared to MWCNT-PEG coating surfaces.

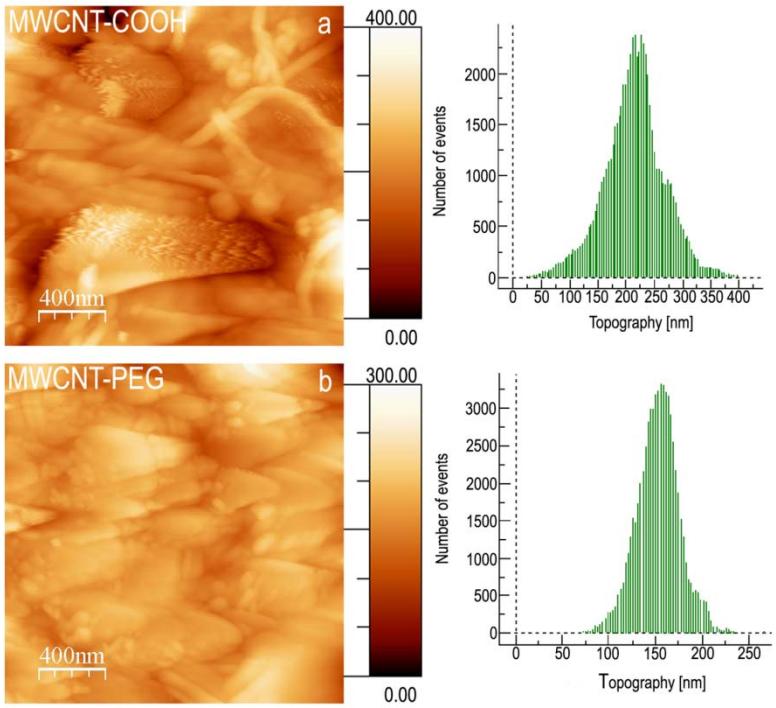

Figure 4.10 Atomic force microscopy images including the topography of the surfaces of (a) MWCNT-COOH and (b) MWCNT-PEG coated cover slips.

4.5.3 Stem cells growth on coated coverslips

Pristine or non-functionalized CNTs are known to display lower cell viability in comparison to *f*-CNTs. Since our ultrapure MWCNTs are pristine CNTs, therefore, we expected even better profiles with functionalized MWCNT-PEG samples which are coated as thin film onto coverslips; indeed this was confirmed by fluorescence microscopy and calcein acetoxymethyl ester (AM) cell viability assay performed on hMSCs growing on all the thin film samples following a previously reported procedure (Bratosin, Mitrofan et al. 2005). Images under a fluorescence microscope (**Figure 4.11a-d**) showed that cell morphology was, in general, similar across PEG alone, *f*-CNTs samples and cover slips after 15 days of incubation in normal stem cell media. More precisely, stem cells grown on PEG alone (**Figure 4.11b**) and MWCNT-PEG (**Figure 4.11d**) presented an elongated, fibroblast-like morphology comparable to those on cover

slips (**Figure 4.11a**), while in the case of MWCNT-COOH substrates, cells showed slightly irregular shapes (**Figure 4.11c**). Additionally it was clearly visible a remarkable decrease in cell viability in case of MWCNT-COOH coated cover slips.

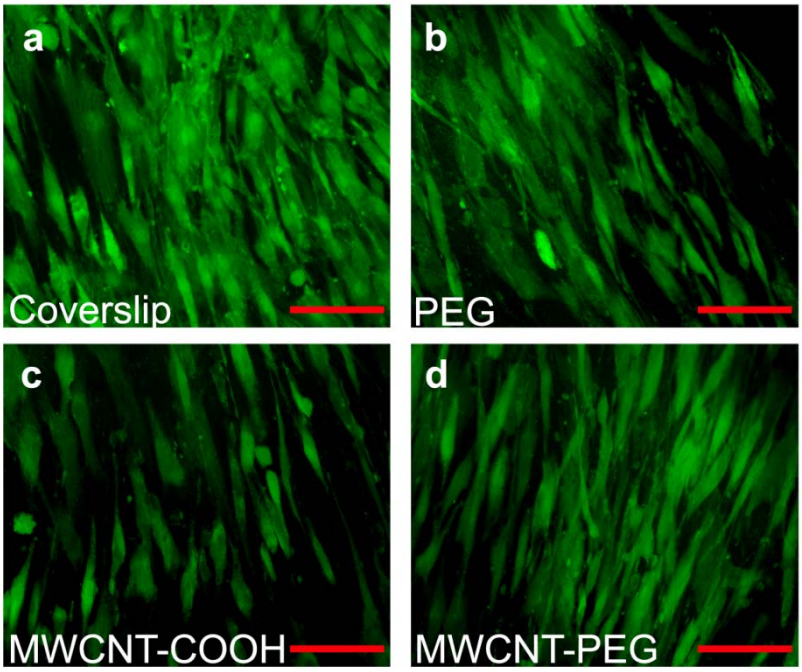

Figure 4.11 Fluorescence microscopic imaging of hMSCs growing on **(a)** normal cover slip; **(b)** PEG coated cover slip; **(c)** MWCNT-COOH coated cover slip; **(d)** MWCNT-PEG coated cover slips. Scale bars are 100 μm.

The results pertaining to above fluorescence microscopy were further confirmed by calcein AM cell viability assay. As expected, cell viability in case of MWCNT-PEG coated cover slips showed no significant difference ($p>0.05$) when compared with cell viability on plain or only PEG-coated cover slips (**Figure 4.12**). This indicates that MWCNT-PEG thin film can be utilized as a scaffold for stem cell growth. However, there was significant decrease in cell viability in case of cover slips coated with MWCNT-COOH ($p<0.05$).

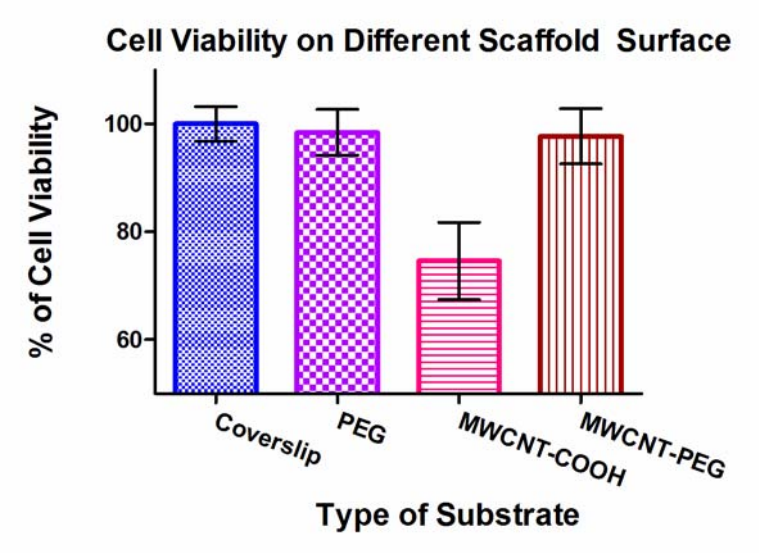

Figure 4.12 Graph showing percentage of cell viability for hMSCs growing on different scaffold surfaces.

Cell proliferation was confirmed by SEM imaging. **Figure 4.13a** clearly showed the distribution of hMSCs growing on a uniform substrate, while a zoomed area (**Figure 4.13b**) enabled the identification of a typical cell with its reticular fibrils on a homogeneous lattice of CNTs. In contrast, the growth of hMSCs on MWCNT-COOH coated cover slips could not be visualized by SEM as the coating was unstable during the process of critical point drying.

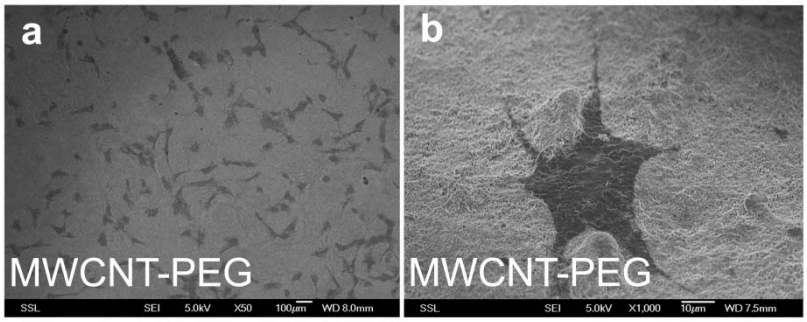

Figure 4.13 SEM images of hMSCs growing in normal medium on MWCNT-PEG coated cover slips at DAY 4 of incubation. **(a)** Large field of view showing growth of lots of cells. Scale bar is 100 µm. **(b)** Small field of view showing a single cell. Scale bar is 10 µm.

4.5.4 Osteogenic induction and differentiation

Numerous pre-clinical studies have shown that recombinant bone morphogenetic proteins (BMPs) play a critical role in bone healing by stimulating the differentiation of mesenchymal stem cells to an osteogenic lineage (Wang, Israel et al. 1993). Similarly Rawadi *et al.* (Rawadi, Vayssiere et al. 2003) have reported the control of osteogenic induction and mineralization by BMP-2 in pluripotent mesenchymal cell lines C3H10T1/2, C2C12, ST2 and the osteoblast cell line MC3T3-E1. In our case, hMSCs were cultured in osteogenic medium with and without BMP-2. An additional sample consisted of BMP-2 covalently attached to MWCNT-COOH via carbodiimide chemistry (Asuri, Karajanagi et al. 2006). Due to the coating procedures that require heating the cover slips at 160ºC (which would have hampered the activity of any protein, including BMP-2), we used the cover slips already coated with MWCNT-COOH for the subsequent covalent immobilization of BMP-2. After repeated washes to remove unspecific adsorption of inducer, the amount of BMP-2 covalently attached onto the MWCNT-COOH coating was analyzed by BCA protein assay using a previously prepared BMP-2 standard curve and it was found to be 70 ng. This was comparable to the amount of BMP-2 (75ng/well) added to the osteogenic media in case of osteoinduction experiments with hMSCs. Post confluence (12-14 days), cell cultured on different substrates (i.e. a) plain cover slips with and without BMP-2; b) PEG alone; c) MWCNT-PEG with and without BMP-2; d) MWCNT-COOH with BMP-2 covalently bound) were subjected to quantitative Alizarin red staining, which stains the calcium deposition as part of matrix mineralization (**Figure 4.14**).

Figure 4.14 shows the important role of BMP-2 as biochemical inducer in both osteogenic differentiation and matrix mineralization. In particular, hMSCs grown on plain

or only PEG-coated cover slips were not able to form calcium deposits. Notably, although calcium can be deposited on some scaffolds, we did not observe any non-specific staining from CNTs alone (without cells) exposed to Alizarin red. Conversely, all the substrates with hMSCs treated with 70-75 ng/well of BMP-2 clearly showed abundant calcium deposition as indicated by a high normalized alizarin red quantity. Only the sample of MWCNT-COOH covalently bound to BMP-2 presented fewer calcium deposits. Interestingly, both BMP-2 treated substrates and MWNT-PEG (without BMP-2) coated cover slips showed comparable ($p>0.05$) deposition of calcium as part of matrix mineralization. In other words, the uniform coating of MWCNT-PEG provided a suitable microenvironment for hMSCs proliferation and differentiation even in the absence of the standard biochemical inducer.

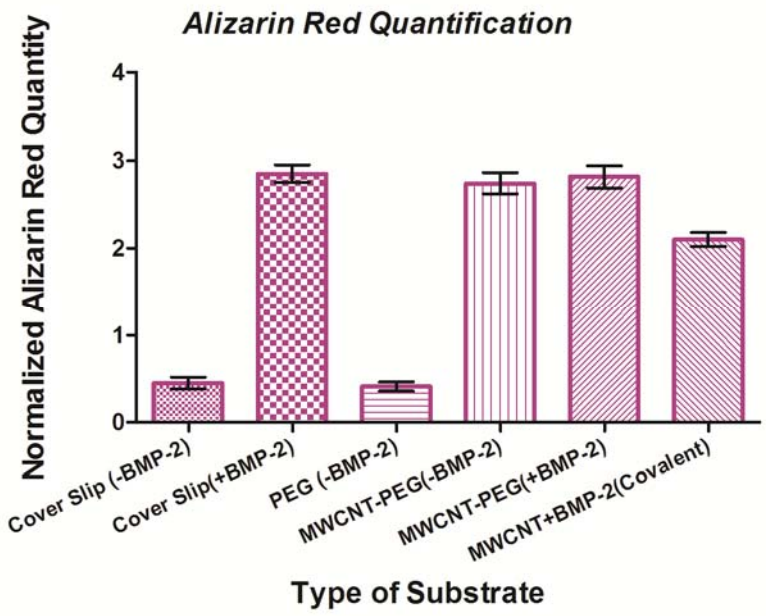

Figure 4.14 Graph showing normalized Alizarin Red Quantity in cells growing on different scaffold surfaces with or without BMP-2.

This differentiation into osteogenic lineages was confirmed by immunofluorescent staining of two common protein markers: *CD44* for hMSCs and osteocalcin (*OCN*) for

osteoblasts (**Figure 4.15**). This investigation was performed after two weeks of incubation of hMSCs onto different substrates in the presence of osteogenic media. The immunofluorescence results clearly showed that cells growing on plain (**Figure 4.15a**) and only PEG-coated (**Figure 4.15c**) cover slips bound to the fluorescent antibody specific for *CD44* expression, confirming the fact that hMSCs maintained a certain degree of "stemness" (i.e. lack of complete differentiation into osteogenic lineage). At the same time, these cells did not immunostain for *OCN* (**Figure 4.15d&f)** because they were not differentiated into osteoblast-like cells. Conversely, MWCNT-PEG samples did not express *CD44* (**Figure 4.15b**) and instead they showed high fluorescence in correspondence of *OCN* immunostaining (**Figure 4.15e**), confirming a successful differentiation of hMSCs into osteoblasts even in absence of BMP-2.

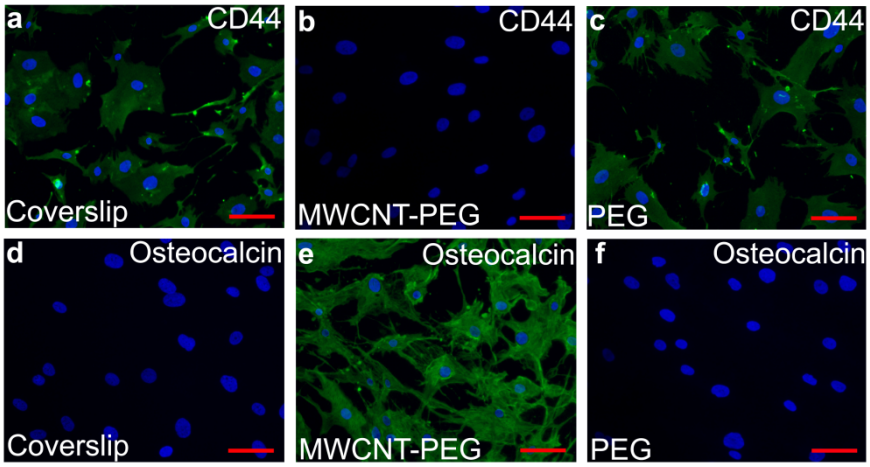

Figure 4.15 Immunofluorescence image of cells subjected to osteoinduction without BMP-2. Cells growing on **(a, d)** plain cover slips showing the presence of CD44 and absence of osteocalcin; **(b, e)** MWCNT-PEG coated cover slips showing the absence of CD44 and presence of osteocalcin; **(c, f)** only PEG-coated cover slips showing the presence of CD44 and absence of osteocalcin. Scale bars are 100 μm.

To substantiate the observation of MWCNT-PEG inducing the differentiation of hMSCs into osteoblasts, we characterized the transcriptional upregulation of osteopontin (*OPN*), an early biomarker for osteogenesis (**Figure 4.16**) (Liu, Akiyama et al. 2008) in

hMSCs grown onto different substrates and cultured for 14 days in osteogenic media with or without the osteogenic inducer (e.g. recombinant bone morphogenetic protein, BMP-2, at a concentration of 75ng/well). Expression changes in various samples were measured as fold change with respect to control cells (i.e. positive control in form of hMSCs grown on cover slip in the presence of BMP-2 with osteoinductive media and negative control consisting of cover slips without BMP-2 and cultured in normal stem cell media).

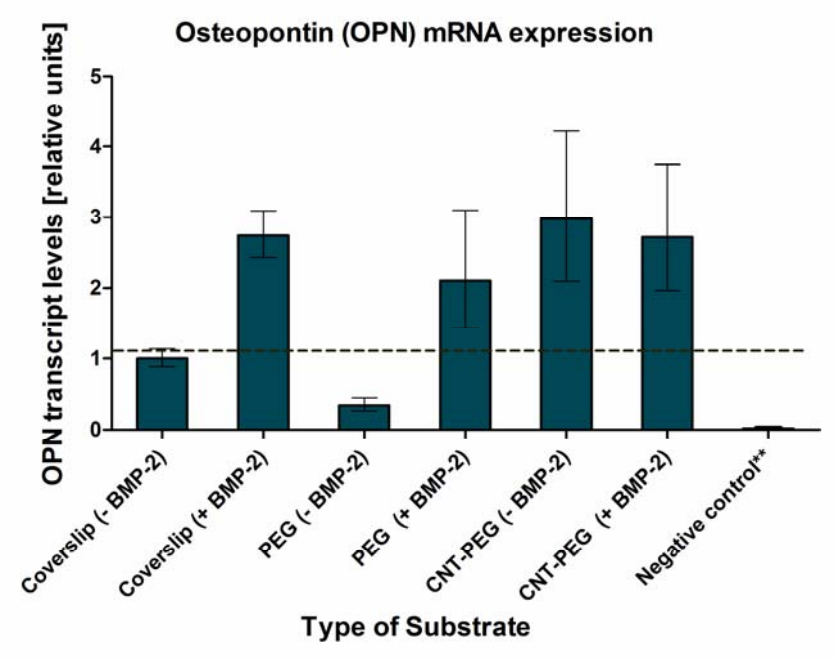

Figure 4.16 qPCR analysis of relative expression levels of osteopontin for hMSCs cultured on different types of substrates and osteoinduced with osteogenic media with or without BMP-2 for 14 days. **Negative control consists of cover slip without BMP-2 and without induction with osteogenic media.

As can be seen from the **Figure 4.16** and **Appendix IV**, BMP-2 mediated greater than two-fold elevation of *OPN* expression for hMSCs grown on either cover slip or PEG coated layer. Strikingly, MWCNT-PEG, even in the absence of BMP-2, demonstrated an elevated *OPN* transcript level that was indistinguishable from the cells undergoing BMP-2 stimulation. The extent of *OPN* expression for MWCNT-PEG alone was in fact similar

to that for PEG (+BMP-2) cells, confirming that the combination of nanotubes and PEG successfully guided cell differentiation towards bone formation.

4.6 DISCUSSION

Recent advances have shown that besides cell surface interactions, distinct nanopatterning of biomimetic surfaces (Park, Cannizzaro et al. 2007; Park, Bauer et al. 2009) contributes significantly to cell behavior and cell differentiation (Engler, Sen et al. 2006; Dalby, Gadegaard et al. 2007; Engler, Sweeney et al. 2007). More precisely, cell adhesion, spreading, proliferation and differentiation seem to be influenced by the substrates on which stem cells grow. In this article we have shown for the first time that multi-walled carbon nanotubes, once functionalized with hydrophilic PEG chains, become biocompatible scaffolds to support hMSCs' growth and proliferation, since they do not affect cell viability. Furthermore, we demonstrated that a compact and uniform thin film of tubes presenting some nanometric irregularities can provide a suitable environment to enable stem cells to differentiate into osteogenic lineage. Indeed we speculated that the combination of the mechanical properties of CNTs, together with the efficient differentiation of stem cells into bone, could pave the way towards the extensive use of this material for the regeneration of functional tissues.

4.6.1 Functionalization of MWCNTs and their characterization

The first and foremost challenge in this work consisted of the surface modification to achieve biocompatible MWCNT materials. The ultrapure MWCNTs were functionalized following the previously established procedure (Zhao, Hu et al. 2005). This functionalization was confirmed by TGA measurements (figure 4.8), by which we estimated the extent of PEG complexed with MWCNTs to be 0.8%. From earlier studies

done with regard to ultrapure, pristine MWCNTs (Nayak, Leow et al. 2010), the dispersibility has been reported to be less than 3mg/ml. However, as can be seen from **Table 4.2**, the additional presence of PEG helped in the formation of a more uniform suspension and resulted in a dispersed network of interconnected MWCNT-PEGs. Indeed, the dispersibility of MWCNT-COOH has increased by more than 3 times until 10 mg/ml; in case of MWCNT-PEG, due to the presence of PEG, an increase of more than 5 times up to 15 mg/ml was observed. So the above results suggest that functionalization of pristine MWCNTs, which are hydrophobic in nature, reduce agglomeration and improve dispersibility of nanotubes in water. The dispersibility is even higher when the functional groups are more hydrophilic in nature. This is evident from the dispersibility data of PEG functionalized CNTs. PEG also helps in getting a uniform coating of nanotubes on the cover slips. This may be due to the PEG helping MWCNT-PEG not only to adhere strongly to each other, but also to adhere strongly to the cover slips (**Figure 4.9**).

4.6.2 Characterization of coated coverslips

Thin films of PEG, MWCNT-COOH and MWCNT-PEG were obtained by coating them uniformly using an airbrush onto pre-heated cover slips and further drying in air. Optical images of the above thin films presented some irregularities and uneven layers (i.e. breaks of cover slips without CNTs) in the case of MWCNT-COOH, while they showed a full and compact film with MWCNT-PEG (**Figure 4.9**). Since it is known that surface regularity is an important factor in cell proliferation and differentiation (Bowers, Keller et al. 1992; Keller, Collins et al. 1997), these results predicted a better cell growth in case of MWCNT-PEGs.

Furthermore, it had been shown that a certain type of topography, specifically the roughness of the underlying substrate (in our case CNT thin film), influences spatial

distribution and cell differentiation (Gomi and Davies 1993; Curtis and Wilkinson 1998), since it affects the specific adsorption of proteins at the surface and the subsequent cell reactions. Therefore, AFM measurements were taken to determine the roughness of cover slips coated with different *f*-CNTs (**Figure 4.10**). Our results indicated that the roughness obtained in the coated samples consisted of nanometric irregularities in the form of either randomized (as in MWCNT-COOH, **Figure 4.10a**) or slightly parallel (as in MWCNT-PEG, **Figure 4.10b**) grooves and ridges. We hypothesized that these parallel grooves helped in the proper growth of stem cells over the whole period of incubation and eventually favored their further differentiation into bone lineage. In fact it has been shown that stem cells' fate can be selectively guided by regulating nanometric dimensions of the substrates (Oh, Brammer et al. 2009), although further investigations are required to fully understand the mechano-sensing phenomenon behind such observation.

In addition, since a prerequisite for successful tissue engineering implant is its stability over time, additional samples of *f*-MWCNT-coatings were subjected to durability study by shaking in distilled water using a shaker at 30 RPM. While MWCNT-COOH coatings were destroyed within the first two hours, MWCNT-PEG coating were stable during the whole period of experiment. Due to the fact that in real implants, these thin films would be embedded inside the damaged tissue rather than freely suspended in solutions, this result suggests that the use of thin films made up of PEG-functionalized carbon nanotubes could provide a solid and stable structure for the growth of cells.

4.6.3 Stem cells growth and characteristics

From our previous cytotoxicity studies (**Figure 3.19** in **chapter 3**), we have confirmed enhanced biocompatibility of these ultrapure MWCNTs, with respect to hMSCs. Briefly, no cytotoxicity was observed until a MWCNT concentration of

100µg/ml even when incubated for a period up to 72 hours. It was also warranted to analyze the behavior of hMSCs in terms of their morphology and cell viability when grown onto thin films of such ultrapure MWCNTs functionalized with different groups as scaffold for bone tissue engineering. From **Figure 4.11** pertaining to fluorescence microscopy and **Figure 4.12** pertaining to calceinAM cell viability assay, we observed a similar morphology and cell viability across PEG alone, MWCNT-PEG and plain coverslips after 15 days of incubation in normal stem cell medium. While hMSCs growing MWCNT-PEG thin film showed elongated, fibroblast-like morphology and cell viability comparable ($p>0.05$) to those on PEG alone and plain coverslips, hMSCs growing on MWCNT-COOH thin film showed slightly irregular shapes and also lower cell growth (($p<0.05$). This result in fact is in agreement with some articles indicating that cytotoxicity is inversely correlated to the extent of CNTs' functionalization(Dumortier, Lacotte et al. 2006; Sayes, Liang et al. 2006; Nayak, Leow et al. 2010), and it supports the promising role of these ultra-pure, functionalized MWCNTs as biocompatible scaffolds. The decrease in cell viability of hMSCs in case of MWCNT-COOH also confirmed the study performed by Liu *et al.* (Liu, Yi et al. 2010), where cell proliferation and osteogenic differentiation of hMSCs were inhibited by carboxylated single-walled and multi-walled carbon nanotubes. This can also be due to poor adherence of hMSCs onto the MWCNT-COOH coating owing to the visible cracks as shown in **Figure 4.9**. On the contrary, this was not true in case of hMSCs growing on the MWCNT-PEG thin film, where the uniform and stable coating formed on the coverslips provided an excellent scaffold surface for unhindered growth and morphogenesis. This result was also further confirmed by SEM imaging of hMSCs growing on MWCNT-PEG thin films which not only showed the uniform growth and distribution of hMSCs on the substrate, but also enabled the identification of a typical cell with its reticular fibrils on a homogeneous lattice of CNTs.

4.6.4 Osteogenic induction and differentiation

Although mesenchymal stem cells are known to represent a heterogeneous population of cells, in the present study we speculated that, once grown onto MWCNT-PEG substrates, they were capable of osteogenic differentiation. To corroborate such hypothesis we characterized osteogenic induction and differentiation in terms of a) matrix mineralization (by quantifying calcium deposition) and b) immunofluorescence (with regard to expression of osteocalcin and qPCR analysis in terms of osteopontin expression).

Alizarin red quantification was done to quantify calcium deposits as part of bone mineralization and the quantity was normalized to protein content as determined by BCA protein assay. As indicated in the **Figure 4.14,** hMSCs grown on plain cover slips and only PEG coated cover slips were not able to mineralize without BMP-2 stimulation, suggesting that osteogenic medium or PEG alone were not sufficient to induce proper differentiation of hMSCs into osteoblasts. In contrast, hMSCs growing on different substrates and osteoinduced with BMP-2 showed profuse calcium deposition. Remarkably, hMSCs growing on MWCNT-PEG coated coverslips showed calcium deposition comparable ($p>0.05$) to BMP-2 treated substrates even without osteoinduction with BMP-2. This result indicates the fact that MWCNT-PEG thin film not only provides a uniform and stable surface for the growth of hMSCs, but also imitates a favorable microenvironment for hMSCs osteogenic differentiation even in the absence of the standard biochemical inducer. In exception, hMSCs growing on thin film of MWCNT-COOH covalently bound to BMP-2 showed comparatively fewer calcium deposits, most probably due to less uniform and unstable coating obtained with MWCNT-COOH, or to a partial denaturation of BMP-2 immobilized onto CNTs. With regard to this last aspect, it

had already been demonstrated that immobilization of enzymes and proteins onto substrates sometimes affects their secondary structures and often decreases their activity (Cang-Rong and Pastorin 2009). From the cell viability and alizarin red quantification studies it was confirmed that hMSCs grown on MWCNT-COOH coated cover slips showed decrease not only in cell viability but also in calcium deposition, as determined by alizarin red quantification even with covalently bonded BMP-2. In contrast to MWCNT-COOH, hMSCs grown on MWCNT-PEG coated cover slips showed comparable cell viability and normalized alizarin red quantity even when osteoinduced without BMP-2. Therefore for further experiments we utilized only MWCNT-PEG coated cover slips for osteogenic differentiation and osteoinduction.

Figure **4.15** shows immunofluorescent staining of two common protein markers, *CD44* for hMSCs and osteocalcin (*OCN*) for osteoblasts, performed after two weeks of growth of hMSCs on different substrates, in the presence of osteogenic medium without osteoinduction by BMP-2. The fact that hMSCs growing on plain and PEG coated coverslips did not show *OCN* expression, but were able to bind to the fluorescent antibody specific for *CD44* expression, confirms that hMSCs maintained significant features of "stemness" character (i.e. lack of complete differentiation into osteogenic lineage). In contrast hMSCs growing on MWCNT-PEG thin films did not show expression of *CD44* after two weeks, but they displayed high fluorescence with respect to *OCN* immunostaining, confirming their successful differentiation into osteoblasts even in absence of BMP-2. Moreover, since *OCN* is normally expressed after 21 days of in vitro osteogenesis of MSCs (Tataria, Quarto et al. 2006), we theorized that MWCNT-PEG samples acted as biochemical enhancer, accelerating the process of hMSCs differentiation into osteocyte phenotype. Such attributes may help to strengthen the bone structure and

eventual implants, e.g. the area of defect could be quickly covered and bridged to surrounding bone by the thin film of nanotubes, which are strong enough to support and anchor the initial monolayer of cells over the whole period, from proliferation to differentiation, for the deposition of new bone.

The above result was further confirmed by qPCR analysis of transcriptional upregulation of osteopontin (*OPN*), an early biomarker for osteogenesis. As can be seen from the qPCR analysis (**Figure 4.16**) of hMSCs, growing on MWCNT-PEG thin films demonstrated an elevated *OPN* transcript level that was comparable (p>0.05) to the hMSCs undergoing BMP-2 stimulation on different substrates. The extent of *OPN* expression for MWCNT-PEG alone was in fact similar to that for MWCNT-PEG (+BMP-2) cells, confirming that the combination of nanotubes and PEG successfully guided cell differentiation towards bone formation. Interestingly, Briggs *et al*.,(Briggs, Treiser et al. 2009) observed that, while osteopontin is a gene up regulated during the initial mineralization phases of osteogenesis other marker genes are critically up-regulated along with downstream programs for osteogenesis, as demonstrated by alkaline phosphatase activity and osteocalcin expression. This effect was also observed when hMSCs were grown on polycarbonates copolymerized with 0-5% PEG.

Altogether, MWCNT-PEG successfully transformed hMSC into bone-like cells even in the absence of any osteogenic inducer, as evidenced by multiple independent criteria at the transcript (e.g. osteopontin), protein (e.g. osteocalcin) and functional (e.g. calcium deposition) levels.

4.7 CONCLUSIONS

It is widely known that extracellular matrix can exert highly complex biochemical effects in a similar way that growth factors can (e.g. BMP-2) (Hidalgo-Bastida and Cartmell 2010), resulting in dramatic changes to cell phenotypes. This study clearly illustrates that by subjecting mesenchymal stem cells to an appropriately selected biomaterial, it is possible to propel the cells to differentiate into a targeted tissue type like osteoblasts. As this finding presents the next challenge of understanding the mechanistic basis for the differentiating pressure of MWCNT-PEG, it also underlies the promise of the ability that such material can differentiate into other tissue types (such as chondrocytes and myocytes) through subtle modification of the matrix and induction with specific media. Taken together, these results suggest a promising role for functionalized CNTs as reinforcing agents due to their high mechanical strength, as well as their use as biocompatible scaffolds for applications in tissue engineering and bone repair.

Chapter 5

Application of ZnO Nanorods for Transdermal Delivery of Vaccines

Continuing with previous two chapters of my thesis involving biomedical applications of carbon nanotubes, this chapter also began as a project corresponding to application of aligned carbon nanotubes grown on silica substrate for transdermal delivery of vaccines. However, during initial experiments with the chips having aligned carbon nanotubes, we observed that the carbon nanotubes were very weakly attached to the silica support resulting in their detachment from the silica support when applied onto the skin sample. Subsequently, after searching for a few alternative nanomaterials, we opted for aligned zinc oxide (ZnO) nanorods grown on silica substrate for the purpose. It is to be noted that zinc oxide not only has antimicrobial and astringent characteristics, but also as nano material, it is already approved by USFDA for use on skin as cosmetic products. Therefore we modified our project for utilizing aligned ZnO nanorods grown on silica substrates, for transdermal delivery of vaccines.

5.1 INTRODUCTION

The creation of vaccines is one of medicine's most important accomplishments as it represents a valuable modality for immunization against human pathogens and treatment of diseases. While diseases like smallpox have been completely eradicated and polio is on the verge of elimination, infections due to measles, mumps, rubella, diphtheria, tetanus, pertussis, Haemophilus influenzae type b (Hib) disease, and yellow fever are now under higher control because of vaccination (Plotkin and Plotkin 2004). Although vaccines have been effective in reducing morbidity and mortality of some of the above diseases, new ones, such as AIDS, influenza (H1N1), hepatitis B virus (HBV) are constantly emerging. Adding to these complications are aging adult population with diminishing immune function, increased use of immunosuppressive agents for cancer, tissue transplantation, and autoimmune disease; and an upwardly spiralling cost of health-

care delivery that makes some existing vaccines unaffordable by the populations at greatest risk (Lawson, Freytag et al. 2007).

Many vaccine delivery methods are currently available in the market for preventive inoculation against various diseases. These methods include (1) needle injections (subcutaneous, intramuscular), (2) oral, sublingual and nasal administrations and (3) transdermal applications (e.g. needle-free systems). Among them, conventional techniques are based on the administration of vaccines with needles and syringes. As a consequence, even though the efficacy of this method of drug delivery is indisputable, it is limited by several drawbacks in terms of safety and acceptability (Zeldis, Jain et al. 1992). Prominent, among these, is the potential for opportunistic infections and transmission of blood borne diseases such as Hepatitis A, B, C and HIV viruses (Garfein, Vlahov et al. 1996); hence, in many cases the use of needles for drug administration is associated to a prophylaxis with expensive and toxic drugs. An additional disadvantage of hypodermic needles is that many patients are needle-averse, which can lead to significant problems with compliance. Studies indicate that approximately 20% of children suffered "serious distress" from vaccinations, and 8.2% of young adults had an "unreasonably intense" fear of injections"(Del Guidice and Sebastian 2006). Therefore, there is the urgent need for a patient-friendly vaccine delivery system.

The major non-invasive routes for the successful administration of vaccines and immunotherapeutics include oral, nasal/pulmonary and transdermal drug delivery. Oral delivery offers the advantage of an easy and non-invasive administration, but it is often associated with a limited bioavailability because of gastrointestinal degradation and epithelial barriers. Conversely, nasal administration provides a particularly ready access to systemic circulation and brain; however, it still faces several challenges, including

quantification and sufficient residence time of the exact dose that should be adsorbed either *via* transcytotic uptake by the so-called M-cells or by paracellular absorption through the nose. Finally, transdermal delivery offers a few advantages over the other technologies; therefore it will be discussed in more details in the following paragraphs.

5.1.1 Transdermal vaccine delivery

As part of the solution to the above problems, recently a great deal of effort is being directed towards developing nonparenteral alternatives to traditional vaccine delivery. One such approach, transdermal vaccine delivery (TVD), is a safe and non-invasive method of delivering antigens directly onto bare skin. The transdermal delivery systems represent an attractive alternative to several vaccines and in particular to hypodermic injection (Guy and Hadgraft 2003; Williams 2003; Prausnitz, Mitragotri et al. 2004; Bronaugh and Maibach 2005).

Transdermal vaccine delivery systems offer several important advantages over more traditional approaches. They avoid variations associated with gastrointestinal drug adsorption and first pass effect of liver, leading to improved bioavailability for vaccines that are prematurely metabolized when delivered orally (Cleary 1993; Henzl and Loomba 2003; Kornick, Santiago-Palma et al. 2003). Unlike hypodermic injections, they are neither painful, nor generate dangerous medical waste and pose the risk of disease transmission by needle re-use (Cleary 1993; Henzl and Loomba 2003). Since they are non-invasive and can be self-administered, therefore patient's compliance is increased. They can provide sustained and controlled delivery for a prolonged period of time (up to one week) resulting in reduction in dosing frequency (Varvel, Shafer et al. 1989; Yang, Park et al. 2004). They provide flexibility of terminating the drug administration in the event of any adverse reactions, either systemic or local by simply removing the delivery

system from the skin. They have reduced side effects associated with systemic toxicity and improved therapy due to maintenance of uniform plasma levels up to the end of the dosing interval (Varvel, Shafer et al. 1989; Cramer and Saks 1994; Kornick, Santiago-Palma et al. 2003; Yang, Park et al. 2004). The systems are generally easy to use (hence there is no need for trained personnel) and inexpensive, leading to reduced overall healthcare treatment costs (Payne, Mathias et al. 1998; Jarupanich, Lamlertkittikul et al. 2003; Archer, Cullins et al. 2004). In a few cases, they provide direct access to target or diseased site, e.g. in the treatment of skin disorders such as psoriasis, eczema and fungal infections (Long 2002). They provide an alternative in circumstances where oral dosing is not possible (e.g. in unconscious or nauseated patients) (Kornick, Santiago-Palma et al. 2003).

Simultaneously they also have several limitations. A molecular weight less than 500 Da is essential to ensure ease of diffusion across the skin's outmost layer, the Stratum Corneum (SC), (Bos and Meinardi 2000) since solute diffusivity is inversely related to its size. Sufficient aqueous and lipid solubility, with a log P (octanol/water) between 1 and 3, is required for the permeant to successfully traverse the SC and its underlying aqueous layers for systemic delivery to occur (Yano, Nakagawa et al. 1986). Intra- and inter-variability is associated with the permeability of intact and diseased human skin, which implies that there will be variable biological response depending on the skin conditions (Southwell, Barry et al. 1984; Larsen, Nielsen et al. 2003). Pre-systemic metabolism; the presence of enzymes, such as peptidases, esterases, in the skin might metabolise the peptides associated with vaccine into a form that is immunologically inactive, thereby reducing the immunogenicity of the vaccine (Steinstrasser and Merkle 1995). They also lead to skin irritation and sensitization, referred to as the "Achilles heel" of dermal and

transdermal delivery. The skin may become sensitive by exposure to certain stimuli; this may include vaccine itself, adjuvants or components of delivery devices, resulting in skin irritation and sensitization like erythema, oedema, etc (Hogan and Maibach 1990; Carmichael 1994; Murphy and Carmichael 2000; Toole, Silagy et al. 2002).

5.1.2 Skin composition

All the above limitations pertaining to transdermal vaccine delivery are attributes of human skin, which has a multifunctional role, primary among which is its role as a barrier against both the egress of endogenous substances such as water and the ingress of xenobiotic material (chemicals and drugs). This barrier function of the skin is reflected in its multi-layered structure (**Figure 5.1**).

As mentioned before, anatomically, the skin has many histologic layers, but in general, it is described in terms of three tissue layers: the epidermis, the dermis and the subcutaneous fat layer called hypodermis. The major rate limiting barrier within the skin that restricts the inward and outward movement of chemical or biochemical substances is the stratum corneum, the top layer of the epidermis consisting of compacted, flattened and dead keratinized cells in stratified layers with a density of 1.55 g/cc. Because of the dense nature of the stratum corneum, values of diffusion coefficients in this tissue are a thousand or more times smaller than in any other skin tissue, which results in higher resistance and general impenetrability. (Scheuplein and Blank 1971) The stratum corneum exhibits regional differences in thickness over the body. It is as thick as several hundred micrometres on the palms of the hand and soles of the feet in an adult, but over most of the body it is about 10 μm thick when dry, increasing to about 40 to 50 μm when fully hydrated. (Gennaro 2003)

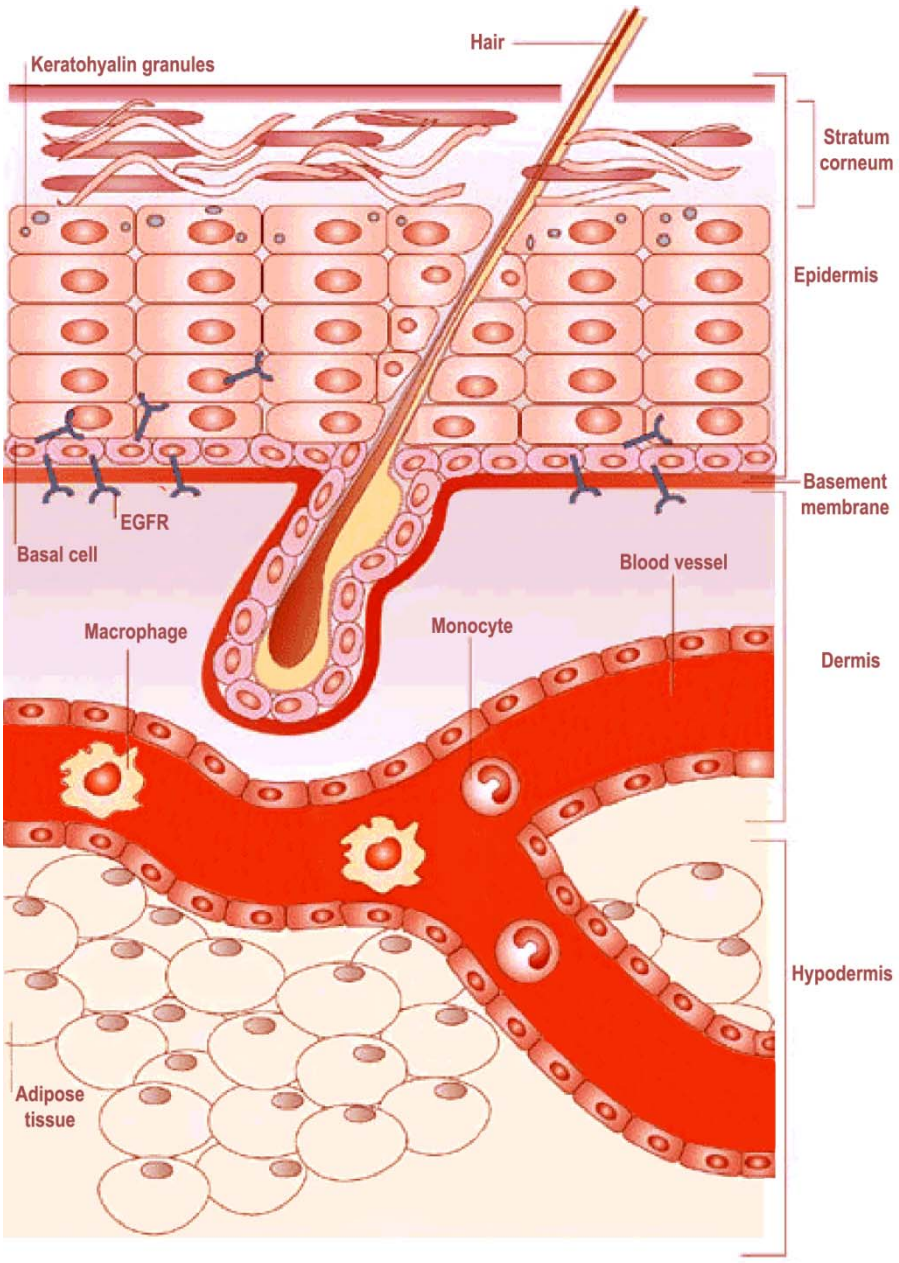

Figure 5.1: Schematic representation of the skin layers. From the outside to the inside there are Epidermis (with the SC), Dermis and Hypodermis (with blood vessels).

5.1.3 The Skin as a Target for Vaccination

The skin is an active immune organ which responds to foreign antigens through activation of the immune system comprising of number of antigen presenting cells (APCs) including the Langerhans cells (LCs) in the viable epidermis and the dermal

dendritic cells (DCs) in the dermis. These APCs play an important role in induction of both cellular and humoral immune response respectively. While LCs effectively prime peptide-specific naive CD8+ T cells and induce their differentiation into cytotoxic T lymphocyte (CTL) that express high levels of cytotoxic molecules as part of cellular immunity, CD14+ dermal DCs display a unique efficiency at inducing the differentiation of naive B cells into antibody secreting cells (ASC) as part of humoral immune response (Stoitzner, Sparber et al. 2010; Ueno, Schmitt et al. 2010). Tissues such as muscles, which are generally targeted by hypodermic needles for delivery of conventional vaccines, have few resident APCs. Conversely the sheer abundance and superficial location of LCs and dendritic cells, and their potent APC activity makes the skin as an attractive tissue for vaccine delivery (Ziegler 2008).

5.1.4 Routes of Penetration

Although the stratum corneum is an efficient barrier, some chemical substances are able to penetrate it and reach the underlying tissues and blood vessels. These "successful" substances are characterized by low molecular weight (≤ 500 Da), lipophilicity, and effectiveness at low dosage. One such substance currently being used is nicotine which has the largest daily dose among drugs in patch form: twenty-one milligrams (Prausnitz, Mitragotri et al. 2004).

Drug molecules (including vaccines) in contact with the skin surface can penetrate by three potential pathways: through the sweat ducts, *via* the hair follicles and sebaceous glands (collectively called the shunt or appendageal route), or directly across the stratum corneum. However it is generally accepted that the appendages comprise a fractional area for permeation of approximately 0.1%, (Higuchi 1962) and their contribution to steady state flux of most drugs is minimal. This assumption has resulted in the majority of skin

penetration enhancement techniques being focused on increasing transport across the stratum corneum rather than via the appendages. Exceptions are iontophoresis, which uses an electrical charge to drive molecules into the skin primarily via the shunt routes as they provide less electrical resistance, and vesicular delivery. (Benson 2005)

These skin penetration enhancement techniques can be broadly divided in to two main categories defined as either passive or active methods.

5.1.4.1 Passive methods for enhancing transdermal drug delivery

Passive transdermal delivery includes conventional means of applying drugs to skin using vehicles such as ointments, creams, gels and skin patch technology. Such methods have been further improved or developed over the last decades in order to enhance the driving force of drug diffusion (thermodynamic activity) and/or increase the permeability of the skin using penetration enhancers (Williams and Barry 2004), supersaturated systems (Pellett, Raghavan et al. 2003), prodrugs or metabolic approaches (Tsai, Guy et al. 1996; Elias, Feingold et al. 2003), liposomes and other vesicles (Schreier 1994; Cevc 1996; Cevc 2003; Godin and Touitou 2003). However, the amount of drug that can be delivered by the above indicated methods is still limited, as these advanced strategies do not bring about any fundamental change in barrier properties of the skin or more specifically of the stratum corneum. Furthermore, advent of biotechnology has led to the generation of therapeutically active, large molecular weight (>500 Da) polar and hydrophilic molecules, mostly peptides in form of vaccines. Such molecules are susceptible to degradation by gastrointestinal enzymes when delivered via oral route and hence they suggest the need to achieve efficient delivery by alternative administration routes. Since passive methods of skin delivery are incapable of enhancing permeation of

such large molecules, therefore studies involving the use of active techniques have gained importance lately.

5.1.4.2 Active methods for enhancing transdermal drug delivery

These methods are poised to make significant impact on transdermal vaccine delivery as they target to reduce the barrier of stratum corneum by enabling its stronger disruption in order to enhance permeation of antigens without disturbing deeper tissues of the skin. Recent technologies (e.g. electroporation, thermal ablation, microdermabrasion and microneedles) have progressed as a result of advances in precision engineering (bioengineering), computing, chemical engineering and material sciences, all of which have helped to achieve the creation of miniaturized, powerful devices that have been shown to deliver macromolecules, including therapeutic proteins and vaccines, across the skin in human clinical trials (Arora, Prausnitz et al. 2008; Jain 2008). However, each of these methods has specific practical limitations, including scale-up, translation from animals to humans, safety, bioavailability, device development, and regulatory approval (Mitragotri 2004).

5.1.4.2.1 Electroporation

It involves the application of high-voltage (≥100 V) pulses for duration of milliseconds to induce skin perturbation. The increase in skin permeability is suggested to be caused by reversible disruption of lipid bilayer structures (Denet, Vanbever et al. 2004; Li 2008) in the skin leading to the generation of transient pores called electropores (Weaver, Vaughan et al. 1999). The electric field applied for milliseconds duration provides electrophoretic driving force, which helps in molecular diffusion via these long-lived electropores, increasing the magnitude of transdermal transport of molecules with

differing lipophilicity and size (i.e. small molecules, proteins, peptides, vaccines and DNA), including biopharmaceuticals with a molecular weight greater than 7 kDa (Denet, Vanbever et al. 2004). Recently, electroporation was shown to deliver a model peptide vaccine into the skin of mice to generate a strong cytotoxic T lymphocyte response (Zhao, Murthy et al. 2006). Although electroporation has been studied extensively in animals, this approach to transdermal delivery has received limited attention in humans thus far due largely to the complexity of device design and pain and muscle stimulation associated with distribution of electric field to sensory and motor neurons in the deeper tissues (Prausnitz and Langer 2008).

5.1.4.2.2 Microdermabrasion

It is a widely used method involving direct removal or disruption of the upper layers of the skin to enhance the permeation of topically applied compounds. This abrasive mechanism related to sand blasting on the microscopic scale, has been shown to increase skin permeability to some of the vaccines and biopharmaceuticals, which suggests possible applications in transdermal vaccine delivery. However, these abrasion devices are generally expensive and usually require trained personnel to operate them, therefore limiting applicability of the technique (Jain 2008).

5.1.4.2.3 Thermal ablation

Thermal ablation is achieved by selectively and transiently heating the skin surface to hundreds of degrees for microseconds to milliseconds, in order to generate micron-scale perforations in the stratum corneum without allowing heat to propagate to the viable tissues below (Bramson, Dayball et al. 2003; Levin, Gershonowitz et al. 2005). It may involve rapidly vaporizing water in the stratum corneum, such that the resulting

volumetric expansion ablates micron-scale craters in the skin's surface (Park, Lee et al. 2008). Animal studies have demonstrated the ability of thermal ablation to deliver a number of different compounds, such as human growth hormone and interferon α-2b (Levin, Gershonowitz et al. 2005; Badkar, Smith et al. 2007). However, regulatory compliance may be necessary for exposure to such a high temperature. In addition, the issue of vaccine stability may also need to be addressed when elevated temperature are used (Jain 2008).

5.1.4.2.4 Sonophoresis

It involves the use of ultrasonic energy to enhance the transdermal delivery of drugs either simultaneously or via pre-treatment. The mechanism behind the enhanced skin permeability is attributed to the formation of gaseous cavities or bubbles within the intercellular lipids on exposure to ultrasound, resulting in disruption of the SC (Mitragotri, Blankschtein et al. 1996). Although frequencies between 20 kHz – 16 MHz have been reported to increase skin permeation, frequencies at the lower end of this range (<100 kHz) are believed to have a more significant effect on transdermal drug delivery, with the delivery of macromolecules of molecular weight up to 48 kDa being reported (Mitragotri, Blankschtein et al. 1995; Mitragotri, Blankschtein et al. 1996; Liu, Li et al. 2006). Sonophoresis has been approved for enhanced delivery of lidocaine through the skin (Becker, Helfrich et al. 2005) and has been studied extensively in animals for delivery of insulin, as well as heparin, tetanus toxoid vaccine and other compounds (Ogura, Paliwal et al. 2008). But Sonophoresis can be time consuming to administer as proper adjustment of ultrasound is necessary, not only to keep the stratum corneum intact for effective drug penetration, but also to minimize or eradicate tingling, irritation and burning associated with it (Escobar-Chavez, Bonilla-Martinez et al. 2009).

5.1.4.2.5 Microneedles

These are micron-scale structures that pierce into the skin and thus allow the unhindered movement of any topically applied drugs in a minimally invasive and targeted manner (Sullivan, Koutsonanos et al. 2010). The length of these microneedles has been estimated to be variable between 0.10-1.00 mm The microneedles can actively drive drugs, vaccines, peptides, nanoparticles and a variety of small molecules into the skin either as coated or encapsulated cargo introduced during solid microrod insertion or via convective flow through hollow microneedles.

Several recent advances have been made in microneedle design and formulation with regard to transdermal delivery of drugs. Notable among them are microneedles made up of water soluble, biocompatible polymers like polyvinylpyrrolidone (PVP) that can encapsulate various compounds within the needle matrix (Sullivan, Koutsonanos et al. 2010). These microneedles dissolve in the skin over a timescale of minutes and thereby leave no sharp medical waste after use (Lee, Park et al. 2008). Sullivan et al.(Sullivan, Koutsonanos et al. 2010) have recently designed and fabricated dissolving polymer microneedle measuring 650 μm in height and 10 μm in radius of curvature, which encapsulated influenza virus vaccine and successfully immunized mice with robust antibody response and cellular immune responses. This year, the pharmaceutical company Sanofi Pasteur has introduced in the market the inactivated influenza vaccine in form an intradermal microinjector (INTANZA ^{TM}), showing both efficacy and safety profiles comparable to conventional intramuscular systems.

However, microneedles are usually penetrating both the epidermis and the dermis (Prausnitz, Gill et al. 2008), thus encountering the pain-transmitting-nerves with concomitant painful sensation. In addition to that, microneedle-generated pores may

allow pathogenic microorganisms such as *Staphylococcus aureus* to penetrate the stratum corneum layer of the epidermis and cause local or systemic infection (Gittard, Narayan et al. 2009).

5.1.4.2.6 Jet injectors

It involves the administration of drugs to the skin by firing the liquid or solid particles at supersonic speeds through its outer layers by using a suitable energy source. A number of needle-free or jet injector systems, both for liquid (Ped-O-Jet®, Iject®, Biojector2000®, Medi-jector® and Intraject®) and powder (PMED™ device, formerly known as powderject® injector) are currently in use (Giudice and Campbell 2006). The latter has been reported to deliver successfully testosterone, lidocaine hydrochloride and macromolecules such as calcitonin and insulin (Burkoth, Bellhouse et al. 1999).

However, due to concerns over cross-contamination during splash back (Hoffman, Abuknesha et al. 2001), poor reliability of dose and depth of delivery(Theintz and Sizonenko 1991; Schramm and Mitragotri 2002), and complaints of painful bruising and bleeding (Schneider, Birnbacher et al. 1994; Mitragotri 2006), jet injectors have not gained wide acceptance. The lack of reliability associated with jet injectors is thought to arise partly from the failure of current devices to respond to the large variations in the mechanical properties of the skin (Schramm and Mitragotri 2002). Additionally, the large dose sizes (Mitragotri 2006) (tens to hundreds of microliters) and nozzle diameters (100–500 μm) used in these devices likely worsen the reliability problem by causing splash back of the drugs or vaccine from the skin and may be responsible for pain.

5.1.5 Nanotechnology for Transdermal vaccine delivery

The study of nanotechnology for transdermal delivery of vaccines is burgeoning. Vaccines based on combination of nanotechnology and transdermal delivery may prove superior to existing vaccines and can simultaneously open new therapeutic avenues for treating infectious disease and malignancy (Nasir 2009). Several products utilizing aspects of nanotechnology in their transdermal formulation are already in the developmental pipeline, and these technologies are also simultaneously being applied to future vaccine development. The most important transdermal delivery system currently being investigated for such purpose is represented by nanoneedles.

5.1.6 Nanoneedles

These consist of a small patch full of tiny needles made up of suitable bio-compatible materials. Unlike previously discussed microneedles, these nanoneedles are of 5-100 μm in length having a base radius of 100-200 nm. These needles can be formed into arrays and used to deliver just about any active ingredient, including antigens for vaccination. The array is pressed against the skin and, because the length of the nanoneedle is so less, the patient feels nothing. Due to this reduced dimensions, they have several advantages compared to both upcoming and conventional transdermal delivery methods. Nanoneedles can deliver vaccines in form of antigens through nanopores created onto the skin; such holes tend to close quickly, thus re-equilibrating the skin to a much higher extent than any microscopic counterpart. Even more important, unlike the micropores formed during the use of microneedle, the nanopores formed on the skin during the use of nanoneedles may not be permeable to pathogenic microbes.

Similar to microneedles, they can be solid where they can be precoated with vaccine, or hollow through which vaccine can pass from the external reservoir. Regarding safety aspect of transdermal delivery systems based on nanoneedles, these nanoneedles must be made up of materials having known clinical biocompatibility data. One such material being used to manufacture nanoneedle is zinc oxide (ZnO). Zinc oxide itself is effective as an antimicrobial agent and has been shown to provide cytoprotection to tissue cells (Soderberg, Sunzel et al. 1990). In addition, zinc oxide is also currently used in dentistry and cosmetic ointments, creams, and lotions to protect against sunburn and skin damage caused by ultraviolet light. Gopikrishnan et al. have shown that synthesized ZnO nanorods exposure on Hela cells had no significant induction of oxidative stress or cell death even in higher concentration (10μg/ml) (Gopikrishnan, Zhang et al. 2010). This suggests that ZnO nanoneedles might be a safer nanomaterial for application in transdermal delivery of vaccines. Therefore, in the study reported below, we have explored aligned ZnO nanorods on solid support for transdermal delivery of a vaccine prototype.

5.2 OBJECTIVE

The aim and objective of this study was to carry out feasibility study with regard to use of ZnO nanoneedles or nanorods grown successfully on silicon chip for transdermal delivery of vaccines. In other words we evaluated the ability of this novel device, made up of nanometric rods to act as an efficient tool for the penetration of the SC and the stimulation of immunological response. Being a preliminary study, we utilized ovalbumin (OVA) as a vaccine prototype with a hope that the data obtained will be useful for further future investigations of this novel device with regard to vaccine such as pertussis, tetanus, influenza etc.

5.3 MATERIALS

5.3.1 Chemicals

Albumin-FITC (Albumin, Fluorescein isothiocyanate conjugate from bovine, A9771), Goat anti-mouse IgG horse radish peroxidases (HRP) conjugate (A4416), Aluminum hydroxide gel (Alum, A8222) and 3, 3', 5, 5' – tetramethylbenzidine (TMB, T0440) were bought from Sigma Aldrich. Fetal bovine serum (FBS, research grade) was bought from HyClone, UK. Phosphate buffer saline (PBS, ultrapure grade was bought from 1st BASE, Singapore. Tween 20 (polyethylene glycol sorbitan monolaurate, A R Grade) was bought from NUMI, NUS. Concentrated sulfuric acid (H_2SO_4) was bought from Merck. Endograde Ovalbumin (lyophilized) was bought from Hyglos GmbH, Germany.

5.3.2 Animals for *in-vivo* experiments

The *in vivo* experiments including process of immunization and collection of serum were done by Dr Jan Fric, Singapore Immunology Network. The experimental plans were formulated by Dr Florent Ginhoux, Singapore Immunology Network. The female BALB/c mice, of 6-8 weeks age at the beginning of each experiment, were sourced from Biopolis animal facility, Singapore. The animals were kept under standardized conditions at the animal facility during the whole period of the experiment. They had free access to rodent chow and water and they were used in accordance with the guidelines of the National Research Council.

5.3.3 Preparation of excised human epidermis

Human abdominal skin was obtained from skin sample of a 22-year-old Indian lady from the Singapore General Hospital (SGH), with prior consent of the donor. Epidermis

was prepared by immersing the whole skin in 60 ºC water for 10 minutes, followed by careful removal of the epidermis from the connective tissues (Kligman and Christophers 1963). Briefly the piece of skin was put into the preheated beaker, whose temperature was kept within the range of 60-65 ºC. After 10 minutes the skin was taken out of the beaker and transferred into a petri dish. With the help of a forceps with sharp ending, a tiny bit of skin was scrapped on its edge, thereby revealing an open area, where the upper part of the skin had disappeared. With another forceps having flat end, the skin was further scrapped, moving it towards the part still covered with skin. By making gentle horizontal movements, the forceps was pressed down on to the underlying collagen until the whole stratum corneum of the epidermis came off. Finally it was stored in plastic bags at -80 ºC until use. Prior to experiments, these membranes with the *stratum corneum* sides up were floated over PBS to.

5.3.4 Preparation of aligned ZnO nanoneedles on a silicon substrate

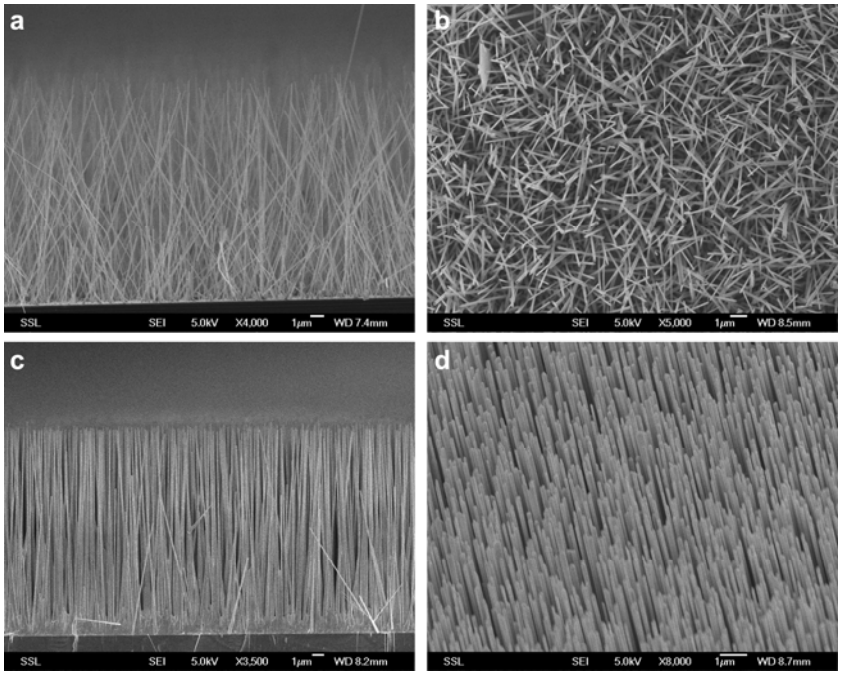

Figure 5.2: SEM images showing side view (a, c) and top view (b, d) of nonaligned and aligned ZnO nano chips, respectively.

Vertically aligned *Zinc Oxide* Nanoneedles chips (courtesy of Professor Sow Chorng Haur of the Department of Physics, National University of Singapore) were synthesized following the procedure described elsewhere (Li, Fang et al. 2006), that is using a vapor-solid (VS) mechanism on Silicon wafers coated with a *Zinc Oxide* seed layer of approximately 200nm. The density was about 5 tubes/μm^2. The obtained chips were of 1cm X 1cm dimension and consisted of ZnO pyramidal nanoneedles (Scheme 1-3) with a tip size of 60 nm and a length ranging from 25-49 μm. The base size of the needles was 150 nm, and the distance between 2 nanorods was of about 0.3 μm.

5.4 METHODS

5.4.1 Skin penetration study

5.4.1.1 Adsorption of vaccine prototype onto chip

About 16 mg of *Albumin-FITC* were weighed and mixed with 3 ml of Phosphate Buffer Saline (PBS) in a 5ml centrifuge tube for *in vitro* skin permeation study. The suspension was sonicated for 1 minute. Out of which 1ml was poured in to a well of 24 well plate (Greiner bio-one, Germany). The silicon chips grown with *Zinc Oxide* nanorods (courtesy of Professor Sow Chorng Haur of the Department of Physics-National University of Singapore) were placed in the same well and finally kept inside freeze at 4 ºC for the adsorption of *Albumin-FITC* onto the chip.

For *in vivo* skin penetration study, higher initial concentration of *albumin-FITC* (10mg/ml) was used. We also changed the method of functionalization of the chip owing to loss of vaccine prototype during previous method used for the purpose of in vitro skin penetration study. About 1.8 mg of *albumin-FITC* was added to 180 μl of PBS and

mixed properly. 60 µl of this solution was adsorbed on to each chip using micropipette. Sufficient care was taken for not allowing the *albumin-FITC* solution to flow out of the chip, for which each time 20 µl of the solution was put on to the chip for adsorption. This process was repeated for three times to have 60 µl of this solution adsorbed on to the chip.

5.4.1.2 *In vitro* skin penetration study

In vitro skin penetration studies were conducted in Prof Chan Sui Yung's lab to investigate the degree of adsorption and penetration of *Albumin-FITC* across the previously prepared stratum corneum (SC). Franz flow-through type diffusion cells (**Figure 5.3**) were used for the skin penetration study.

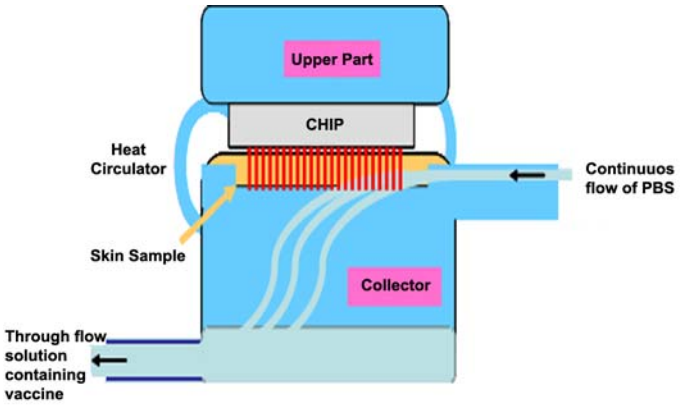

Figure 5.3: Schematic representation of *in vitro* skin penetration study using Franz flow-through type diffusion cell.

The chip was mounted on to the donor having nanorods facing the receptor chamber. Human SC was mounted on to the chip attached to the donor with the top of stratum corneum facing the nanorods. Subsequently the donor having the chip and SC attached to it was mounted on to the receptor compartment. The receptor solution of 500 ml of PBS was placed in the reservoir bottle and allowed to flow through the receptor compartment

at 0.50 ml/h. The receptor solution was thoroughly degassed to prevent the formation of bubbles beneath the membrane. Temperature of the cells was controlled at 37 ºC by a heater/circulator (Haake, Germany). The receptor solution was pumped by a 16 channel peristaltic cassette pump (Ismatec, Switzerland) continuously through the receptor compartment and drained into the test-tube sitting in the fraction collector (ISCO Retriever IV, US). Cumulated receptor liquid samples were taken at 3 h intervals for protein assay. Experiments were carried out in triplicate, performed in different times over a period of 4 months.

The nanorod chips used for the purpose were visualized through SEM (JEOL JSM-6701F field-emission scanning electron microscope) and fluorescence microscopy (Nikon AZ-100) both before and after the *in-vitro* skin permeation study to analyze the integrity of the nanorods on the silica support and to determine condition of *albumin-FITC* adsorbed on to the nanoneedles. The human skin used for the purpose was visualized under Nikon Eclipse Ti-E inverted microscope with Nikon C1si laser scanning confocal for depth and uniformity of the penetration.

5.4.1.3 *In vivo* skin penetration study

The three albumin-FITC functionalized chips were applied to dorsal part of the right ear of each mouse for 1 minute using manual pressure. Finally the ear of each mouse applied with ZnO nanoneedles were cut and split in to dorsal (test) and ventral (control) skin. These skin samples were subjected to confocal microscopy (Nikon A1R Fast Laser Scanning Confocal) to determine the depth of penetration of the nanoneedles across the stratum corneum.

5.4.2 Transepidermal water loss (TEWL)

Among the various methods aimed to measure skin's appearance and its eventual modification (Andersen and Maibach 1995), trans epidermal water loss (TEWL) is widely used being a quick and non-invasive biophysical technique (Pinnagoda, Tupker et al. 1990; Fluhr, Kuss et al. 2001). TEWL is defined as the measurement of the quantity of water that passes from inside a body through the epidermal layer (skin) to the surrounding atmosphere via diffusion and evaporation processes. Such measurement might be useful to determine skin damage or, in our specific case, to evaluate the ZnO nanorod mediated enhancement of skin permeation.

TEWL was measured with a Tewameter, which consisted of a closed transparent chamber containing sensors for relative humidity and temperature. The scheme below (**Figure 5.4**) shows a linear increase of relative humidity (RH %) in the chamber shortly after placing the device in contact with the skin. The TEWL is calculated from the increase in RH %.

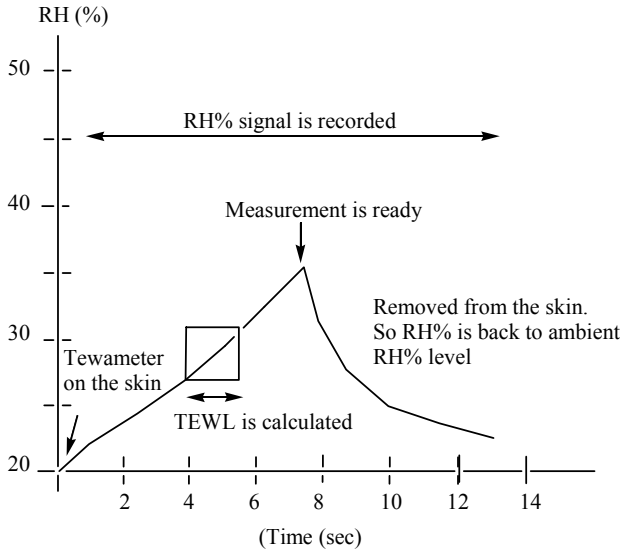

Figure 5.4: Graph showing working principle of the VapoMeter

The study was conducted by Dr Giorgia Pastorin, assistant professor, department of Pharmacy, National University of Singapore, Singapore in the early afternoon (13.30) in a temperature controlled room (temperature was kept at 21ºC) and the subject acclimatized for about 20 minutes prior to start the experiment. Prof Hans Junginger, Faculty of Pharmaceutical Sciences, Naresuan University, Phitsanulok, Thailand, volunteered as a subject for this experiment. Four angles of a squared area were marked on each forearm in the center of which the TEWL were measured before and after the chips were placed (**Figure 5.5a**). Before applying the nanoneedle device, baseline values were recorded for the barrier function (TEWL). TEWL was measured using Tewameter TM 300 Courage+Khazaka (Cologne, Germany) (**Figure 5.5b**) at the Cosmetic and Natural Product Research Centre (**COSNAT**), Naresuan Hospital, (Phitsanulok, Thailand).

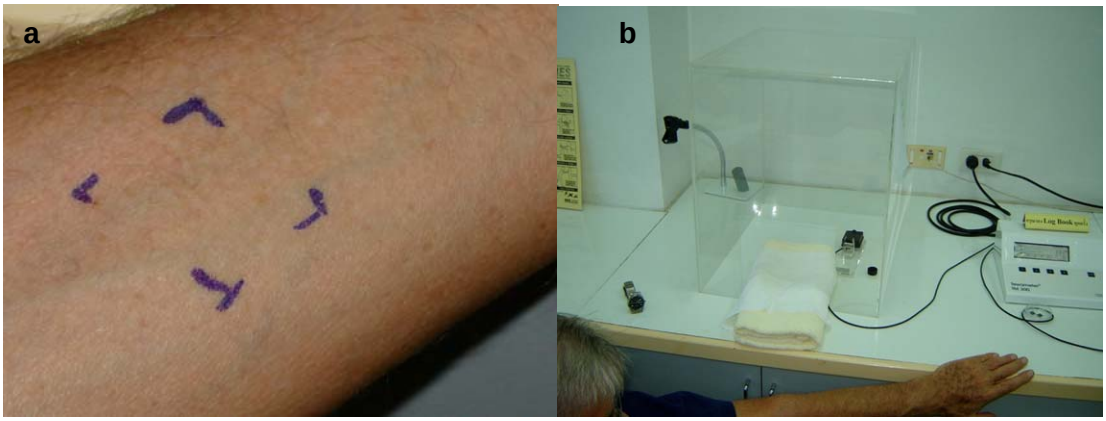

Figure 5.5: Image showing (a) skin area where the TEWL measurements were performed, (b) Tewameter and the chamber of measurement.

The probe of the apparatus was placed gently onto center of the marked square on the skin, and values were collected over a period of 30 seconds, after which an average reading was automatically generated. Measurements on the 2 arms were performed at different time. Baseline measurements were made every 5 minutes for 20 minutes. The values were expressed as g h^{-1} m^{-2} and were calculated from a mean of 3 consecutive

measurements. The measurements were performed directly after a two-fold application (0 minutes) and repeated every 5 minutes over a period of 25 minutes.

5.4.3 Tape stripping

To verify whether the protein delivered from the chips was not stacked at the surface and, on the contrary, it was able to effectively penetrate through the skin, a tape stripping experiment was associated with this study (conducted by Dr Giorgia Pastorin, Department of Pharmacy, National University of Singapore): a chip, adsorbed with *albumin-FITC* through the same procedure as described previously in *in vitro* skin penetration study, was applied onto the skin of the dorsal part of the forearm of Prof Hans Junginger, Faculty of Pharmaceutical Sciences, Phitsanulok, Thailand, who volunteered for the experiment, for a period of one hour (**Figure 5.6a**), after which the skin correspondent to the treated area underwent 18 cycles of application-removal tape stripping (**Figures 5.6b** and **5.6c**).

Figure 5.6: Image showing (a) application of the chip on the forearm skin for one hour, (b) tape stripping in the area where the chip was applied previously, (c) skin appearance after 18 tape stripping.

Tape strips were removed from the skin area of the forearm of the volunteer after 1-hour application of one chip previously adsorbed with Albumin-FITC until a shiny watery layer appeared (wet epidermis layer). The adhesive tape (Transpore tape" from 3M

Company) was pressed onto the surface of the skin and removed with one quick movement and fixed directly to a slide frame. The tape stripping procedure was repeated 18 times on the same skin area, and the correspondent slide frames were analyzed under fluorescence microscope.

5.4.4 Immunization of mice and determination of immune responses

The immunization on the back of the mice has been routinely conducted after shaving of the skin surface to remove hair. The shaving procedure may assists in the controlled delivery of the antigen and simultaneously allows visual assessment of the applied area. However, an important concern with regard to this method has been that small abrasions resulting from the shaving process itself may contribute to the potent systemic immune response observed (Scharton-Kersten, M. Glenn et al. 1999). To exclude this possibility we have immunized mice on the ear which does not require shaving because of its naturally hairless surface. Thus the penetration of the ZnO nanoneedle adsorbed with endograde OVA and immunization of mice ear skin is not dependent upon shaving insults to the stratum corneum.

5.4.4.1 Preparation of endograde OVA solution

2.4 mg of endograde ova was added to 240 µl of sterile PBS. Each was added with 40 µl of this solution to have 400 µg of OVA on each chip.

5.4.4.2 Preparation of OVA in alum suspension

The OVA in alum suspension was prepared following the procedure mentioned elsewhere (Boonyo, Junginger et al. 2007). Briefly 28 µl of alum (13mg/ml) was mixed with 332 µl of PBS to get 360 µl of alum suspension (100 µg/ 100 µl) and was autoclaved before use. The sterile alum suspension was added to 2.4 mg of endograde OVA to get

360 µl of alum suspension with OVA. The PH of this suspension was adjusted to 7.4 with 0.5 N NaOH. Each chip was added with 60 µl of this suspension to have 400 µg of OVA and 60 µg of alum adsorbed in it.

5.4.4.3 Functionalization of chips

Altogether 12 ZnO nanoneedle chips were used for the purpose. All the functionalized chips were stored at 4ºC to prevent drying of the nanoneedle surface.

Group 1: 3 chips were charged with 60 µl of PBS each and applied on to the ear of the mice to be used as negative control.

Group 2: 3 chips were charged with 40 µl endograde OVA solution (10 mg/ml) and were applied on to ear of mice for the purpose of immunization.

Group 3: 3 chips were adsorbed with 40 µl endograde OVA solution (10 mg/ml) and were applied to mice ear stripped of stratum corneum.

Group 4: 3 chips were adsorbed with 60 µl of endograde OVA with alum suspension to have 400 µg of OVA and 60 µg of alum (adjuvant).

5.4.4.4 Application functionalized chips on to the mice ear

For the purpose dorsal surface of the mice ear was gently swabbed with cotton tipped applicator containing 70% ethanol and was allowed to dry. Since hydration of the skin allows better penetration of the antigen in to the epidermis (Glenn, Rao et al. 1998), therefore functionalized chips, in some cases were charged with 10 µl of PBS to avoid the chips surface becoming dry before application on to the ear of the mice. While functionalized chips were applied for 1 minute by manual pressure to the dorsal part of

the right ears of the anesthetized mice, the left ears of the mice were punched for identification.

5.4.4.5 Collection of mice serum

Blood samples (0.2 ml) per animal were collected from the cut tail tip of mice after 1 week from the day of immunization from 12 mice used for the purpose. Each of these samples in microcentrifuge tubes was spinned down at 3000 RPM for 15 minutes. The supernatant (serum) was separated and transferred to respective marked centrifuge tubes and stored at -80ºC till further use.

5.4.4.6 Enzyme-Linked Immunosorbent Assay (ELISA)

Immune responses to various OVA formulations including the negative control were analyzed after 1 week by Enzyme-Linked Immunosorbent Assay (ELISA) in order to determine the levels of OVA-specific serum immunoglobulin G (IgG) antibody as mentioned elsewhere(Boonyo, Junginger et al. 2007).

5.4.4.6.1 Preparation of coating buffer

Coating buffer (0.05 M bicarbonate buffer, PH-9.6) for coating antibody on to wells of NUNC Maxisorp plates was prepared by adding 1.59 g of Na_2CO_3, 2.93 g of $NaHCO_3$ and 0.2 g of NaN_3 to 900 ml of water and properly mixed. The volume was finally made up to 1 Liter by adding extra milliQ water. The PH of 9.6 was confirmed by using pH meter.

5.4.4.6.2 Preparation of coating solution

3.0 mg of endograde OVA was added to 30 ml of 0.05 M bicarbonate buffer (PH 9.6) and stored inside freeze at 4ºC for future use.

5.4.4.6.3 Preparation of washing buffer

400 ml of PBS was added with 250 µl Tween 20 (T20) and mixed properly. The volume was made up to 500 ml by adding more PBS to have 0.05% Tween 20 in PBS (T20/PBS) washing buffer.

5.4.4.6.4 Preparation of blocking buffer

50 ml of fetal bovine serum (FBS) was added with 450 ml of PBS to get 10% FBS in PBS (10 FBS/PBS) buffer.

5.4.4.6.5 Preparation of 1N H_2SO_4

10 ml of concentrated (36N) H_2SO_4 was added to 350 ml of milliQ water to get 1N H_2SO_4.

5.4.4.6.6 Procedure

Briefly, four 96 well Maxisorp NUNC-Immuno ™ flat bottom plate (properly labeled), were coated with 50 µl/well of 100 µg/ml OVA in coating solution (0.05 M bicarbonate buffer, PH 9.6). After overnight incubation at 4ºC, the plates were washed 6 times with 0.05% v/v Tween 20 in phosphate buffer saline solution (T20/PBS). Blocking was carried out by adding 200 µl of 10% v/v FBS in PBS (10 FBS/PBS) into the wells followed by a 2 h incubation at room temperature. The plates were then washed with T20/PBS for 3 times. 40 µl of each serum sample was added with 160 µl of 10 FBS/PBS to give a 1: 5 dilution of serum. 100 µl of 1:5 diluted serums from each sample were added to wells of respective marked well plate in duplicate. Two fold serial dilutions were done using 10 FBS/PBS in ELISA plates starting from 1:10 to 1:20480 dilutions. Blanks were also set up in duplicate using 100 µl of 10FBS/PBS and the absorbance of these blanks will be subtracted from the absorbance of the standards and samples. The ELISA

plates were incubated for 1 hr at room temperature and then washed with T20/PBS for 3 times. Goat anti-mouse IgG HRP conjugate was diluted with 10FBS/PBS to have 1:5000 diluted secondary antibody solutions and 100 µl of this diluted solution was added into each well and further incubated for 45 min at room temperature. The plates were washed with T20/PBS and 100 µl of TMB were then added into each well. After the color development, the reaction was stopped by adding 100 µl/well of 1N H_2SO_4. The absorbance was measured at a wavelength of 450 nm using a micro plate reader (Spectra count, Perkin Elmer, USA).

5.4.5 Bradford protein quantification

5.4.5.1 Standard curve for albumin-FITC

1 mg of *Albumin-FITC* was weighed and dissolved in 1 ml of PBS in a 2ml centrifuge tube. Different concentrations (0.02-0.08mg/ml) of Albumin-*FITC* were prepared by diluting this solution with different volume of PBS. 100 µl of each of these concentration samples were taken in 5 ml test tubes and were added with 5 ml of Bradford reagent (Bio-Rad). Then Optical Density (OD) was taken at 595 nm for all the concentrations and a graph was plotted to get the standard curve (**Appendix-V**).

5.4.5.2 Standard curve for endograde OVA

The original given solution (10mg/ml) was diluted to have 1 mg/ml solution. Serial dilution was done to have different dilutions (100 µg/ml - 1000 µg/ml) of endograde OVA solution. 20 µl of the above dilutions of endograde OVA were taken in a 96 micro well plate in triplicates and 200 µl of the Bradford reagent was added to each well and mixed properly. Finally the absorbance reading was taken at 595 nm to plot the standard curve (**Appendix VI**).

5.4.5.3 Protein quantitation

Albumin-FITC samples, collected from the washing of the chips, both before and after their use in *in-vitro* skin permeation study and the receptor liquid samples were subjected to Bradford protein quantification. 20 µl of each samples were added with 80 µl of PBS to give a 5 times dilution of the protein concentration. It was further added with 5 ml of Bradford reagent and OD was taken at 595 nm. This OD was then compared with the standard curve to get the appropriate protein concentration. This concentration was then multiplied with 5 to get original concentration of the protein sample.

Similarly the chips used for immunization of mice were washed with PBS to have the endograde ova samples which were also subjected to Bradford protein quantification to determine the approximate amount of protein that may have been delivered to the mice skin.

5.5 RESULTS

5.5.1 *In vitro* skin penetration study

In vitro skin permeation study was conducted to investigate the degree of penetration of nanorods through human skin samples using Franz diffusion cells. Since our vaccine prototype (albumin) was incorporated with the fluorescent molecule FITC, we could visualize our protein adsorbed onto the nanorods both before and after the skin penetration study.

5.5.1.1 Scanning electron microscopy

Figure 5.7 shows the SEM image of the ZnO nanorod chip before and after skin penetration study *in vitro*. This was done to verify the state of the nanorods and the

condition of their alignment. Although from the figure change in the shape of the nanorods was evident, it is also important to note that nanorods remained attached to the chip, since no reduction in their density was noticed all along the sample. Additionally most of the nanorods preserved certain degree of alignment and only the tips were affected.

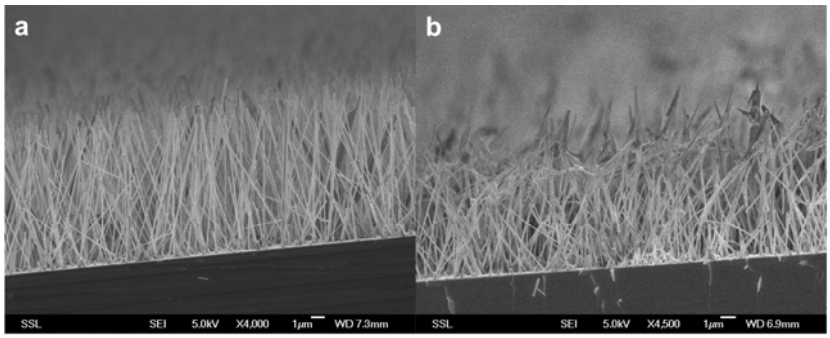

Figure 5.7: SEM of the chip before and after the skin penetration study. (a) Chip Before skin penetration study. (B) Chip After skin penetration study.

5.5.1.2 Fluorescence and confocal microscopy

From **Figure 5.8,** it can be seen that before application onto the skin, the chip shows uniform presence of albumin-FITC adsorbed on to each nanorods, whereas after the skin penetration study, some blank patches have been formed on the chip suggesting detachment of Albumin-FITC from the chip. To determine the fate of the above detached albumin-FITC, human skin used for the purpose was subjected to confocal laser scanning microscopy after the skin penetration study. **Figure 5.9 (a)** represents a 3D image of the human skin as obtained from confocal microscopy, confirming a uniform distribution of the vaccine prototype onto the skin layer. Similarly, another confocal image (**Figure 5.9 (b))** shows the formation of nanoscopic tunnels through the skin layer in XYZ direction due to the penetration of ZnO nanorods adsorbed with albumin-FITC. . From this image it

was possible to calculate the length of each channel. The average length of the channel formed through the skin was found to be about 9 µm.

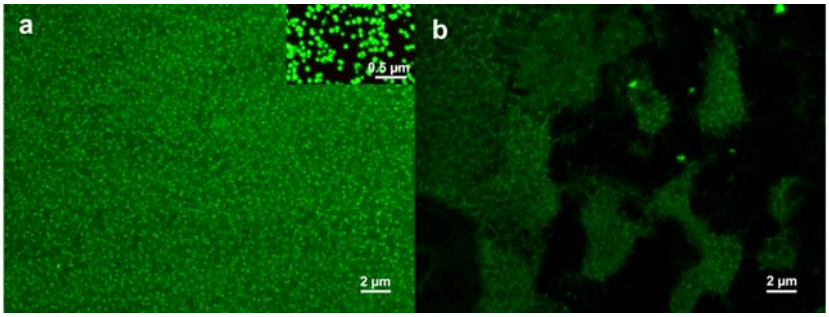

Figure 5.8: Fluorescence microscopy of the ZnO nanorod chip adsorbed with albumin-FITC (a) before application on to the skin and (b) after application on to the skin for in vitro skin penetration study. The top right corner of the figure (a) shows magnification of the chip's surface.

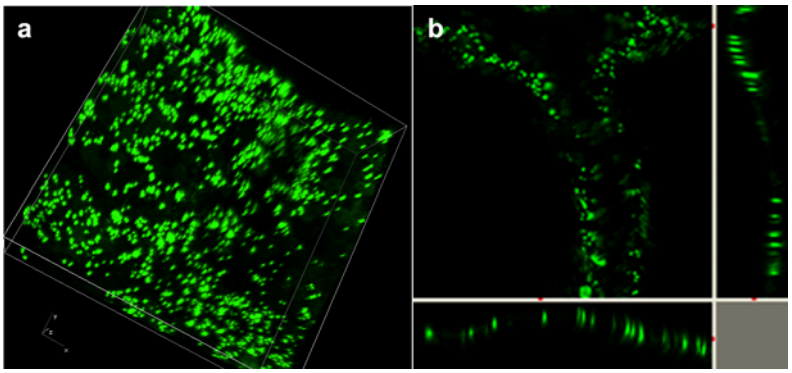

Figure 5.9: Confocal images of the skin after *in vitro* skin penetration study showing (a). image of the skin showing channel formed because of the nanoneedles adsorbed with Albumin-FITC. Please note that the image has been taken from the original video file showing channel formed along the thickness of the skin layer by layer.

5.5.1.3 Bradford protein quantitation

The receptor liquid samples collected at 3 hour-intervals during *in vitro* skin penetration study were subjected to Bradford assay to determine protein quantity and trans-diffusion rate of albumin-FITC. As it can be seen from the **Table 5.1** and **Figure 5.10**, a significant quantity of albumin FITC diffused within the first 12 hours including

the maximum peak observed during the initial 4 hours. The quantity of protein decresed in the subsequent samples collected in the next 12 hours.

Sample (every 3 hours)	**Sample volume** (µl)	**Average OD** (595 nm, $x10^{-3}$)	**Protein Concentration** (µg/ml)	**Total Protein** (µg)
0	0	0.00	0.0	0.0
3	20	6.39	31.4	47.10
6	20	4.22	20.7	31.05
9	20	3.81	18.7	28.05
12	20	3.05	12.7	19.05
15	20	3.46	16.9	25.35
18	20	3.38	16.6	24.90
21	20	1.86	9.1	13.65
24	20	0.46	2.3	3.45
Total protein				**192.60**

Table 5.1: Protein concentration as determined by Bradford assay of receptor liquid samples collected every 3 hours during skin penetration study.

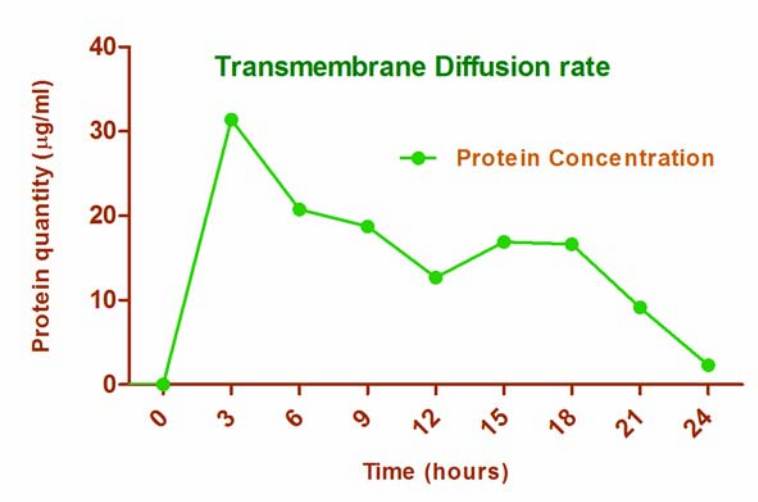

Figure 5.10: Graph showing transdiffusion rate of albumin-FITC determined during *in vitro* skin penetration study.

In order to translate these observations into more concrete values, albumin-FITC adsorbed on to the chip was quantified in terms of difference between initial and final concentration of albumin-FITC solution used for the purpose. Additionally we washed the chip after skin penetration study and determined amount of albumin-FITC that remained attached onto the chip even after application onto the skin.

Protein sample	OD (595nm)	Average OD	Protein quantity(mg)
Protein sample before adsorption on to chip (stock solution)	0.9486 0.9463 0.9545	0.9498 (SD-0.004)	5.397
Protein sample after adsorption onto chip	0.8012 0.7982 0.7967	0.7987 (SD-0.002)	4.544
Protein adsorbed onto the chip	-		0.853
Protein sample from washing of chip	0.0431 0.0461 0.0479	0.0457 (SD-0.002)	0.302
Protein sample collected from receptor chamber	(**Table 5.1**)		0.193

Table 5.2: Analysis of quantity of *albumin-FITC* adosrbed on to the chip and amount released in to the skin during the *in vitro* skin penetration study by Bradford assay. Where possible, the experiments were repeated in triplicates.

As reported in the **table 5.2**, around 0.853 mg of *albumin-FITC* was initially adsorbed onto the chip. However, only 193 µg of *albumin-FITC* actually could be collected from the receptor chamber. Moreover maximum amount of *albumin-FITC* was found to remain adsorbed with chip even after application. Therefore we decresed the amount of albumin to be adsorbed on to the chip during *in vivo* skin penetration study.

5.5.2 *In vivo* skin penetration study

The above results pertaining to *in vitro* skin penetration study was further confirmed by applying ZnO nanorod chips adsorbed with albumin-FITC to ear of the mice as part of the *in vivo* skin penetration study. While the chips were applied to dorsal part of the ear, ventral part of the ear was used as control for confocal laser scanning microscopy to make sure that nanorods did not completely penetrated across the thin ear. From the confocal microscopic image of the ear skin used for in vivo skin penetration study**,** it can be observed that the dorsal part of the skin (**Figure 5.11a)** possesses fluorescent channels due to the penetration of nanorods adsorbed with albumin-FITC. However the same is not true with respect to ventral part of the skin (**Figure 5.11b)** as it is devoid of any fluorescence except few self-fluorescing hairs.

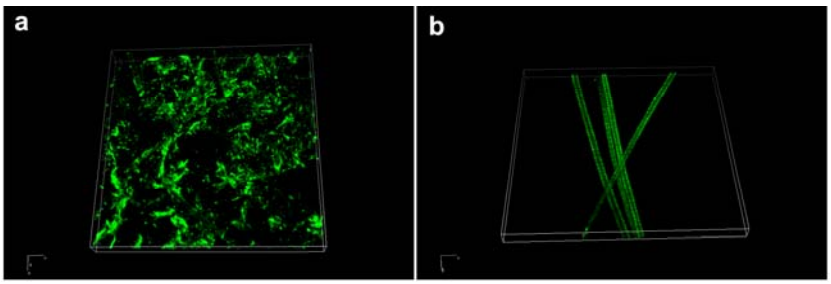

Figure 5.11: Confocal microscopic image of (a) dorsal and (b) ventral part of mice ear used in *in vivo* skin penetration study. While the functionalized chip was applied to dorsal part of the ear, ventral part was used as control.

.

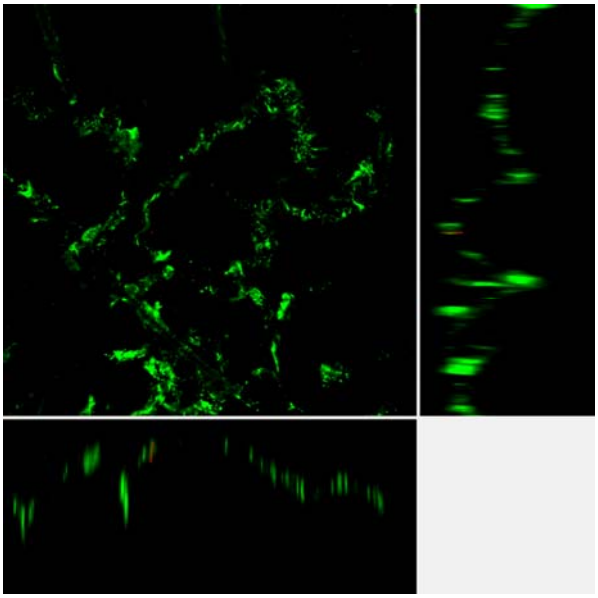

Figure 5.12: Confocal microscopy image of the mice ear skin sample utilized for in vivo skin penetration study represented in XYZ direction.

Channel	Sample 1 Length (µm)	Sample 2 Length (µm)	Sample 3 Length (µm)
1	11.50	16.10	4.60
2	11.50	12.30	6.90
3	11.50	6.90	6.90
4	11.50	9.20	13.80
5	9.20	13.80	16.10
6	6.90	13.80	16.10
7	13.80	11.50	9.20
8	9.20	12.30	6.90
9	13.80	16.10	11.50
10	11.50	9.20	12.10
Average		**11.19**	**SD=3.16**

Table 5.3: Length of fluorescing channels formed in the ear skin of the mice due to the penetration of ZnO nanorods adsorbed with albumin-FITC used for *in vivo* skin penetration study.

Further analysis of 3D confocal images in XYZ direction was done to determine the length of the fluorescing channels formed due to the penetration of aligned ZnO nanorods and adsorption of albumin-FITC. Ten of these fluorescence channels were randomly selected from each of the three mice ear skin samples by using Nikon elements Ar software and their length was calculated using inbuilt scale. From the **Figure 5.12** and **Table 5.3** it can be observed that the average length of the fluorescence channels formed due to penetration of ZnO nanorods was 11.19 µm. while the maximum length of the channel formed was around 16.10 µm and minimum length of the channel formed was 4.60 µm

5.5.3 Transepidermal water loss

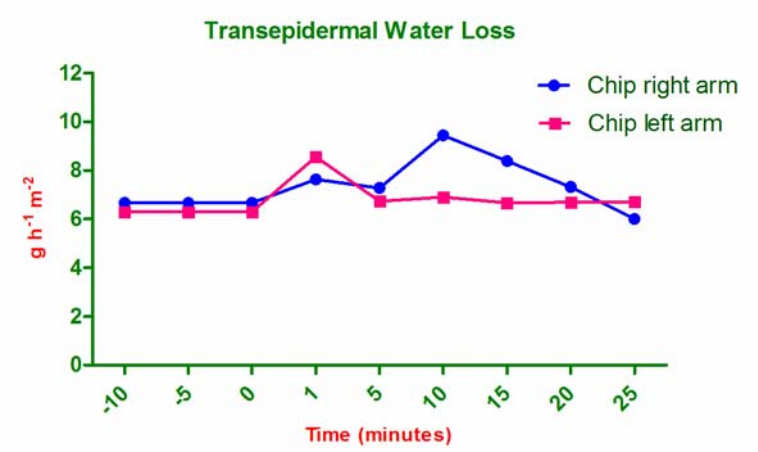

Figure 5.13: Graph showing TEWL values in both the arms after treatment with chips having nanorods calculated over a period of 25 minutes.

The TEWL values after treatment with the devices are provided in the following graph (**Figure 5.13**). As concerns the left arm (pink line), prior to treatment TEWL values were about 6.30 g h^{-1} m^{-2} (SD ± 0.7). After the application of the chip on to the skin, the TEWL values increased immediately above 8.57. After 5 minutes of rest, the following TEWL value decreased rapidly to a much lower value (≤ 7.00). Although the

measurements were continued for a period of 70 minutes (data not shown), the values did not change remarkably after the initial 15-25 minutes. Therefore, further points in the final graph are not included. In the case of the right arm (blue line), we noticed a different behavior, with baseline levels of about 6.68 g h^{-1} m^{-2} (SD ± 0.7): the increase in TEWL was comparable, but it originated only after 10 minutes from the application, and its effect decreased slowly until it reached baseline values within about 15 minute.

5.5.5 Tape stripping

The skin layers collected by tape stripping after 1 hour of application of the ZnO nano rods chip adsorbed with albumin-FITC were subjected to analysis under confocal microscope. As can be seen from the 3D confocal images (**Figure 5.14)**, all the skin layers (only 1st, 11th and 18th layers shown) beginning from first till the last revealed the presence of fluorescence signals.

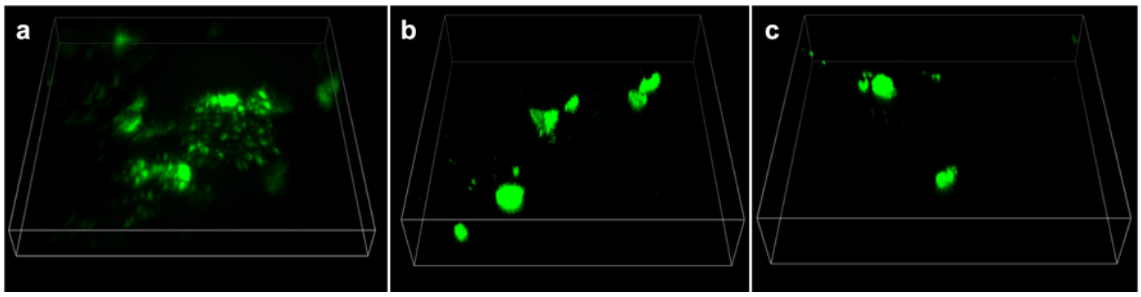

Figure 5.14: 3D images of obtained by confocal microscopy of (a) 1st skin layer (b) 11th skin layer and (c) 18th skin layer obtained during tape stripping experiment.

5.5.6 *In vivo* immunization using ZnO nanorods

For the purpose we adsorbed six ZnO nanorod chips with endograde OVA; while three chips were applied onto normal dorsal skin of right ear of the mice, three chips were applied onto right ear of mice whose dorsal skin layer was stripped of stratum corneum.

As discussed before, the stratum corneum is the major barrier for delivery of large molecules like peptide antigens (Prausnitz 2004). Therefore to increase the delivery of OVA and immune response, we stripped the stratum corneum from the dorsal part of the right of the mice.

Similarly we used additional three chips for adsorbing endograde OVA with alum. Alum is currently the most commonly used and only approved adjuvant for routine use with human vaccines (Li, Willingham et al. 2008). The mechanism of adjuvanticity of alum includes a) formation of a depot; b) efficient uptake of aluminum adsorbed antigen particles by antigen presenting cells due to their particulate nature and optimal size (<10 μm); c) stimulation of immune competent cells of the body through activation of complement and activation of macrophages (Gupta 1998). In other words alum as an adjuvant can enhance the immunogenicity of vaccine and hence increase immune response. Additionally we used three nanorod chips adsorbed with PBS only as negative control for immune response to our prototype vaccine. The immune response observed with respect to other chips will be compared to this negative control to determine titer of antibody.

All the chips used for the purpose, excluding PBS loaded chips, were adsorbed with 400 μg of OVA irrespective of the presence of adjuvant. After application of the chips for immunization, they were subjected to washing with PBS to wash off any left-over OVA still attached to the nanorods of the chips. The washed OVA were further quantified by Bradford assay to determine expected delivery of OVA from each chip in to the skin of mice ear during immunization process. From **Table 5.4**, it can be seen that around 25% of OVA was delivered from all the chips used for the purpose. It can also be seen that

OVA-adsorbed chips applied on to stripped ear showing maximum delivery of OVA (± 30%) compared to others.

Chip No	Formulation	Original Loading (µg)	1st Washing (µg)	2nd Washing (µg)	Total Washing (µg)	Expected Delivery (µg)
1	PBS	0	0	0	0	NA
2	PBS	0	0	0	0	NA
3	PBS	0	0	0	0	NA
4	OVA	400	297.52	2.8	300.32	99.68
5	OVA	400	300.97	2.244	303.214	96.79
6	OVA	400	311.58	1.633	313.213	86.78
7	OVA+alum	400	266.26	42.88	309.14	90.86
8	OVA+alum	400	278.93	25.88	304.81	95.19
9	OVA+alum	400	273.15	17.26	290.42	109.58
10	OVA (stripped ear)	400	241.49	21.49	262.97	137.03
11	OVA (stripped ear)	400	242.21	24.32	266.53	133.47
12	OVA (stripped ear)	400	253.54	17.99	271.53	128.47

Table 5.4: Loading and expected delivery of endograde OVA from different ZnO nanorod chips used for *in vivo* immunization.

The serum separated from blood collected from each mouse was subjected to ELISA to determine antibody titer produced in response to immunization with OVA as a vaccine prototype. A '**Titer'** is defined as the dilution of serum of OVA treated mouse sufficient to give a change in absorbance of 1.0 from the untreated (PBS) mouse at 450 nm after 30 minutes of substrate conversion at 25 °C. It can be observed from **Figure 5.15** that for only OVA treated mouse the antibody titer was produced at serum dilution of 1:160-1:320. But for OVA with ALUM treated mouse and OVA treated to mouse with

stripped ear, the antibody titer was produced at serum dilution of 1:640-1280. In other words the immune response for OVA with ALUM (chips 7-9) and OVA applied to stripped ear (chips 10-12) shows no significant difference ($p>0.05$) in immune response although OVA delivery for stripped ear was significantly higher. In contrast they show significant difference ($p< 0.05$) of immune response in comparison to only OVA treated mouse (chips 4-6).

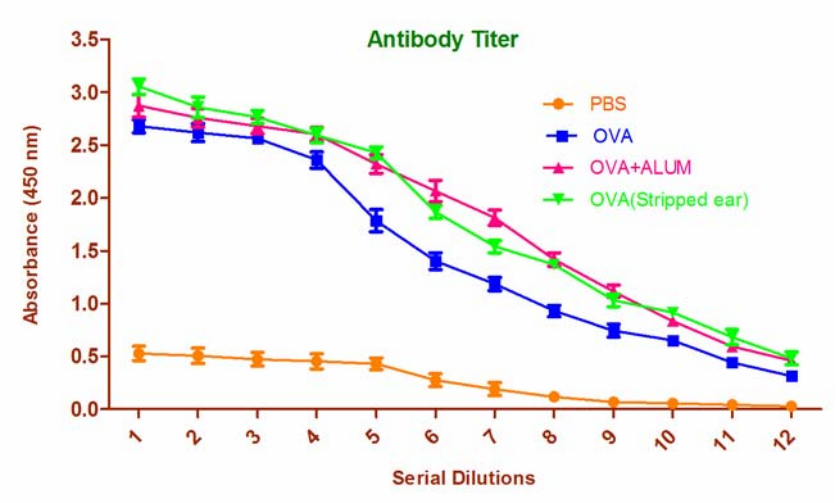

Figure 5.15: Graph plotted for absorbance vs serum dilutions as part of immune response for in vivo immunization of mice with ZnO nanorod chip adsorbed with endograde OVA. Note: - Two fold serial dilutions of serum have been done starting from 1:10 to 1:20480. While 1 in the X axis of the graph is 1:10, 12 stand for 1:20480.

5.6 DISCUSSION

Bacterial, parasitic and viral infections constitute one of the major health problems facing the world. Drug resistance is rapidly escalating and new drug developments, although faster than in the past with the advent of combinatorial methods, are becoming prohibitive. Therefore, the development of new prophylactic and potent therapeutic vaccines including novel delivery systems to combat these types of infections is of utmost importance (Roy 2004). Various novel delivery systems are currently under pipeline and

some of them are even undergoing vigorous clinical trial. As part of that we subjected our novel device composed of ZnO nanorods grown on silica chips to preliminary investigation pertaining to its application in transdermal delivery of vaccine. These chips with nanorods were adsorbed with a vaccine prototype and were analysed for *in vitro* and *in vivo* skin penetration studies including TEWL and *in vivo* immune response.

5.6.1 Skin penetration studies

The chips used for the *in vitro* skin permeation study were analysed by SEM for state of their alignment before and after application onto skin. As indicated in **Figure 5.7** most nanorods preserved a certain degree of alignment and only the tips were affected. The change in the shape of the nanorods was more likely due to the pressure exerted for the effective application of the chip on the skin sample. In further experiments this process could be ameliorated in order to optimize the release of our prototype vaccine through the skin and simultaneously avoid excessive distortion of the tubes. As part of the design of the chips, the base of the nanorods can be strengthened further by increasing their width, so that there is no effect on alignment during their application on to skin.

Our prototype vaccine *albumin-FITC*, constitutes bovine serum albumin, a model protein commonly used as prototype vaccine (Roy 2004), conjugated with a fluorescent molecule, thereby offering the advantage of further characterization of both the ZnO nanorod chips and skin on to which it was applied. Since FITC is covalently bound to albumin, therefore the optical signal can be visualized under fluorescence microscope to trace the presence of our prototype vaccine. With this in mind the chips adsorbed with our prototype vaccine were analyzed under fluorescence microscope. The blank patches formed on the chip (**Figure 5.8b**) after application on to the skin suggest detachment of the *albumin-FITC*. This detached *albumin-FITC seems to be* adsorbed on to the skin as

seen **in its** confocal image (**Figure 5.9**) taken after application of the chips adsorbed with prototype vaccine. The detailed evaluation of the skin by both fluorescence and confocal laser scanning microscopy revealed the penetration of *albumin-FITC* facilitated by the nanorods, as indicated by the formation of fluorescent pathways perfectly corresponding to nano channels created by nanorods along the skin layer (**Figure 5.9a**). In other words, the fluorescent molecule conjugated to our prototype vaccine was mainly adsorbed through these tunnels. As support of this observation, no fluorescence was detected outside the area covered by the chip.

From **Figure 5.9**, the average length of the fluorescence channels formed were found to be 9 μm. However the stratum corneum consists of 10-15 layers of coenocytes and varies in thickness from approximately 10-15 μm in the dry state to 40 μm when hydrated (Scheuplein 1967; Anderson, Cassidy et al. 1973; Holbrook and Odland 1974). In this *in vitro* skin penetration study, the skin sample may be hydrated as it was attached with receptor compartment of Franz diffusion cells having PBS flowing through it. Additionally from confocal video images (data not shown), the thickness of the skin was found to be almost 22-23μm, whereas our nanorods were of 20 μm only. From **Table 5.1** and **5.2** involving Bradford quantification it was observed that only 20-25% of the vaccine passed through the skin in to receptor fluid. Approximately 302 μg of *albumin-FITC* were found to remain adsorbed with the chip out of 853 μg initially adsorbed for the purpose. This indicates that some protein remained entrapped in the skin itself as all the nanorods did not completely penetrated across the stratum corneum. This is confirmed by the presence of fluorescence along the skin layers in form of channels.

The *in vivo* skin penetration study was done with chips having nanorods of length 30-35μm and average length of the corresponding fluorescence channels formed was

found to be around 11 μm (**Figure 5.12** and **Table 5.3**). This is a small improvement over the length of channels formed by earlier chips utilized for in vitro skin permeation study. To exclude the possibility of chips completely perforating the very thin ear of the mice we split the ears in to two parts in form of dorsal part where chips were applied and the ventral part as control and we analyzed these two parts under confocal microscopy. The same fluorescence channels were found in the dorsal part of ear in case of *in vivo* penetration study. The fact that there was no fluorescence in case of ventral part of skin except few self-fluorescing hairs proves that nanorods penetrated only the SC of dorsal part of the ear skin. From both the *in vitro* and *in vivo* skin penetration study it can be suggested for promising application of these ZnO nanorods based chips for efficient transdermal vaccination.

5.6.2 Transepidermal water loss

The aim of this part of the study was to use a TEWL based approach to determine how the application of our nanorod based chips affects skin barrier integrity. TEWL was chosen as it is a much more rapid and user-friendly method in comparison to other drug penetration experiments which involve ethical issues (Fluhr, Elsner et al. 2005). As indicated in **Figure 5.13**, the increase in TEWL for both the arms was comparable, but the origin of TEWL for both arms occurred at different time. While for left arm, it was quite instantaneous, for right arm, TEWL originated only after 5 minutes. An explanation for such difference could be attributed to the temperature inside the room, which at the beginning seemed pleasant but subsequently resulted to be too cold for the subject under investigation. Although there are many reasons for inter group variations in TEWL readings (Elmahjoubi, Frum et al. 2009), it is particularly sensitive to environmental factors such as humidity, temperature, time of year (season variation) and moisture

content of the skin (hydration level). Additionally there is inherent natural variability of human skin (Meidan and Roper 2008), even though, they are two arms of the same person. While the humidity was controlled by the chamber of the apparatus, the ambient temperature on the individual was maintained constantly at 21 °C but it was perceived as uncomfortable.

In every case, it was important to observe an increase in permeability and enhancement of water loss values (TEWL in both arms increased of at least 2.3 g h^{-1} m^{-2}) with the use of the chips, as a demonstration of their efficacy in penetrating the skin with a total absence of pain. Therefore, they seemed to be able to disrupt the *stratum corneum* barrier to a higher extent, while inducing no irritation on the treated area. On the other side, the subsequent decrease of TEWL values to normal ranges suggested that the nanopores, once formed, rapidly closed after the application of the chips on the skin, thus minimizing both skin irritation and any potential adverse effect.

5.6.3 Tape stripping

As demonstrated through tape stripping experiment, our prototype vaccine effectively penetrated through the skin and did not stacked at the surface confirmed by the fact that all the 18 layers stripped from the dorsal skin of the forearm of a 65 years old volunteer applied with chips with vaccine, showed presence of fluorescence under confocal microscopy. As expected, the fluorescence decreased from the first layer to the eighteenth layer, but its mere presence confirms the delivery of our vaccine.

5.6.4 *In vivo* immune response

According to the results obtained in above preliminary studies, the nanorod patches have high possibility to be used as a device for vaccination. Therefore in subsequent step

we investigated the ability of the nanorod chips adsorbed with our vaccine prototype to evoke an immune reaction when applied onto the skin of BALB/c mice. The immune response was determined by ELISA of the serum collected from the mice subjected to chips with different OVA formulations. Overall the antibody titer found in case of serum of test mice was at a serum dilution of 1:160 (**Figure 5.15**) compared to serum of mice applied with PBS adsorbed chips (negative control). Since the chips used as negative control had no OVA adsorbed onto them, therefore this increased antibody titer in case of mice applied with test chips could only be due to immune response corresponding to OVA.

As observed from **Table 5.4,** the OVA adsorbed chips applied to stripped ear showed higher delivery of OVA (± 30%) compared to chips applied to normal skin (± 25%) of ear of mice. This could be possibly due to decreased thickness of stratum corneum obtained by tape stripping the ear. However immune response (**Figure 5.15**) obtained in case of OVA applied to stripped ear did not show any significant difference ($P>0.05$) compared to OVA with alum as adjuvant. Furthermore the OVA with alum showed better antibody titer (1:640) compared to mice applied with chips adsorbed with only OVA (1:160). This suggests that alum as an adjuvant not only effective at increasing the immune response of mice exposed to the vaccine, but it also helps in decreasing the dose of vaccine needed to be delivered for the same immune response.

5.7 CONCLUSION

The preliminary data reported in this on-going study provide useful information about the applicability of our novel nanorod device for the purpose of transdermal delivery of vaccines. These silica chips having ZnO nanorods grown on them were not

only effective at enhancing the permeability of the skin to large molecules including peptide antigens, but they also helped in increasing the immune response against our prototype vaccine. The above can be suggested by the fact that nanorods of 30-35μm length were able to deliver the vaccine prototype more than 11μm across the skin. Since stratum corneum of normal skin has average thickness of 10 μm, therefore our device can be expected to deliver any vaccine across this great barrier into the skin. Similarly, the increase in TEWL during application of the chip and its rapid decrease after the application proves that our chips with nanorods are able to form reversible nanopores in the stratum corneum without inducing any evident irritation. Furthermore a significant increase in antibody titer as part of the immune response against our prototype vaccine delivered using this novel nano device confirms its efficacy. In summary these results pave the way for a further development of the project for transdermal delivery of vaccine using this novel nano device.

Currently this device is being further investigated with respect to other vaccines such as pertussis and influenza utilizing the above preliminary data.

Chapter 6

Conclusions and Future Directions

Nanomaterials, which can be manipulated on previously impossible scales, represent valuable tools for a wide area of applications. As such, scientist and research communities are currently exploiting unique properties of several nanomaterials for various purposes including biomedical applications. In this thesis we have investigated carbon nanotubes (CNTs) and ZnO nanorods as they possess unique physicochemical and biological characteristics potentially suitable for specific biomedical applications. They have been depicted in form of three experimental chapters.

The first experimental chapter of this thesis examined several physicochemical and biological parameters (e.g. length, concentration, dispersibility, functionalization, purity, cell lines, cell viability assay methods and different hydrophilic polar chains) pertaining to pristine and functionalized carbon nanotubes, and evaluated their influence on cytotoxicity and biocompatibility. The results from the above study revealed remarkable biocompatibility of ultrapure sample of multi-walled CNTs (MWCNTs). There was no sign of cytotoxicity till a dose of 150µg/ml, establishing the fact that the presence of metallic impurities (such as iron and cobalt) was responsible for eventual cytotoxicity of CNTs. In other words, purity was identified as the most crucial among several parameters that can guarantee CNTs' potential application in biomedical fields. However, it should be noted that this study was limited to biological characterization of CNTs involving *in vitro* cytotoxicity studies only. Further research involving *in vivo* toxicity studies, environmental exposure, bioaccumulation, and interaction with cellular constituents is therefore needed to verify the above results. These further investigations may result beneficial not only for the use of CNTs in biomedical applications such as drug delivery, but also to understand the fundamental processes associated with their interaction with the environment and living systems.

The second experimental chapter of this thesis explored the use of the above highly biocompatible ultrapure MWCNTs functionalized with polyethylene glycol (PEG) as a bio-composite scaffold in the form of a thin film to support human mesenchymal stem cells (hMSCs) growth, proliferation and their osteogenic differentiation. It was found that pegylated ultrapure MWCNT thin film not only provides uniform and stable surface for the growth of hMSCs, but also imitates a favourable microenvironment for osteogenic differentiation even in the absence of the standard osteogenic inducer such as BMP-2. This finding is significant as it suggests that these ultrapure MWCNTs functionalized with appropriate natural or synthetic polymer can be utilized as biocompatible scaffolds for applications in tissue engineering and regenerative medicine. However, the mechanisms underlying the enhancement of osteogenesis of hMSCs growing on MWCNT-PEG thin film is still unknown, therefore further research is needed to identify the chemical and mechanical cues involved for such favourable osteogenic microenvironment. Simultaneously the biochemical characteristics of the MWCNT-PEG scaffold can be standardized further before it is subjected to clinical studies.

The primary objective of the third experimental part of this thesis was to carry out a preliminary study of transdermal delivery of a vaccine prototype using aligned ZnO nanorods grown successfully on silicon chip as part of a future platform for transdermal delivery of therapeutics. The results provided an interesting perspective of penetration of ZnO nanorods across the stratum corneum and a significant increase in antibody titer as part of the immune response against our prototype vaccine. This paves the way for further studies involving this novel nano device for transdermal delivery of pertussis, tetanus and influenza vaccines. Furthermore the device can be improved with regard to length and alignment of the ZnO nanorods to increase its applicability for the purpose.

References

Ajayan, P. M. (1999). "Nanotubes from Carbon." Chem Rev **99**(7): 1787-1800.

Ali-Boucetta, H., K. T. Al-Jamal, et al. (2008). "Multiwalled carbon nanotube-doxorubicin supramolecular complexes for cancer therapeutics." Chemical Communications **8**(4): 459-461.

Andersen, P. H. and H. I. Maibach (1995). "Skin irritation in man: a comparative bioengineering study using improved reflectance spectroscopy." Contact Dermatitis **33**(5): 315-322.

Anderson, M. L., W. J. Dhert, et al. (1999). "Critical size defect in the goat's os ilium. A model to evaluate bone grafts and substitutes." Clin Orthop Relat Res(364): 231-239.

Anderson, R. L., J. M. Cassidy, et al. (1973). "The effect of in vivo occlusion on human stratum corneum hydration-dehydration in vitro." J Invest Dermatol **61**(6): 375-379.

Archer, D. F., V. Cullins, et al. (2004). "The impact of improved compliance with a weekly contraceptive transdermal system (Ortho Evra) on contraceptive efficacy." Contraception **69**(3): 189-195.

Arnold, M. S., S. I. Stupp, et al. (2005). "Enrichment of single-walled carbon nanotubes by diameter in density gradients." Nano Letters **5**(4): 713-718.

Arora, A., M. R. Prausnitz, et al. (2008). "Micro-scale devices for transdermal drug delivery." International Journal of Pharmaceutics **364**(2): 227-236.

Arrington, E. D., W. J. Smith, et al. (1996). "Complications of iliac crest bone graft harvesting." Clin Orthop Relat Res(329): 300-309.

Asuri, P., S. S. Karajanagi, et al. (2006). "Water-soluble carbon nanotube-enzyme conjugates as functional biocatalytic formulations." Biotechnol Bioeng **95**(5): 804-811.

Atala, A., R. Lanza, et al. (2008). Principles of Regenerative Medicine, Academic Press.

Badkar, A. V., A. M. Smith, et al. (2007). "Transdermal delivery of interferon alpha-2B using microporation and iontophoresis in hairless rats." Pharm Res **24**(7): 1389-1395.

Bai, R., W. Wang, et al. (2007). "Review on biological security of nanomaterials." J Environ Health **24**: 59-61.

Bąkowicz, K. and S. Mitura (2002). "Biocompatibility of NCD." Journal of Wide Bandgap Materials **9**(4): 261-272.

Balasubramanian, K. and M. Burghard (2005). "Chemically functionalized carbon nanotubes." Small **1**(2): 180-192.

Bandow, S., A. M. Rao, et al. (1997). "Purification of single-wall carbon nanotubes by microfiltration." Journal of Physical Chemistry B **101**(44): 8839-8842.

Bawarski, W. E., E. Chidlowsky, et al. (2008). "Emerging nanopharmaceuticals." Nanomedicine **4**(4): 273-282.

Bawendi, M. G., M. L. Steigerwald, et al. (1990). "The Quantum-Mechanics of Larger Semiconductor Clusters (Quantum Dots)." Annual Review of Physical Chemistry **41**: 477-496.

Baylink, D. J., R. D. Finkelman, et al. (1993). "Growth factors to stimulate bone formation." J Bone Miner Res **8 Suppl 2**: S565-572.

Becker, B. M., S. Helfrich, et al. (2005). "Ultrasound with topical anesthetic rapidly decreases pain of intravenous cannulation." Acad Emerg Med **12**(4): 289-295.

Benson, H. A. (2005). "Transdermal drug delivery: penetration enhancement techniques." Curr Drug Deliv **2**(1): 23-33.

Bentzen, E. L., F. House, et al. (2005). "Progression of respiratory syncytial virus infection monitored by fluorescent quantum dot probes." Nano Lett **5**(4): 591-595.

Bernstein, D., V. Castranova, et al. (2005). "Testing of fibrous particles: short-term assays and strategies." Inhal Toxicol **17**(10): 497-537.

Bianco, A., K. Kostarelos, et al. (2005). "Biomedical applications of functionalised carbon nanotubes." Chem Commun (Camb)(5): 571-577.

Bianco, A., K. Kostarelos, et al. (2005). "Applications of carbon nanotubes in drug delivery." Curr Opin Chem Biol **9**(6): 674-679.

Blaheta, R. A., M. Franz, et al. (1991). "A rapid non-radioactive fluorescence assay for the measurement of both cell number and proliferation." J Immunol Methods **142**(2): 199-206.

Bobyn, J. D., E. S. Mortimer, et al. (1992). "Producing and avoiding stress shielding. Laboratory and clinical observations of noncemented total hip arthroplasty." Clin Orthop Relat Res(274): 79-96.

Bogunia-Kubik, K. and M. Sugisaka (2002). "From molecular biology to nanotechnology and nanomedicine." Biosystems **65**(2-3): 123-138.

Bolskar, R. D., A. F. Benedetto, et al. (2003). "First soluble M@C60 derivatives provide enhanced access to metallofullerenes and permit in vivo evaluation of Gd@C60[C(COOH)2]10 as a MRI contrast agent." J Am Chem Soc **125**(18): 5471-5478.

Bonassar, L. J. and C. A. Vacanti (1998). "Tissue engineering: the first decade and beyond." J Cell Biochem Suppl **30-31**: 297-303.

Bondar', V. S., I. O. Pozdnyakova, et al. (2004). "Applications of nanodiamonds for separation and purification of proteins." Physics of the Solid State **46**(4): 758-760.

Boonyo, W., H. E. Junginger, et al. (2007). "Chitosan and trimethyl chitosan chloride (TMC) as adjuvants for inducing immune responses to ovalbumin in mice following nasal administration." J Control Release **121**(3): 168-175.

Boquest, A. C., A. Shahdadfar, et al. (2005). "Isolation and transcription profiling of purified uncultured human stromal stem cells: alteration of gene expression after in vitro cell culture." Mol Biol Cell **16**(3): 1131-1141.

Bos, J. D. and M. M. Meinardi (2000). "The 500 Dalton rule for the skin penetration of chemical compounds and drugs." Exp Dermatol **9**(3): 165-169.

Bosi, S., T. Da Ros, et al. (2003). "Synthesis and anti-HIV properties of new water-soluble bis-functionalized[60]fullerene derivatives." Bioorg Med Chem Lett **13**(24): 4437-4440.

Bottini, M., S. Bruckner, et al. (2006). "Multi-walled carbon nanotubes induce T lymphocyte apoptosis." Toxicol Lett **160**(2): 121-126.

Bowers, K. T., J. C. Keller, et al. (1992). "Optimization of surface micromorphology for enhanced osteoblast responses in vitro." Int J Oral Maxillofac Implants **7**(3): 302-310.

Boyne, P. J., L. C. Lilly, et al. (2005). "De novo bone induction by recombinant human bone morphogenetic protein-2 (rhBMP-2) in maxillary sinus floor augmentation." J Oral Maxillofac Surg **63**(12): 1693-1707.

Bramson, J., K. Dayball, et al. (2003). "Enabling topical immunization via microporation: a novel method for pain-free and needle-free delivery of adenovirus-based vaccines." Gene Ther **10**(3): 251-260.

Bratosin, D., L. Mitrofan, et al. (2005). "Novel fluorescence assay using calcein-AM for the determination of human erythrocyte viability and aging." Cytometry A **66**(1): 78-84.

Briggs, T., M. D. Treiser, et al. (2009). "Osteogenic differentiation of human mesenchymal stem cells on poly(ethylene glycol)-variant biomaterials." J Biomed Mater Res A **91**(4): 975-984.

Bronaugh, R. L. and H. I. Maibach, Eds. (2005). Percutaneous Absorption. Drugs and Pharmaceutical Sciences. New York, Taylor & Francis.

Brown, K. L. and R. L. Cruess (1982). "Bone and cartilage transplantation in orthopaedic surgery. A review." J Bone Joint Surg Am **64**(2): 270-279.

Burkoth, T. L., B. J. Bellhouse, et al. (1999). "Transdermal and transmucosal powdered drug delivery." Crit Rev Ther Drug Carrier Syst **16**(4): 331-384.

Byrne, S. J., Y. Williams, et al. (2007). ""Jelly dots": synthesis and cytotoxicity studies of CdTe quantum dot-gelatin nanocomposites." Small **3**(7): 1152-1156.

Cang-Rong, J. T. and G. Pastorin (2009). "The influence of carbon nanotubes on enzyme activity and structure: investigation of different immobilization procedures through enzyme kinetics and circular dichroism studies." Nanotechnology **20**(25).

Carmichael, A. J. (1994). "Skin Sensitivity and Transdermal Drug-Delivery - a Review of the Problem." Drug Safety **10**(2): 151-159.

Cevc, G. (1996). "Transfersomes, liposomes and other lipid suspensions on the skin: permeation enhancement, vesicle penetration, and transdermal drug delivery." Crit Rev Ther Drug Carrier Syst **13**(3-4): 257-388.

Cevc, G. (2003). Transferosomes: innovative transdermal drug carriers. Modified release drug delivery technology. M. J. Rathbone, J. Hadgraft and M. S. Roberts. New York, Marcel Dekker. **126**.

Chang, C. C., I. K. Hsu, et al. (2010). "A New Lower Limit for the Ultimate Breaking Strain of Carbon Nanotubes." ACS Nano.

Chang, S. Q., Y. D. Dai, et al. (2009). "UV-enhanced cytotoxicity of thiol-capped CdTe quantum dots in human pancreatic carcinoma cells." Toxicol Lett **188**(2): 104-111.

Chen, R. J., S. Bangsaruntip, et al. (2003). "Noncovalent functionalization of carbon nanotubes for highly specific electronic biosensors." Proc Natl Acad Sci U S A **100**(9): 4984-4989.

Chen, R. J., Y. G. Zhang, et al. (2001). "Noncovalent sidewall functionalization of single-walled carbon nanotubes for protein immobilization." Journal of the American Chemical Society **123**(16): 3838-3839.

Chiaretti, M., G. Mazzanti, et al. (2008). "Carbon nanotubes toxicology and effects on metabolism and immunological modification in vitro and in vivo." Journal of Physics-Condensed Matter **20**(47).

Chung, P. H., E. Perevedentseva, et al. (2006). "Spectroscopic study of bio-functionalized nanodiamonds." Diamond and Related Materials **15**(4-8): 622-625.

Cleary, G. W. (1993). Transdermal delivery systems; a medical rationale. Topical drug bioavailability, bioequivalence and penetration. V. P. Shah and H. I. Maibach. New York, Plenum**:** 17-68.

Collins, P. G. and P. Avouris (2000). "Nanotubes for electronics." Sci Am **283**(6): 62-69.

Colomer, J. F., P. Piedigrosso, et al. (1998). "Purification of catalytically produced multi-wall nanotubes." Journal of the Chemical Society - Faraday Transactions **94**(24): 3753-3758.

Coombes, A. G. and M. C. Meikle (1994). "Resorbable synthetic polymers as replacements for bone graft." Clin Mater **17**(1): 35-67.

Coventry, M. B. and E. M. Tapper (1972). "Pelvic instability: a consequence of removing iliac bone for grafting." J Bone Joint Surg Am **54**(1): 83-101.

Cowley, S. P. and L. D. Anderson (1983). "Hernias through donor sites for iliac-bone grafts." J Bone Joint Surg Am **65**(7): 1023-1025.

Cramer, M. P. and S. R. Saks (1994). "Translating Safety, Efficacy and Compliance into Economic Value for Controlled-Release Dosage Forms." Pharmacoeconomics **5**(6): 482-504.

Cui, D., F. Tian, et al. (2005). "Effect of single wall carbon nanotubes on human HEK293 cells." Toxicol Lett **155**(1): 73-85.

Curtis, A. and C. Wilkinson (2001). "Nantotechniques and approaches in biotechnology." Trends Biotechnol **19**(3): 97-101.

Curtis, A. S. and C. D. Wilkinson (1998). "Reactions of cells to topography." J Biomater Sci Polym Ed **9**(12): 1313-1329.

Da Ros, T. and M. Prato (1999). "Medicinal chemistry with fullerenes and fullerene derivatives." Chemical Communications(8): 663-669.

da Silva Meirelles, L., A. I. Caplan, et al. (2008). "In search of the in vivo identity of mesenchymal stem cells." Stem Cells **26**(9): 2287-2299.

Dai, H. J. (2001). Nanotube growth and characterization. Carbon Nanotubes: Synthesis, Structure, Properties and Applications. M. S. Dresselhaus, G. Dresselhaus and P. Avouris. Berlin, springer. **80:** 29-53.

Dai, H. J. (2002). "Carbon nanotubes: opportunities and challenges." Surface Science **500**(1-3): 218-241.

Dalby, M. J., N. Gadegaard, et al. (2007). "The control of human mesenchymal cell differentiation using nanoscale symmetry and disorder." Nat Mater **6**(12): 997-1003.

Dalton, A. B., A. Ortiz-Acevedo, et al. (2004). "Hierarchical self-assembly of peptide-coated carbon nanotubes." Advanced Functional Materials **14**(12): 1147-1151.

Damien, C. J. and J. R. Parsons (1991). "Bone graft and bone graft substitutes: a review of current technology and applications." J Appl Biomater **2**(3): 187-208.

Davis, H. E. and J. K. Leach (2008). Hybrid and Composite Biomaterials in Tissue Engineering. Topics in Multifunctional Biomaterials and Devices. N. Ashammakhi. **1**.

Davis, J. J., M. L. H. Green, et al. (1998). "The immobilisation of proteins in carbon nanotubes." Inorganica Chimica Acta **272**(1-2): 261-266.

Davoren, M., E. Herzog, et al. (2007). "In vitro toxicity evaluation of single walled carbon nanotubes on human A549 lung cells." Toxicology in Vitro **21**(3): 438-448.

De Bari, C., F. Dell'Accio, et al. (2001). "Multipotent mesenchymal stem cells from adult human synovial membrane." Arthritis Rheum **44**(8): 1928-1942.

de Boer, H. H. (1988). "The history of bone grafts." Clin Orthop Relat Res(226): 292-298.

de Caestecker, M. (2004). "The transforming growth factor-beta superfamily of receptors." Cytokine Growth Factor Rev **15**(1): 1-11.

De Rosa, G., D. De Stefano, et al. (2008). "Novel cationic liposome formulation for the delivery of an oligonucleotide decoy to NF-kappa B into activated macrophages." European Journal of Pharmaceutics and Biopharmaceutics **70**(1): 7-18.

Dee, K. C. and R. Bizios (1996). "Mini-review: Proactive biomaterials and bone tissue engineering." Biotechnol Bioeng **50**(4): 438-442.

Del Guidice, M. and M. Sebastian (2006). "Nurses financial handbook." Pa Nurse **61**(2): 14-15.

Demczyk, B. G., Y. M. Wang, et al. (2002). "Direct mechanical measurement of the tensile strength and elastic modulus of multiwalled carbon nanotubes." Materials Science and Engineering a-Structural Materials Properties Microstructure and Processing **334**(1-2): 173-178.

Denet, A. R., R. Vanbever, et al. (2004). "Skin electroporation for transdermal and topical delivery." Adv Drug Deliv Rev **56**(5): 659-674.

Di Marco, M., C. Sadun, et al. (2007). "Physicochemical characterization of ultrasmall superparamagnetic iron oxide particles (USPIO) for biomedical application as MRI contrast agents." Int J Nanomedicine **2**(4): 609-622.

Didenko, V. V., V. C. Moore, et al. (2005). "Visualization of individual single-walled carbon nanotubes by fluorescent polymer wrapping." Nano Letters **5**(8): 1563-1567.

Dieckmann, G. R., A. B. Dalton, et al. (2003). "Controlled assembly of carbon nanotubes by designed amphiphilic Peptide helices." J Am Chem Soc **125**(7): 1770-1777.

Dikin, D. A., S. Stankovich, et al. (2007). "Preparation and characterization of graphene oxide paper." Nature **448**(7152): 457-460.

Dillon, A. C., M. Yudasaka, et al. (2004). "Employing Raman spectroscopy to qualitatively evaluate the purity of carbon single-wall nanotube materials." J Nanosci Nanotechnol **4**(7): 691-703.

Dominici, M., K. Le Blanc, et al. (2006). "Minimal criteria for defining multipotent mesenchymal stromal cells. The International Society for Cellular Therapy position statement." Cytotherapy **8**(4): 315-317.

Donaldson, K., R. Aitken, et al. (2006). "Carbon nanotubes: a review of their properties in relation to pulmonary toxicology and workplace safety." Toxicol Sci **92**(1): 5-22.

Donaldson, K. and C. L. Tran (2002). "Inflammation caused by particles and fibers." Inhal Toxicol **14**(1): 5-27.

Dong, L., K. L. Joseph, et al. (2008). "Cytotoxicity of single-walled carbon nanotubes suspended in various surfactants." Nanotechnology **19**(25).

Dubertret, B., P. Skourides, et al. (2002). "In vivo imaging of quantum dots encapsulated in phospholipid micelles." Science **298**(5599): 1759-1762.

Dumortier, H., S. Lacotte, et al. (2006). "Functionalized carbon nanotubes are non-cytotoxic and preserve the functionality of primary immune cells." Nano Lett **6**(7): 1522-1528.

Dyke, C. A., M. P. Stewart, et al. (2005). "Separation of single-walled carbon nanotubes on silica gel. Materials morphology and Raman excitation wavelength affect data interpretation." Journal of the American Chemical Society **127**(12): 4497-4509.

Dyke, C. A. and J. M. Tour (2004). "Overcoming the insolubility of carbon nanotubes through high degrees of sidewall functionalization." Chemistry-a European Journal **10**(4): 813-817.

Elias, P. M., K. R. Feingold, et al. (2003). Metabolic approach to transdermal drug delivery. Transdermal drug delivery. R. H. Guy and J. Hadgraft. New York, Marcel Dekker. **123:** 285-304.

Elisseeff, J., C. Puleo, et al. (2005). "Advances in skeletal tissue engineering with hydrogels." Orthod Craniofac Res **8**(3): 150-161.

Elmahjoubi, E., Y. Frum, et al. (2009). "Transepidermal water loss for probing full-thickness skin barrier function: correlation with tritiated water flux, sensitivity to punctures and diverse surfactant exposures." Toxicol In Vitro **23**(7): 1429-1435.

Engler, A. J., S. Sen, et al. (2006). "Matrix elasticity directs stem cell lineage specification." Cell **126**(4): 677-689.

Engler, A. J., H. L. Sweeney, et al. (2007). "Extracellular matrix elasticity directs stem cell differentiation." J Musculoskelet Neuronal Interact **7**(4): 335.

Enneking, W. F., J. L. Eady, et al. (1980). "Autogenous cortical bone grafts in the reconstruction of segmental skeletal defects." J Bone Joint Surg Am **62**(7): 1039-1058.

Escobar-Chavez, J. J., D. Bonilla-Martinez, et al. (2009). "The use of sonophoresis in the administration of drugs throughout the skin." J Pharm Pharm Sci **12**(1): 88-115.

Flahaut, E., M. C. Durrieu, et al. (2006). "Investigation of the cytotoxicity of CCVD carbon nanotubes towards human umbilical vein endothelial cells." Carbon **44**(6): 1093-1099.

Fluhr, J. W., P. Elsner, et al. (2005). Bioengineering of the Skin: Water and the Stratum Corneum. Boca Raton, FL, CRC Press.

Fluhr, J. W., O. Kuss, et al. (2001). "Testing for irritation with a multifactorial approach: comparison of eight non-invasive measuring techniques on five different irritation types." Br J Dermatol **145**(5): 696-703.

Fraczek, A., E. Menaszek, et al. (2008). "Comparative in vivo biocompatibility study of single- and multi-wall carbon nanotubes." Acta Biomaterialia **4**(6): 1593-1602.

Freed, L. E. and G. Vunjak-Novakovic (2000). Tissue engineering bioreactors. Principles of Tissue Engineering. R. P. Lanza, R. Langer and J. Vacanti. San Diego, Academic Press**:** 143-156.

Garfein, R. S., D. Vlahov, et al. (1996). "Viral infections in short-term injection drug users: the prevalence of the hepatitis C, hepatitis B, human immunodeficiency, and human T-lymphotropic viruses." Am J Public Health **86**(5): 655-661.

Garibaldi, S., C. Brunelli, et al. (2006). "Carbon nanotube biocompatibility with cardiac muscle cells." Nanotechnology **17**(2): 391-397.

Geim, A. K. and K. S. Novoselov (2007). "The rise of graphene." Nat Mater **6**(3): 183-191.

Gennaro, A. R., Ed. (2003). Remington: The Science and Practice of Pharmacy. Baltimore, Lippincott Williams & Wilkins.

Georgakilas, V., K. Kordatos, et al. (2002). "Organic functionalization of carbon nanotubes." Journal of the American Chemical Society **124**(5): 760-761.

Georgakilas, V., D. Voulgaris, et al. (2002). "Purification of HiPCO carbon nanotubes via organic functionalization." Journal of the American Chemical Society **124**(48): 14318-14319.

Gharbi, N., M. Pressac, et al. (2005). "[60]fullerene is a powerful antioxidant in vivo with no acute or subacute toxicity." Nano Lett **5**(12): 2578-2585.

Gittard, S. D., R. J. Narayan, et al. (2009). "Pulsed laser deposition of antimicrobial silver coating on Ormocer microneedles." Biofabrication **1**(4): 041001.

Giudice, E. L. and J. D. Campbell (2006). "Needle-free vaccine delivery." Adv Drug Deliv Rev **58**(1): 68-89.

Glenn, G. M., M. Rao, et al. (1998). "Skin immunization made possible by cholera toxin." Nature **391**(6670): 851.

Godin, B. and E. Touitou (2003). "Ethosomes: new prospects in transdermal delivery." Crit Rev Ther Drug Carrier Syst **20**(1): 63-102.

Goldstein, J., D. Newbury, et al. (2003). Scanning Electron Microscopy and X-ray Microanalysis, 3rd Ed., springer.

Gomi, K. and J. E. Davies (1993). "Guided bone tissue elaboration by osteogenic cells in vitro." J Biomed Mater Res **27**(4): 429-431.

Gonsalves, K., C. Halberstadt, et al. (2007). Biomedical Nanostructures. Hoboken, New Jersey, John Wiley & Sons, Inc.

Gonzalez, K. A., L. J. Wilson, et al. (2002). "Synthesis and in vitro characterization of a tissue-selective fullerene: vectoring C(60)(OH)(16)AMBP to mineralized bone." Bioorg Med Chem **10**(6): 1991-1997.

Gopikrishnan, R., K. Zhang, et al. (2010). "Synthesis, Characterization and Biocompatibility Studies of Zinc oxide (ZnO) Nanorods for Biomedical Application." Nano-Micro Letters **2**(1): 4.

Granjeiro, J. M., R. C. Oliveira, et al. (2005). "Bone morphogenetic proteins: from structure to clinical use." Braz J Med Biol Res **38**(10): 1463-1473.

Gupta, R. K. (1998). "Aluminum compounds as vaccine adjuvants." Advanced Drug Delivery Reviews **32**(3): 155-172.

Guy, R. H. and J. Hadgraft, Eds. (2003). Transdermal Drug Delivery. New York, Marcel Dekker.

Haddon, R. C. (2002). "Carbon nanotubes." Acc Chem Res **35**(12): 997.

Hamon, M. A., J. Chen, et al. (1999). "Dissolution of single-walled carbon nanotubes." Advanced Materials **11**(10): 834-+.

Hatano, K., H. Inoue, et al. (1999). "Effect of surface roughness on proliferation and alkaline phosphatase expression of rat calvarial cells cultured on polystyrene." Bone **25**(4): 439-445.

Heald, C. G. R., G. G. Wildgoose, et al. (2004). "Chemical derivatisation of multiwalled carbon nanotubes using diazonium salts." Chemphyschem **5**(11): 1794-1799.

Henzl, M. R. and P. K. Loomba (2003). "Transdermal delivery of sex steroids for hormone replacement therapy and contraception - A review of principles and practice." Journal of Reproductive Medicine **48**(7): 525-540.

Hidalgo-Bastida, L. A. and S. H. Cartmell (2010). "Mesenchymal stem cells, osteoblasts and extracellular matrix proteins: enhancing cell adhesion and differentiation for bone tissue engineering." Tissue Eng Part B Rev **16**(4): 405-412.

Higuchi, W. I. (1962). "Analysis of data on the medicament release from ointments." J Pharm Sci **51**: 802-804.

Hilding, J., E. A. Grulke, et al. (2003). "Dispersion of carbon nanotubes in liquids." Journal of Dispersion Science and Technology **24**(1): 1-41.

Hirsch, A. (2002). "Functionalization of single-walled carbon nanotubes." Angewandte Chemie - International Edition **41**(11): 1853-1859.

Hoffman, P. N., R. A. Abuknesha, et al. (2001). "A model to assess the infection potential of jet injectors used in mass immunisation." Vaccine **19**(28-29): 4020-4027.

Hogan, D. J. and H. I. Maibach (1990). "Adverse dermatologic reactions to transdermal drug delivery systems." J Am Acad Dermatol **22**(5 Pt 1): 811-814.

Holbrook, K. A. and G. F. Odland (1974). "Regional differences in the thickness (cell layers) of the human stratum corneum: an ultrastructural analysis." J Invest Dermatol **62**(4): 415-422.

Holzinger, M., J. Abraham, et al. (2003). "Functionalization of single-walled carbon nanotubes with (R-)oxycarbonyl nitrenes." J Am Chem Soc **125**(28): 8566-8580.

Holzinger, M., O. Vostrowsky, et al. (2001). "Sidewall Functionalization of Carbon Nanotubes This work was supported by the European Union under the 5th Framework Research Training Network 1999, HPRNT 1999-00011 FUNCARS." Angew Chem Int Ed Engl **40**(21): 4002-4005.

Hu, H., P. Bhowmik, et al. (2001). "Determination of the acidic sites of purified single-walled carbon nanotubes by acid-base titration." Chemical Physics Letters **345**(1-2): 25-28.

Hu, H., Y. C. Ni, et al. (2004). "Chemically functionalized carbon nanotubes as substrates for neuronal growth." Nano Letters **4**(3): 507-511.

Huang, H., E. Pierstorff, et al. (2007). "Active nanodiamond hydrogels for chemotherapeutic delivery." Nano Lett **7**(11): 3305-3314.

Huang, H. J., M. Chen, et al. (2009). "Ultrananocrystalline Diamond Thin Films Functionalized with Therapeutically Active Collagen Networks." Journal of Physical Chemistry B **113**(10): 2966-2971.

Huang, L. C. L. and H. C. Chang (2004). "Adsorption and immobilization of cytochrome c on nanodiamonds." Langmuir **20**(14): 5879-5884.

Hudson, J. L., M. J. Casavant, et al. (2004). "Water-soluble, exfoliated, nonroping single-wall carbon nanotubes." J Am Chem Soc **126**(36): 11158-11159.

Iijima, S. (1991). "Helical microtubules of graphitic carbon." Nature **354**(6348): 56-58.

Im, G. I., Y. W. Shin, et al. (2005). "Do adipose tissue-derived mesenchymal stem cells have the same osteogenic and chondrogenic potential as bone marrow-derived cells?" Osteoarthritis and Cartilage **13**(10): 845-853.

in 'tAnker, P. S., S. A. Scherjon, et al. (2003). "Amniotic fluid as a novel source of mesenchymal stem cells for therapeutic transplantation." Blood **102**(4): 1548-1549.

Ishijima, A. and T. Yanagida (2001). "Single molecule nanobioscience." Trends Biochem Sci **26**(7): 438-444.

Islam, M. F., E. Rojas, et al. (2003). "High weight fraction surfactant solubilization of single-wall carbon nanotubes in water." Nano Letters **3**(2): 269-273.

Jain, K. K., Ed. (2008). Drug Delivery Systems. Methods in Molecular Biology. Totowa, NJ, Humana Press.

Jarupanich, T., S. Lamlertkittikul, et al. (2003). "Efficacy, safety and acceptability of a seven-day, transdermal estradiol patch for estrogen replacement therapy." J Med Assoc Thai **86**(9): 836-845.

Jell, G., R. Verdejo, et al. (2008). "Carbon nanotube-enhanced polyurethane scaffolds fabricated by thermally induced phase separation." Journal of Materials Chemistry **18**(16): 1865-1872.

Jia, G., H. Wang, et al. (2005). "Cytotoxicity of carbon nanomaterials: single-wall nanotube, multi-wall nanotube, and fullerene." Environ Sci Technol **39**(5): 1378-1383.

Jia, H., W. Hou, et al. (2008). "The structures and antibacterial properties of nano-SiO_2 supported silver/zinc-silver materials." Dental Materials **24**(2): 244-249.

Jongpaiboonkit, L., W. J. King, et al. (2009). "Screening for 3D environments that support human mesenchymal stem cell viability using hydrogel arrays." Tissue Eng Part A **15**(2): 343-353.

Kagan, V. E., Y. Y. Tyurina, et al. (2006). "Direct and indirect effects of single walled carbon nanotubes on RAW 264.7 macrophages: role of iron." Toxicol Lett **165**(1): 88-100.

Kam, N. W. and H. Dai (2005). "Carbon nanotubes as intracellular protein transporters: generality and biological functionality." J Am Chem Soc **127**(16): 6021-6026.

Kam, N. W. S., T. C. Jessop, et al. (2004). "Nanotube molecular transporters: Internalization of carbon nanotube-protein conjugates into mammalian cells." Journal of the American Chemical Society **126**(22): 6850-6851.

Karachevtsev, V. A., A. Y. Glamazda, et al. (2006). "Spectroscopic and SEM studies of SWNTs: Polymer solutions and films." Carbon **44**(7): 1292-1297.

Kawamoto, H., T. Uchida, et al. (2006). "G band Raman features of DNA-wrapped single-wall carbon nanotubes in aqueous solution and air." Chemical Physics Letters **432**(1-3): 172-176.

Kawamoto, H., T. Uchida, et al. (2006). "Raman study of DNA-wrapped single-wall carbon nanotube hybrids under various humidity conditions." Chemical Physics Letters **431**(1-3): 118-120.

Keller, J. C., J. G. Collins, et al. (1997). "In vitro attachment of osteoblast-like cells to osteoceramic materials." Dent Mater **13**(1): 62-68.

Khademhosseini, A., J. P. Vacanti, et al. (2009). "Progress in Tissue Engineering." Scientific American **300**(5): 64-+.

Khang, D., S. Y. Kim, et al. (2007). "Enhanced fibronectin adsorption on carbon nanotube/poly(carbonate) urethane: independent role of surface nano-roughness and associated surface energy." Biomaterials **28**(32): 4756-4768.

Kim, K. Y. (2007). "Nanotechnology platforms and physiological challenges for cancer therapeutics." Nanomedicine **3**(2): 103-110.

Kligman, A. M. and E. Christophers (1963). "Preparation of Isolated Sheets of Human Stratum Corneum." Arch Dermatol **88**: 702-705.

Klumpp, C., K. Kostarelos, et al. (2006). "Functionalized carbon nanotubes as emerging nanovectors for the delivery of therapeutics." Biochimica et Biophysica Acta (BBA) - Biomembranes **1758**(3): 404-412.

Kong, J. and H. J. Dai (2001). "Full and modulated chemical gating of individual carbon nanotubes by organic amine compounds." Journal of Physical Chemistry B **105**(15): 2890-2893.

Koole, R. (1994). "Ectomesenchymal mandibular symphysis bone graft: an improvement in alveolar cleft grafting?" Cleft Palate Craniofac J **31**(3): 217-223.

Kornick, C. A., J. Santiago-Palma, et al. (2003). "Benefit-risk assessment of transdermal fentanyl for the treatment of chronic pain." Drug Safety **26**(13): 951-973.

Kroto, H. W., J. R. Heath, et al. (1985). "C-60 - Buckminsterfullerene." Nature **318**(6042): 162-163.

Krueger, A., J. Stegk, et al. (2008). "Biotinylated nanodiamond: Simple and efficient functionalization of detonation diamond." Langmuir **24**(8): 4200-4204.

Kruger, A. (2006). "Hard and soft: Biofunctionalized diamond." Angewandte Chemie-International Edition **45**(39): 6426-6427.

Kruger, A., Y. J. Liang, et al. (2006). "Surface functionalisation of detonation diamond suitable for biological applications." Journal of Materials Chemistry **16**(24): 2322-2328.

Krumov, N., I. Perner-Nochta, et al. (2009). "Production of Inorganic Nanoparticles by Microorganisms." Chemical Engineering & Technology **32**(7): 1026-1035.

Lacerda, L., H. Ali-Boucettal, et al. (2008). "Tissue histology and physiology following intravenous administration of different types of functionalized multiwalled carbon nanotubes." Nanomedicine **3**(2): 149-161.

Lacerda, L., A. Bianco, et al. (2006). "Carbon nanotubes as nanomedicines: From toxicology to pharmacology☆." Advanced Drug Delivery Reviews **58**(14): 1460-1470.

Lam, R., M. Chen, et al. (2008). "Nanodiamond-embedded microfilm devices for localized chemotherapeutic elution." ACS Nano **2**(10): 2095-2102.

Lane, J. M., E. Tomin, et al. (1999). "Biosynthetic bone grafting." Clin Orthop Relat Res(367 Suppl): S107-117.

Langer, R. and J. P. Vacanti (1993). "Tissue engineering." Science **260**(5110): 920-926.

Lanone, S. and J. Boczkowski (2006). "Biomedical applications and potential health risks of nanomaterials: molecular mechanisms." Curr Mol Med **6**(6): 651-663.

Larsen, R. H., F. Nielsen, et al. (2003). "Dermal penetration of fentanyl: Inter- and intraindividual variations." Pharmacology & Toxicology **93**(5): 244-248.

Lawson, L. B., L. C. Freytag, et al. (2007). "Use of nanocarriers for transdermal vaccine delivery." Clinical Pharmacology and Therapeutics **82**(6): 641-643.

Lee, J. W., J. H. Park, et al. (2008). "Dissolving microneedles for transdermal drug delivery." Biomaterials **29**(13): 2113-2124.

Lee, O. K., T. K. Kuo, et al. (2004). "Isolation of multipotent mesenchymal stem cells from umbilical cord blood." Blood **103**(5): 1669-1675.

Levin, G., A. Gershonowitz, et al. (2005). "Transdermal delivery of human growth hormone through RF-microchannels." Pharm Res **22**(4): 550-555.

Li, C., G. Fang, et al. (2006). "Effect of substrate temperature on the growth and photoluminescence properties of vertically aligned ZnO nanostructures." Journal of Crystal Growth **292**(1): 19-25.

Li, D., M. B. Muller, et al. (2008). "Processable aqueous dispersions of graphene nanosheets." Nat Nanotechnol **3**(2): 101-105.

Li, H., S. B. Willingham, et al. (2008). "Cutting edge: inflammasome activation by alum and alum's adjuvant effect are mediated by NLRP3." J Immunol **181**(1): 17-21.

Li, S., Ed. (2008). Electroporation Protocols: Preclinical and Clinical Gene Medicine. Methods in Molecular Biology. Totowa, NJ, Humana press.

Li, X., X. Wang, et al. (2008). "Chemically derived, ultrasmooth graphene nanoribbon semiconductors." Science **319**(5867): 1229-1232.

Li, Z. R., A. S. Biris, et al. (2007). "Influence of impurities on the x-ray photoelectron spectroscopy and Raman spectra of single-wall carbon nanotubes." Journal of Chemical Physics **127**(15): -.

Liang, F., A. K. Sadana, et al. (2004). "A convenient route to functionalized carbon nanotubes." Nano Letters **4**(7): 1257-1260.

Lin, S., X. Xie, et al. (2007). "Quantum dot imaging for embryonic stem cells." BMC Biotechnol **7**: 67.

Lin, Y., S. Taylor, et al. (2004). "Advances toward bioapplications of carbon nanotubes." Journal of Materials Chemistry **14**(4): 527-541.

Liong, M., J. Lu, et al. (2008). "Multifunctional inorganic nanoparticles for imaging, targeting, and drug delivery." ACS Nano **2**(5): 889-896.

Liu, D. D., C. Q. Yi, et al. (2010). "Inhibition of Proliferation and Differentiation of Mesenchymal Stern Cells by Carboxylated Carbon Nanotubes." ACS Nano **4**(4): 2185-2195.

Liu, F., Y. Akiyama, et al. (2008). "Changes in the expression of CD106, osteogenic genes, and transcription factors involved in the osteogenic differentiation of human bone marrow mesenchymal stem cells." J Bone Miner Metab **26**(4): 312-320.

Liu, H., S. Li, et al. (2006). "Investigation into the potential of low-frequency ultrasound facilitated topical delivery of Cyclosporin A." Int J Pharm **326**(1-2): 32-38.

Liu, K. K., C. L. Cheng, et al. (2007). "Biocompatible and detectable carboxylated nanodiamond on human cell." Nanotechnology **18**(32): -.

Liu, Y., C. Chipot, et al. (2010). "Solubilizing carbon nanotubes through noncovalent functionalization. Insight from the reversible wrapping of alginic acid around a

single-walled carbon nanotube." Journal of Physical Chemistry B **114**(17): 5783-5789.

Liu, Z., X. Sun, et al. (2007). "Supramolecular chemistry on water-soluble carbon nanotubes for drug loading and delivery." ACS Nano **1**(1): 50-56.

Liu, Z., S. Tabakman, et al. (2009). "Carbon nanotubes in biology and medicine: In vitro and in vivo detection, imaging and drug delivery." Nano Research **2**(2): 85-120.

Liwarska-Bizukojc, E., K. Miksch, et al. (2005). "Acute toxicity and genotoxicity of five selected anionic and nonionic surfactants." Chemosphere **58**(9): 1249-1253.

Lockman, P. R., J. M. Koziara, et al. (2004). "Nanoparticle surface charges alter blood-brain barrier integrity and permeability." J Drug Target **12**(9-10): 635-641.

Long, C. (2002). Common skin disorders and their topical treatment. Dermatological and transdermal formulations. K. A. Walters. New York, Marcel Dekker**:** 41-60.

Louit, G., T. Asahi, et al. (2009). "Spectral and 3-Dimensional Tracking of Single Gold Nanoparticles in Living Cells Studied by Rayleigh Light Scattering Microscopy." Journal of Physical Chemistry C **113**(27): 11766-11772.

Lu, F., L. Gu, et al. (2009). "Advances in Bioapplications of Carbon Nanotubes." Advanced Materials **21**(2): 139-152.

Lu, Q., J. M. Moore, et al. (2004). "RNA polymer translocation with single-walled carbon nanotubes." Nano Letters **4**(12): 2473-2477.

Maggini, M., G. Scorrano, et al. (1993). "Addition of Azomethine Ylides to C-60 - Synthesis, Characterization, and Functionalization of Fullerene Pyrrolidines." Journal of the American Chemical Society **115**(21): 9798-9799.

Magrez, A., S. Kasas, et al. (2006). "Cellular toxicity of carbon-based nanomaterials." Nano Lett **6**(6): 1121-1125.

Malarkey, E. B., K. A. Fisher, et al. (2009). "Conductive Single-Walled Carbon Nanotube Substrates Modulate Neuronal Growth." Nano Letters **9**(1): 264-268.

Manna, S. K., S. Sarkar, et al. (2005). "Single-walled carbon nanotube induces oxidative stress and activates nuclear transcription factor-kappaB in human keratinocytes." Nano Lett **5**(9): 1676-1684.

Marchesan, S., T. Da Ros, et al. (2005). "Anti-HIV properties of cationic fullerene derivatives." Bioorg Med Chem Lett **15**(15): 3615-3618.

Marrs, B., R. Andrews, et al. (2006). "Augmentation of acrylic bone cement with multiwall carbon nanotubes." J Biomed Mater Res A **77**(2): 269-276.

Martin, C. R. and P. Kohli (2003). "The emerging field of nanotube biotechnology." Nat Rev Drug Discov **2**(1): 29-37.

Martin, J., K. Helm, et al. (2008). "Adult lung side population cells have mesenchymal stem cell potential." Cytotherapy **10**(2): 140-151.

Mashino, T., D. Nishikawa, et al. (2003). "Antibacterial and antiproliferative activity of cationic fullerene derivatives." Bioorg Med Chem Lett **13**(24): 4395-4397.

Mashino, T., K. Shimotohno, et al. (2005). "Human immunodeficiency virus-reverse transcriptase inhibition and hepatitis C virus RNA-dependent RNA polymerase inhibition activities of fullerene derivatives." Bioorg Med Chem Lett **15**(4): 1107-1109.

Mawhinney, D. B., V. Naumenko, et al. (2000). "Surface defect site density on single walled carbon nanotubes by titration." Chemical Physics Letters **324**(1-3): 213-216.

Medintz, I. L., H. T. Uyeda, et al. (2005). "Quantum dot bioconjugates for imaging, labelling and sensing." Nat Mater **4**(6): 435-446.

Meidan, V. M. and C. S. Roper (2008). "Inter- and intra-individual variability in human skin barrier function: a large scale retrospective study." Toxicol In Vitro **22**(4): 1062-1069.

Meinel, L., V. Karageorgiou, et al. (2004). "Bone tissue engineering using human mesenchymal stem cells: effects of scaffold material and medium flow." Ann Biomed Eng **32**(1): 112-122.

Meuer, S., L. Braun, et al. (2009). "Pyrene Containing Polymers for the Non-Covalent Functionalization of Carbon Nanotubes." Macromolecular Chemistry and Physics **210**(18): 1528-1535.

Minko, T. (2005). "Soluble polymer conjugates for drug delivery." Drug Discovery Today: Technologies **2**(1): 15-20.

Minqin, R., J. A. van Kan, et al. (2007). "Nano-imaging of single cells using STIM." Nuclear Instruments & Methods in Physics Research Section B-Beam Interactions with Materials and Atoms **260**(1): 124-129.

Mistry, A. S. and A. G. Mikos (2005). "Tissue engineering strategies for bone regeneration." Adv Biochem Eng Biotechnol **94**: 1-22.

Mitchell, D. T., S. B. Lee, et al. (2002). "Smart nanotubes for bioseparations and biocatalysis." J Am Chem Soc **124**(40): 11864-11865.

Mitragotri, S. (2004). "Breaking the skin barrier." Adv Drug Deliv Rev **56**(5): 555-556.

Mitragotri, S. (2006). "Current status and future prospects of needle-free liquid jet injectors." Nat Rev Drug Discov **5**(7): 543-548.

Mitragotri, S., D. Blankschtein, et al. (1995). "Ultrasound-mediated transdermal protein delivery." Science **269**(5225): 850-853.

Mitragotri, S., D. Blankschtein, et al. (1996). "Transdermal drug delivery using low-frequency sonophoresis." Pharm Res **13**(3): 411-420.

Mohan, S. and D. J. Baylink (1991). "Bone growth factors." Clin Orthop Relat Res(263): 30-48.

Moore, V. C., M. S. Strano, et al. (2003). "Individually Suspended Single-Walled Carbon Nanotubes in Various Surfactants." Nano Letters **3**(10): 1379-1382.

Morones, J. R., J. L. Elechiguerra, et al. (2005). "The bactericidal effect of silver nanoparticles." Nanotechnology **16**(10): 2346-2353.

Moroni, L., J. R. de Wijn, et al. (2008). "Integrating novel technologies to fabricate smart scaffolds." J Biomater Sci Polym Ed **19**(5): 543-572.

Mosmann, T. (1983). "Rapid colorimetric assay for cellular growth and survival: application to proliferation and cytotoxicity assays." J Immunol Methods **65**(1-2): 55-63.

Mundy, G. R. (1993). "Cytokines and growth factors in the regulation of bone remodeling." J Bone Miner Res **8 Suppl 2**: S505-510.

Murakami, T. and K. Tsuchida (2008). "Recent advances in inorganic nanoparticle-based drug delivery systems." Mini Rev Med Chem **8**(2): 175-183.

Murphy, M. and A. J. Carmichael (2000). "Transdermal drug delivery systems and skin sensitivity reactions. Incidence and management." Am J Clin Dermatol **1**(6): 361-368.

Murugan, R. and S. Ramakrishna (2004). "Bioresorbable composite bone paste using polysaccharide based nano hydroxyapatite." Biomaterials **25**(17): 3829-3835.

Nakamura, E. and H. Isobe (2003). "Functionalized fullerenes in water. The first 10 years of their chemistry, biology, and nanoscience." Accounts of Chemical Research **36**(11): 807-815.

Nasir, A. (2009). "Nanotechnology in Vaccine Development: A Step Forward." Journal of Investigative Dermatology **129**(5): 1055-1059.

Nayak, T. R., P. C. Leow, et al. (2010). "Crucial Parameters Responsible for Carbon Nanotubes Toxicity." Current Nanoscience **6**(2): 141-154.

Nguyen, T. T. B., H. C. Chang, et al. (2007). "Adsorption and hydrolytic activity of lysozyme on diamond nanocrystallites." Diamond and Related Materials **16**(4-7): 872-876.

Nikolaev, P., M. J. Bronikowski, et al. (1999). "Gas-phase catalytic growth of single-walled carbon nanotubes from carbon monoxide." Chemical Physics Letters **313**(1-2): 91-97.

Nimmagadda, A., K. Thurston, et al. (2006). "Chemical modification of SWNT alters in vitro cell-SWNT interactions." J Biomed Mater Res A **76**(3): 614-625.

Niyogi, S., M. A. Hamon, et al. (2002). "Chemistry of single-walled carbon nanotubes." Acc Chem Res **35**(12): 1105-1113.

Niyogi, S., H. Hu, et al. (2001). "Chromatographic purification of soluble single-walled carbon nanotubes (s-SWNTS)." J Am Chem Soc **123**(4): 733-734.

Noguchi, Y., A. Ishibashi, et al. (2006). DNA dissolves single-walled carbon nanotubes in water, Nagoya.

Ogura, M., S. Paliwal, et al. (2008). "Low-frequency sonophoresis: current status and future prospects." Adv Drug Deliv Rev **60**(10): 1218-1223.

Oh, S., K. S. Brammer, et al. (2009). "Stem cell fate dictated solely by altered nanotube dimension." Proceedings of the National Academy of Sciences **106**(7): 2130-2135.

Oikarinen, J. and L. K. Korhonen (1979). "The bone inductive capacity of various bone transplanting materials used for treatment of experimental bone defects." Clin Orthop Relat Res(140): 208-215.

Oklund, S. A., D. J. Prolo, et al. (1986). "Quantitative comparisons of healing in cranial fresh autografts, frozen autografts and processed autografts, and allografts in canine skull defects." Clin Orthop Relat Res(205): 269-291.

Okumura, M., M. Mikawa, et al. (2002). "Evaluation of water-soluble metallofullerenes as MRI contrast agents." Academic Radiology **9 Suppl 2**: S495-497.

Ortiz-Acevedo, A., H. Xie, et al. (2005). "Diameter-selective solubilization of single-walled carbon nanotubes by reversible cyclic peptides." J Am Chem Soc **127**(26): 9512-9517.

Ozawa, M., M. Inaguma, et al. (2007). "Preparation and behavior of brownish, clear nanodiamond colloids." Advanced Materials **19**(9): 1201-+.

Pantarotto, D., C. D. Partidos, et al. (2003). "Synthesis, structural characterization, and immunological properties of carbon nanotubes functionalized with peptides." J Am Chem Soc **125**(20): 6160-6164.

Park, H., C. Cannizzaro, et al. (2007). "Nanofabrication and microfabrication of functional materials for tissue engineering." Tissue Eng **13**(8): 1867-1877.

Park, J., S. Bauer, et al. (2009). "TiO2 nanotube surfaces: 15 nm--an optimal length scale of surface topography for cell adhesion and differentiation." Small **5**(6): 666-671.

Park, J. H., J. W. Lee, et al. (2008). "The effect of heat on skin permeability." Int J Pharm **359**(1-2): 94-103.

Park, K. (2007). "Nanotechnology: What it can do for drug delivery." Journal of Controlled Release **120**(1-2): 1-3.

Park, K. H., M. Chhowalla, et al. (2003). "Single-walled carbon nanotubes are a new class of ion channel blockers." J Biol Chem **278**(50): 50212-50216.

Partha, R., L. R. Mitchell, et al. (2008). "Buckysomes: fullerene-based nanocarriers for hydrophobic molecule delivery." ACS Nano **2**(9): 1950-1958.

Pastorin, G., K. Kostarelos, et al. (2005). "Functionalized Carbon Nanotubes: Towards the Delivery of Therapeutic Molecules." Journal of Biomedical Nanotechnology **1**(2): 133-142.

Payne, R., S. D. Mathias, et al. (1998). "Quality of life and cancer pain: satisfaction and side effects with transdermal fentanyl versus oral morphine." J Clin Oncol **16**(4): 1588-1593.

Pellett, M., S. L. Raghavan, et al. (2003). The application of supersaturated systems to percutaneous drug delivery. Transdermal drug delivery. R. H. Guy and J. Hadgraft. New York, Marcel Dekker**:** 285-304.

Pinnagoda, J., R. A. Tupker, et al. (1990). "Guidelines for transepidermal water loss (TEWL) measurement. A report from the Standardization Group of the European Society of Contact Dermatitis." Contact Dermatitis **22**(3): 164-178.

Pittenger, M. F., A. M. Mackay, et al. (1999). "Multilineage potential of adult human mesenchymal stem cells." Science **284**(5411): 143-147.

Plotkin, S. L. and S. A. Plotkin (2004). A short history of vaccination. Vaccines. S. A. Plotkin and W. A. Orenstein. Philadelphia, WB Saunders Company**:** 1-15.

Poland, C. A., R. Duffin, et al. (2008). "Carbon nanotubes introduced into the abdominal cavity of mice show asbestos-like pathogenicity in a pilot study." Nat Nanotechnol **3**(7): 423-428.

Polisetty, N., A. Fatima, et al. (2008). "Mesenchymal cells from limbal stroma of human eye." Molecular Vision **14**(46-53): 431-442.

Prausnitz, M. R. (2004). "Microneedles for transdermal drug delivery." Advanced Drug Delivery Reviews **56**(5): 581-587.

Prausnitz, M. R., H. S. Gill, et al. (2008). Microneedles for Drug Delivery. Modified-Release Drug Delivery Technology. M. J. Rathbone, J. Hadgraft, M. S. Roberts and M. E. Lane. New York, Informa Healthcare. **2:** 295-310.

Prausnitz, M. R. and R. Langer (2008). "Transdermal drug delivery." Nat Biotechnol **26**(11): 1261-1268.

Prausnitz, M. R., S. Mitragotri, et al. (2004). "Current status and future potential of transdermal drug delivery." Nature Reviews Drug Discovery **3**(2): 115-124.

Prolo, D. J. and J. J. Rodrigo (1985). "Contemporary bone graft physiology and surgery." Clin Orthop Relat Res(200): 322-342.

Raja, P. M. V., J. Connolley, et al. (2007). "Impact of carbon nanotube exposure, dosage and aggregation on smooth muscle cells." Toxicology Letters **169**(1): 51-63.

Rakhi, R. B., K. Sethupathi, et al. (2008). "Synthesis and hydrogen storage properties of carbon nanotubes." International Journal of Hydrogen Energy **33**(1): 381-386.

Rancan, F., M. Helmreich, et al. (2005). "Fullerene-pyropheophorbide a complexes as sensitizer for photodynamic therapy: uptake and photo-induced cytotoxicity on Jurkat cells." J Photochem Photobiol B **80**(1): 1-7.

Rawadi, G., B. Vayssiere, et al. (2003). "BMP-2 controls alkaline phosphatase expression and osteoblast mineralization by a Wnt autocrine loop." J Bone Miner Res **18**(10): 1842-1853.

Richard, C. (2003). "Supramolecular Self-Assembly of Lipid Derivatives on Carbon Nanotubes." Science **300**(5620): 775-778.

Roco, M. C. (2003). "Converging science and technology at the nanoscale: opportunities for education and training." Nature Biotechnology **21**(10): 1247-1249.

Roy, R. (2004). "New trends in carbohydrate-based vaccines." Drug Discovery Today: Technologies **1**(3): 327-336.

Ruoff, R. S., D. S. Tse, et al. (1993). "Solubility of C-60 in a Variety of Solvents." Journal of Physical Chemistry **97**(13): 3379-3383.

Sarin, V. K., S. B. Kent, et al. (1981). "Quantitative monitoring of solid-phase peptide synthesis by the ninhydrin reaction." Anal Biochem **117**(1): 147-157.

Satija, N. K., V. K. Singh, et al. (2009). "Mesenchymal stem cell-based therapy: a new paradigm in regenerative medicine." J Cell Mol Med **13**(11-12): 4385-4402.

Sato, Y., A. Yokoyama, et al. (2005). "Influence of length on cytotoxicity of multi-walled carbon nanotubes against human acute monocytic leukemia cell line THP-1 in vitro and subcutaneous tissue of rats in vivo." Mol Biosyst **1**(2): 176-182.

Sayes, C. M., F. Liang, et al. (2006). "Functionalization density dependence of single-walled carbon nanotubes cytotoxicity in vitro." Toxicol Lett **161**(2): 135-142.

Scharton-Kersten, T., G. M. Glenn, et al. (1999). "Principles of transcutaneous immunization using cholera toxin as an adjuvant." Vaccine **17**(SUPPL. 2).

Scheuplein, R. J. (1967). "Mechanism of percutaneous absorption. II. Transient diffusion and the relative importance of various routes of skin penetration." J Invest Dermatol **48**(1): 79-88.

Scheuplein, R. J. and I. H. Blank (1971). "Permeability of the skin." Physiol Rev **51**(4): 702-747.

Schneider, U., R. Birnbacher, et al. (1994). "Painfulness of needle and jet injection in children with diabetes mellitus." Eur J Pediatr **153**(6): 409-410.

Schramm, J. and S. Mitragotri (2002). "Transdermal drug delivery by jet injectors: energetics of jet formation and penetration." Pharm Res **19**(11): 1673-1679.

Schrand, A. M., H. J. Huang, et al. (2007). "Are diamond nanoparticles cytotoxic?" Journal of Physical Chemistry B **111**(1): 2-7.

Schreier, H. (1994). "Liposomes and niosomes as topical drug carriers: Dermal and transdermal drug delivery." Journal of Controlled Release **30**(1): 1-15.

Schultz, O., M. Sittinger, et al. (2000). "Emerging strategies of bone and joint repair." Arthritis Res **2**(6): 433-436.

Seeman, N. C. and A. M. Belcher (2002). "Emulating biology: building nanostructures from the bottom up." Proc Natl Acad Sci U S A **99 Suppl 2**: 6451-6455.

Sekhon, B. S. and S. R. Kamboj (2010). "Inorganic nanomedicine-Part 1." Nanomedicine: Nanotechnology, Biology, and Medicine **6**(4): 516-522.

Sekhon, B. S. and S. R. Kamboj (2010). "Inorganic nanomedicine-Part 2." Nanomedicine: Nanotechnology, Biology, and Medicine **6**(5): 612-618.

Shashkov, E. V., M. Everts, et al. (2008). "Quantum dots as multimodal photoacoustic and photothermal contrast agents." Nano Lett **8**(11): 3953-3958.

Shim, M., N. W. S. Kam, et al. (2002). "Functionalization of carbon nanotubes for biocompatibility and biomolecular recognition." Nano Letters **2**(4): 285-288.

Shvartzman-Cohen, R., E. Nativ-Roth, et al. (2004). "Selective dispersion of single-walled carbon nanotubes in the presence of polymers: The role of molecular and colloidal length scales." Journal of the American Chemical Society **126**(45): 14850-14857.

Sinani, V. A., M. K. Gheith, et al. (2005). "Aqueous dispersions of single-wall and multiwall carbon nanotubes with designed amphiphilic polycations." Journal of the American Chemical Society **127**(10): 3463-3472.

Singh, R., D. Pantarotto, et al. (2005). "Binding and condensation of plasmid DNA onto functionalized carbon nanotubes: toward the construction of nanotube-based gene delivery vectors." J Am Chem Soc **127**(12): 4388-4396.

Sitharaman, B., K. R. Kissell, et al. (2005). "Superparamagnetic gadonanotubes are high-performance MRI contrast agents." Chem Commun (Camb)(31): 3915-3917.

Sittinger, M., J. Bujia, et al. (1996). "Tissue engineering and autologous transplant formation: Practical approaches with resorbable biomaterials and new cell culture techniques." Biomaterials **17**(3): 237-242.

Smart, S., A. Cassady, et al. (2006). "The biocompatibility of carbon nanotubes." Carbon **44**(6): 1034-1047.

Smith, A. M., X. Gao, et al. (2004). "Quantum dot nanocrystals for in vivo molecular and cellular imaging." Photochem Photobiol **80**(3): 377-385.

Soderberg, T. A., B. Sunzel, et al. (1990). "Antibacterial effect of zinc oxide in vitro." Scand J Plast Reconstr Surg Hand Surg **24**(3): 193-197.

Southwell, D., B. W. Barry, et al. (1984). "Variations in Permeability of Human-Skin within and between Specimens." International Journal of Pharmaceutics **18**(3): 299-309.

Stankovich, S., D. A. Dikin, et al. (2006). "Graphene-based composite materials." Nature **442**(7100): 282-286.

Star, A., D. W. Steuerman, et al. (2002). "Starched carbon nanotubes." Angew Chem Int Ed Engl **41**(14): 2508-2512.

Star, A., J. F. Stoddart, et al. (2001). "Preparation and properties of polymer-wrapped single-walled carbon nanotubes." Angewandte Chemie-International Edition **40**(9): 1721-1725.

Steinstrasser, I. and H. P. Merkle (1995). "Dermal metabolism of topically applied drugs: pathways and models reconsidered." Pharm Acta Helv **70**(1): 3-24.

Stevens, J. L., A. Y. Huang, et al. (2003). "Sidewall amino-functionalization of single-walled carbon nanotubes through fluorination and subsequent reactions with terminal diamines." Nano Letters **3**(3): 331-336.

Stoitzner, P., F. Sparber, et al. (2010). "Langerhans cells as targets for immunotherapy against skin cancer." Immunology and Cell Biology **88**(4): 431-437.

Strano, M. S., C. A. Dyke, et al. (2003). "Electronic structure control of single-walled carbon nanotube functionalization." Science **301**(5639): 1519-1522.

Strong, D. M., G. E. Friedlaender, et al. (1996). "Immunologic responses in human recipients of osseous and osteochondral allografts." Clin Orthop Relat Res(326): 107-114.

Sullivan, S. P., D. G. Koutsonanos, et al. (2010). "Dissolving polymer microneedle patches for influenza vaccination." Nat Med **16**(8): 915-920.

Sullivan, S. P., D. G. Koutsonanos, et al. (2010). "Dissolving polymer microneedle patches for influenza vaccination." Nature Medicine **16**(8): 915-U116.

Sun, X., Z. Liu, et al. (2008). "Nano-Graphene Oxide for Cellular Imaging and Drug Delivery." Nano Res **1**(3): 203-212.

Swetha, M., K. Sahithi, et al. (2010). "Biocomposites containing natural polymers and hydroxyapatite for bone tissue engineering." Int J Biol Macromol **47**(1): 1-4.

Tabata, Y., Y. Murakami, et al. (1997). "Photodynamic effect of polyethylene glycol-modified fullerene on tumor." Jpn J Cancer Res **88**(11): 1108-1116.

Tagmatarchis, N., V. Georgakilas, et al. (2002). "Sidewall functionalization of single-walled carbon nanotubes through electrophilic addition." Chemical Communications(18): 2010-2011.

Tagmatarchis, N. and M. Prato (2004). "Functionalization of carbon nanotubes via 1,3-dipolar cycloadditions." Journal of Materials Chemistry **14**(4): 437.

Tagmatarchis, N. and M. Prato (2004). "Functionalization of carbon nanotubes via 1,3-dipolar cycloadditions." Journal of Materials Chemistry **14**(4): 437-439.

Takagi, A., A. Hirose, et al. (2008). "Induction of mesothelioma in p53+/- mouse by intraperitoneal application of multi-wall carbon nanotube." J Toxicol Sci **33**(1): 105-116.

Tataria, M., N. Quarto, et al. (2006). "Absence of the p53 tumor suppressor gene promotes osteogenesis in mesenchymal stem cells." Journal of Pediatric Surgery **41**(4): 624-632.

Theintz, G. E. and P. C. Sizonenko (1991). "Risks of jet injection of insulin in children." Eur J Pediatr **150**(8): 554-556.

Thostenson, E. T., C. Y. Li, et al. (2005). "Nanocomposites in context." Composites Science and Technology **65**(3-4): 491-516.

Toole, J., S. Silagy, et al. (2002). "Evaluation of irritation and sensitisation of two 50 microg/day oestrogen patches." Maturitas **43**(4): 257-263.

Toth, E., R. D. Bolskar, et al. (2005). "Water-soluble gadofullerenes: toward high-relaxivity, pH-responsive MRI contrast agents." J Am Chem Soc **127**(2): 799-805.

Tsai, J. C., R. H. Guy, et al. (1996). "Metabolic approaches to enhance transdermal drug delivery. 1. Effect of lipid synthesis inhibitors." J Pharm Sci **85**(6): 643-648.

Tuli, R., S. Tuli, et al. (2003). "Characterization of multipotential mesenchymal progenitor cells derived from human trabecular bone." Stem Cells **21**(6): 681-693.

Ueno, H., N. Schmitt, et al. (2010). "Dendritic cells and humoral immunity in humans." Immunology and Cell Biology **88**(4): 376-380.

Urist, M. R. (1965). "Bone: formation by autoinduction." Science **150**(698): 893-899.

Ushizawa, K., Y. Sato, et al. (2002). "Covalent immobilization of DNA on diamond and its verification by diffuse reflectance infrared spectroscopy." Chemical Physics Letters **351**(1-2): 105-108.

Vacanti, J. P. and R. Langer (1999). "Tissue engineering: the design and fabrication of living replacement devices for surgical reconstruction and transplantation." Lancet **354 Suppl 1**: SI32-34.

Vaccaro, A. R., T. Patel, et al. (2005). "A 2-year follow-up pilot study evaluating the safety and efficacy of op-1 putty (rhbmp-7) as an adjunct to iliac crest autograft in posterolateral lumbar fusions." Eur Spine J **14**(7): 623-629.

Varvel, J. R., S. L. Shafer, et al. (1989). "Absorption characteristics of transdermally administered fentanyl." Anesthesiology **70**(6): 928-934.

Veetil, J. V. and K. Ye (2009). "Tailored carbon nanotubes for tissue engineering applications." Biotechnol Prog **25**(3): 709-721.

Wang, E. A., D. I. Israel, et al. (1993). "Bone morphogenetic protein-2 causes commitment and differentiation in C3H10T1/2 and 3T3 cells." Growth Factors **9**(1): 57-71.

Wang, J., C. Chen, et al. (2006). "Antioxidative function and biodistribution of [Gd@C82(OH)22]n nanoparticles in tumor-bearing mice." Biochem Pharmacol **71**(6): 872-881.

Wang, J., G. Liu, et al. (2004). "Ultrasensitive electrical biosensing of proteins and DNA: carbon-nanotube derived amplification of the recognition and transduction events." J Am Chem Soc **126**(10): 3010-3011.

Wang, J., G. D. Liu, et al. (2003). "Electrochemical detection of DNA hybridization based on carbon-nanotubes loaded with CdS tags." Electrochemistry Communications **5**(12): 1000-1004.

Wang, S., E. S. Humphreys, et al. (2003). "Peptides with selective affinity for carbon nanotubes." Nature Materials **2**(3): 196-200.

Wang, X., L. H. Liu, et al. (2009). "Engineering nanomaterial surfaces for biomedical applications." Exp Biol Med (Maywood) **234**(10): 1128-1139.

Watcharotone, S., D. A. Dikin, et al. (2007). "Graphene-silica composite thin films as transparent conductors." Nano Lett **7**(7): 1888-1892.

Weaver, J. C., T. E. Vaughan, et al. (1999). "Theory of electrical creation of aqueous pathways across skin transport barriers." Adv Drug Deliv Rev **35**(1): 21-39.

Whitesides, G. M. and M. Boncheva (2002). "Beyond molecules: self-assembly of mesoscopic and macroscopic components." Proc Natl Acad Sci U S A **99**(8): 4769-4774.

Wick, P., P. Manser, et al. (2007). "The degree and kind of agglomeration affect carbon nanotube cytotoxicity." Toxicol Lett **168**(2): 121-131.

Wildoer, J. W., L. C. Venema, et al. (1998). "Electronic structure of atomically resolved carbon nanotubes." Nature **391**(6662): 59-62.

Williams, A. (2003). Transdermal and Topical Drug Delivery: From Theory to Clinical Practice. London, Pharmaceutical Press.

Williams, A. C. and B. W. Barry (2004). "Penetration enhancers." Adv Drug Deliv Rev **56**(5): 603-618.

Wu, W., S. Wieckowski, et al. (2005). "Targeted delivery of amphotericin B to cells by using functionalized carbon nanotubes." Angew Chem Int Ed Engl **44**(39): 6358-6362.

Wu, W., S. Wieckowski, et al. (2005). "Targeted delivery of amphotericin B to cells by using functionalized carbon nanotubes." Angewandte Chemie-International Edition **44**(39): 6358-6362.

Yang, K., S. Zhang, et al. (2010). "Graphene in mice: Ultrahigh in vivo tumor uptake and efficient photothermal therapy." Nano Letters **10**(9): 3318-3323.

Yang, S. I., H. Y. Park, et al. (2004). "Transdermal eperisone elicits more potent and longer-lasting muscle relaxation than oral eperisone." Pharmacology **71**(3): 150-156.

Yang, W., P. Thordarson, et al. (2007). "Carbon nanotubes for biological and biomedical applications." Nanotechnology **18**(41).

Yano, T., A. Nakagawa, et al. (1986). "Skin permeability of various non-steroidal anti-inflammatory drugs in man." Life Sci **39**(12): 1043-1050.

Yaszemski, M. J., R. G. Payne, et al. (1996). "Evolution of bone transplantation: molecular, cellular and tissue strategies to engineer human bone." Biomaterials **17**(2): 175-185.

Yeap, W. S., Y. Y. Tan, et al. (2008). "Using detonation nanodiamond for the specific capture of glycoproteins." Anal Chem **80**(12): 4659-4665.

Yin, J. J., F. Lao, et al. (2009). "The scavenging of reactive oxygen species and the potential for cell protection by functionalized fullerene materials." Biomaterials **30**(4): 611-621.

Young, H. E., T. A. Steele, et al. (2001). "Human reserve pluripotent mesenchymal stem cells are present in the connective tissues of skeletal muscle and dermis derived from fetal, adult, and geriatric donors." Anat Rec **264**(1): 51-62.

Yu, M. F., B. S. Files, et al. (2000). "Tensile loading of ropes of single wall carbon nanotubes and their mechanical properties." Physical Review Letters **84**(24): 5552-5555.

Yu, M. F., O. Lourie, et al. (2000). "Strength and breaking mechanism of multiwalled carbon nanotubes under tensile load." Science **287**(5453): 637-640.

Yu, S. J., M. W. Kang, et al. (2005). "Bright fluorescent nanodiamonds: no photobleaching and low cytotoxicity." J Am Chem Soc **127**(50): 17604-17605.

Zakharian, T. Y., A. Seryshev, et al. (2005). "A fullerene-paclitaxel chemotherapeutic: synthesis, characterization, and study of biological activity in tissue culture." J Am Chem Soc **127**(36): 12508-12509.

Zanello, L. P., B. Zhao, et al. (2006). "Bone cell proliferation on carbon nanotubes." Nano Lett **6**(3): 562-567.

Zeldis, J. B., S. Jain, et al. (1992). "Seroepidemiology of viral infections among intravenous drug users in northern California." West J Med **156**(1): 30-35.

Zhao, B., H. Hu, et al. (2001). "Chromatographic purification and properties of soluble single-walled carbon nanotubes." J Am Chem Soc **123**(47): 11673-11677.

Zhao, B., H. Hu, et al. (2005). "Synthesis and characterization of water soluble single-walled carbon nanotube graft copolymers." J Am Chem Soc **127**(22): 8197-8203.

Zhao, Y. L., S. N. Murthy, et al. (2006). "Induction of cytotoxic T-lymphocytes by electroporation-enhanced needle-free skin immunization." Vaccine **24**(9): 1282-1290.

Zheng, M., A. Jagota, et al. (2003). "DNA-assisted dispersion and separation of carbon nanotubes." Nature Materials **2**(5): 338-342.

Zheng, M., A. Jagota, et al. (2003). "Structure-based carbon nanotube sorting by sequence-dependent DNA assembly." Science **302**(5650): 1545-1548.

Ziegler, A. S. (2008). "Needle-free delivery of powdered protein vaccines: A new and rapidly developing technique." Journal of Pharmaceutical Innovation **3**(3): 204-213.

Ziegler, K. J., Z. Gu, et al. (2005). "Controlled oxidative cutting of single-walled carbon nanotubes." J Am Chem Soc **127**(5): 1541-1547.

Zippel, N., M. Schulze, et al. (2010). "Biomaterials and mesenchymal stem cells for regenerative medicine." Recent patents on biotechnology **4**(1): 1-22.

Zorbas, V., A. Ortiz-Acevedo, et al. (2004). "Preparation and characterization of individual peptide-wrapped single-walled carbon nanotubes." J Am Chem Soc **126**(23): 7222-7227.

Zvaifler, N. J., L. Marinova-Mutafchieva, et al. (2000). "Mesenchymal precursor cells in the blood of normal individuals." Arthritis Res **2**(6): 477-488.

Appendices

Appendix I. Amount of BMP-2 covalently bonded to MWCNT-COOH coated coverslips when applied with specific amount of BMP-2.

Applied BMP-2 (ng)	OD at 562 nm	Amount as shown in BCA assay (ng)	Average (ng)
100	0.00304	38	39
	0.0032	40	
150	0.00544	68	70
	0.00576	72	

Appendix II. Graph showing BMP2 standard curve as prepared by BCA protein assay.

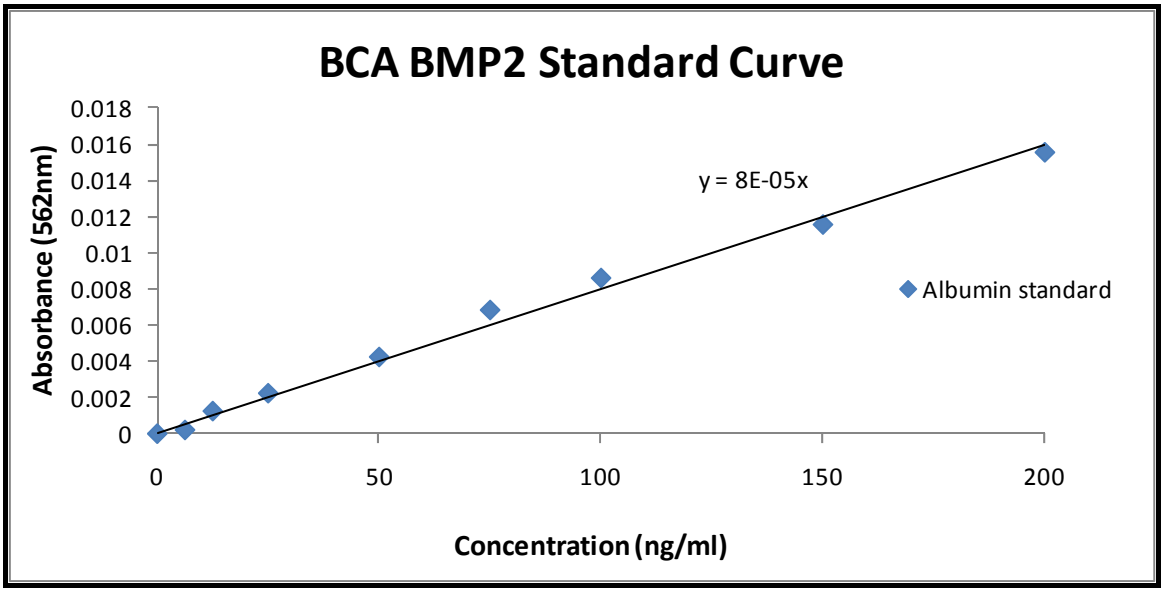

Appendix III: Graph showing standard curve for cell viability of hMSCs as determined by Calcein AM cell viability assay.

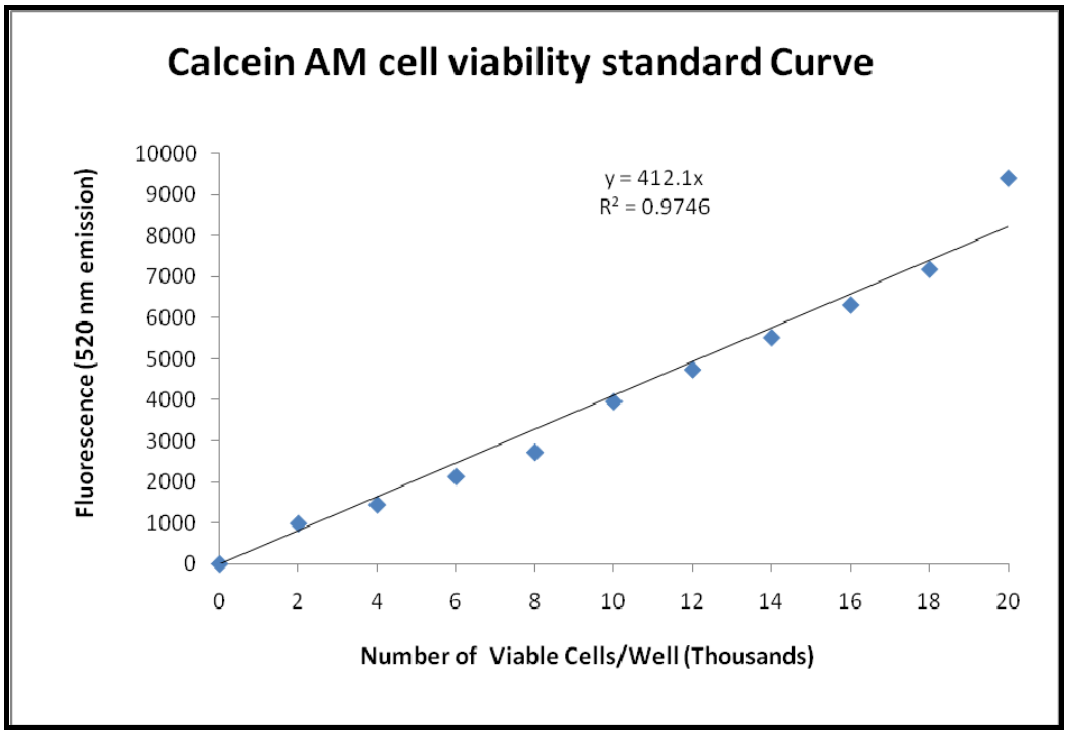

Appendix IV: Fold change expression of osteopontin (*OPN*) in hMSCs cultured on different types of substrates and osteoinduced with osteogenic media with or without BMP-2 for 14 days. Expression changes in various samples were measured as fold change with respect to control cells (i.e. cells grown on cover slip in the absence of BMP-2). **Negative control consists of coverslip without BMP-2 and without induction with osteogenic media.

Sample	**OPN Average C_T**	**18S Average C_T**	**ΔC_T** **($C_{T\ OPN} - C_{T\ 18S}$)**	**$\Delta\Delta C_T$** **(ΔC_T of test sample – ΔC_T of control cells)**	**Fold difference in OPN relative to control cells**
Coverslip without BMP-2	30.17 ± 0.18	14.22 ± 0.02	15.95 ± 0.18	0.00 ± 0.18	1.0 (0.9 – 1.1)
Coverslip with BMP-2	28.38 ± 0.17	13.88 ± 0.03	14.50 ± 0.18	-1.45 ± 0.18	2.7 (2.4 – 3.1)
PEG without BMP-2	31.79 ± 0.38	14.33 ± 0.02	17.46 ± 0.38	1.52 ± 0.38	0.3 (0.3 – 0.5)
PEG with BMP-2	28.95 ± 0.56	14.08 ± 0.03	14.87 ± 0.56	-1.08 ± 0.56	2.1 (1.4 – 3.1)
CNT-PEG without BMP-2	28.47 ± 0.50	14.09 ± 0.05	14.37 ± 0.50	-1.57 ± 0.50	3.0 (2.1 – 4.2)
CNT-PEG with BMP-2	28.58 ± 0.47	14.07 ± 0.02	14.51 ± 0.47	-1.44 ± 0.47	2.7 (2.0 – 3.7)
**Negative control	36.47 ± 0.09	14.28 ± 1.40	22.18 ± 1.41	6.24 ± 1.41	0.0 (0.0 – 0.0)

Appendix V. Graph showing standard curve for albumin-FITC as determined by Bradford assay.

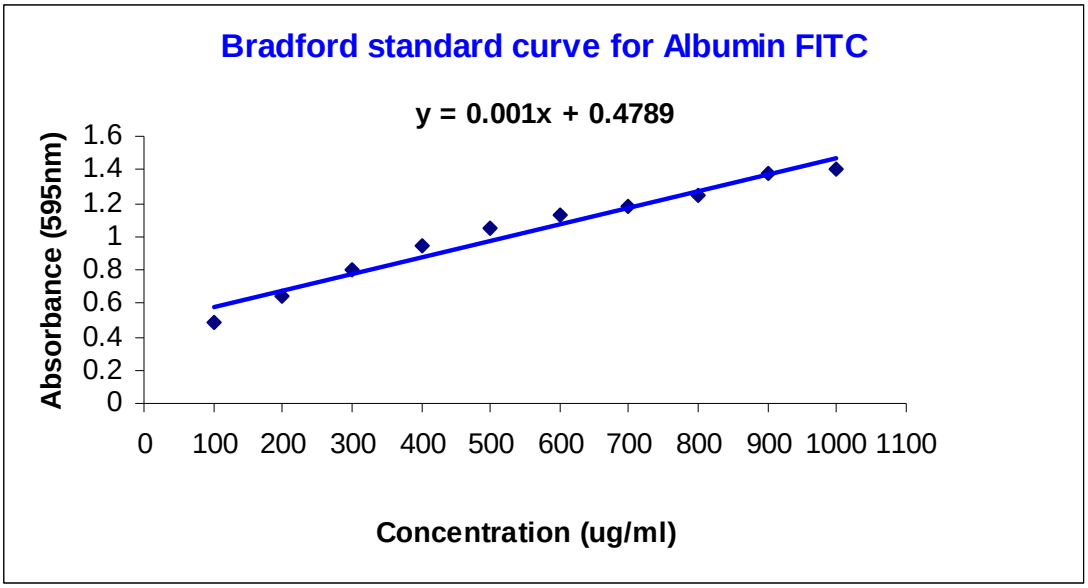

Appendix VI. Graph showing standard curve for endograde OVA solution as determined by Bradford assay.